

Carbazole-benzothiadiazole-based conjugated copolymers : synthesis, electrochromism and electrofluorochromism

Ding, Guoqiang

2014

Ding, G. (2014). Carbazole-benzothiadiazole-based conjugated copolymers : synthesis, electrochromism and electrofluorochromism. Doctoral thesis, Nanyang Technological University, Singapore.

<https://hdl.handle.net/10356/61738>

<https://doi.org/10.32657/10356/61738>



**CARBAZOLE–BENZOTHIADIAZOLE-BASED
CONJUGATED COPOLYMERS: SYNTHESIS,
ELECTROCHROMISM AND
ELECTROFLUOROCHROMISM**

DING GUOQIANG

SCHOOL OF MATERIALS SCIENCE AND ENGINEERING

2014

**CARBAZOLE-BENZOTHIADIAZOLE-BASED
CONJUGATED COPOLYMERS: SYNTHESIS,
ELECTROCHROMISM AND
ELECTROFLUOROCHROMISM**

DING GUOQIANG

DING GUOQIANG

SCHOOL OF MATERIALS SCIENCE AND ENGINEERING

**A THESIS SUBMITTED TO THE NANYANG
TECHNOLOGICAL UNIVERSITY IN PARTIAL
FULFILLMENT OF THE REQUIREMENTS FOR THE
DEGREE OF DOCTOR OF PHILOSOPHY**

2014

Acknowledgement

First of all, I would like to express my deepest appreciation to my supervisor and mentor, Associate Professor, Dr. Lu Xuehong, for her inspiring and patient guidance throughout this challenging journey. Her profound knowledge, invaluable suggestions and warm encouragement enlighten my way pursuing the truth.

I would like to sincerely thank my co-supervisor, Senior Scientist, Dr. Xu Jianwei, who is from Institute of Materials Research and Engineering (IMRE), for his indispensable advice, patient guidance and valuable support. His profound knowledge benefits me a lot in chemical synthesis.

I will show my thanks to my seniors, Dr. Xiong Shanxin and Dr. Jia Pengtao, for their guidance in the electrochemical and electrochromic characterizations. I would like to thank Dr. Yee Wu Aik, Dr. Kong Junhua, Ms. Phua Si Lei and all other colleagues of our group, for their encouragement and help.

Many thanks to Dr. Wang Xiaobai, Dr. Xiao Yang, Dr. Zhou Hui, Ms. Cho Ching Mui, Ms. Angeline Tan Yan Xuan, and other staff as well as students who helped me in IMRE. Thank the technical staff from Organic Materials Service Lab, Facts and E-Space in MSE, for equipment training and technical support.

Especially, I would like to thank my parents and my wife, for their love, understanding, encouragement and support.

Last but not least, I would like to thank all who helped me during the period of my PhD studies.

Abbreviations

ACN	Acetonitrile
BTD	2,1,3-Benzothiadiazole
CIE	Commission Internationale de l'Eclairage
CN ⁻	Cyanide anion
CP	Conjugated polymer
CV	Cyclic voltammetry
D–A	Donor–acceptor
EC	Electrochromic
ECD	Electrochromic device
EFC	Electrofluorochromic
FESEM	Field emission scanning electron microscope
HT	3-Hexylthiophene
ITO	Indium tin oxide
LiClO ₄	Lithium perchlorate
NMR	Nuclear magnetic resonance
PEDOT:PSS	Poly(3,4-ethylenedioxythiophene) doped with poly(styrenesulfonate)
PET	Poly(ethylene terephthalate)
Redox	Reduction–oxidation
TBACN	Tetrabutylammonium cyanide
UV–vis–NIR	Ultraviolet–visible–near infrared

Table of Contents

Acknowledgement	I
Abbreviations.....	III
List of Figures, Schemes and Tables	VII
Abstract.....	XII
1. Introduction.....	1
1.1 Background.....	1
1.2 Motivation, Hypotheses and Objectives	4
1.3 Organization of this thesis	6
2. Literature Review.....	7
2.1 Introduction.....	7
2.2 Electrochromic devices	9
2.2.1 Configuration of ECDs	9
2.2.1.1 Components	9
2.2.1.2 Transmissive ECDs.....	11
2.2.2 Types of ECDs.....	13
2.2.2.1 Visible and Vis–NIR ECDs	13
2.2.2.2 Black ECDs.....	13
2.2.3 Key performance parameters	15
2.3 Electrochromic materials	18
2.3.1 Overview.....	18
2.3.2 Anodically coloring conjugated polymers	22
2.3.2.1 Polyaniline	22
2.3.2.2 Carbazole-based conjugated polymers.....	23
2.3.2.3 Azulene-based conjugated polymers	25
2.3.2.4 Others.....	26
2.3.3 Cathodically coloring conjugated polymers	27
2.3.3.1 PEDOT.....	27
2.3.3.2 Others.....	28
2.3.4 Donor–Acceptor conjugated polymers	28

2.3.5 Synthesis of conjugated polymers via Suzuki coupling.....	31
2.4 Electrofluorochromic materials and devices.....	32
2.4.1 Fluorescence from conjugated polymers	32
2.4.1.1 Principles	32
2.4.1.2 Fluorescent conjugated polymers for sensor application and cyanide detection ..	33
2.4.2 EFC materials.....	35
2.4.3 EFC devices	38
2.4.4 Applications of EFC materials.....	39
2.5 Characterization of electrochemical, EC and EFC properties	40
2.5.1 Three-electrode electrochemical cell	40
2.5.2 Main characterization methods	41
3. Black-to-Transmissive Electrochromism of Carbazole–Benzothiadiazole–Azulene- Based Donor–Acceptor Conjugated Polymers Complemented by PEDOT:PSS.....	43
3.1 Introduction.....	43
3.2 Experimental	45
3.2.1 Materials	45
3.2.2 Chemical characterization.....	45
3.2.4 Cyclic voltammetry and spectroelectrochemical characterization.....	48
3.2.5 ECD fabrication and characterization.....	48
3.3 Results and discussion	49
3.3.1 Synthesis and structure verification	49
3.3.2 Cyclic voltammetry.....	56
3.3.3 Spectroelectrochemical behavior	59
3.3.4 Black-to-transmissive ECD	60
3.4 Conclusions.....	62
4. Electrofluorochromic Detection of Cyanide Anion Using A Benzothiadiazole- Containing Conjugated Copolymer	63
4.1 Introduction.....	63
4.2 Experimental	64
4.2.1 Materials	64
4.2.2 Chemical characterization.....	65
4.2.3 Synthesis	65
4.2.4 Cyclic voltammetry and spectroelectrochemical characterization.....	69
4.3 Results and discussion	70

4.3.1 Synthesis and structural characterization	70
4.3.2 Optical and electrochemical properties	73
4.3.3 Electrochromic and electrofluorochromic properties.....	75
4.3.4 Cyanide detection.....	77
4.4 Conclusions.....	81
5. Nanoporous Carbazole–Benzothiadiazole-Based Copolymer Electrode for Electrofluorochromic Detection of Cyanide Anion	83
5.1 Introduction.....	83
5.2. Experimental	85
5.2.1 Materials	85
5.2.2 Chemical and morphological characterization.....	85
5.2.3 Monomer synthesis	86
5.2.4 Electropolymerization, cyclic voltammetry and spectroelectrochemical characterization	86
5.3. Results and discussion	87
5.3.1 Synthesis and structural verification	87
5.3.2 Effect of morphology on electrochemical properties	93
5.3.3 Electrochromic and electrofluorochromic properties.....	96
5.3.4 Cyanide detection and possible mechanism.....	99
5.3.5 Detection of cyanide in partially aqueous media	104
5.4. Conclusions.....	108
6. Conclusions and Recommendations	110
6.1 Conclusions.....	110
6.1.1 Dual-active-layer complementary black ECD	110
6.1.2 Electrofluorochromic sensor towards cyanide detection	111
6.1.3 Electrofluorochromic cyanide detection in partially aqueous media.....	112
6.2 Recommendations for further research	113
References.....	116
List of Publications	128
Appendix.....	129

List of Figures, Schemes and Tables

Figure 2.1 (a) Anti-glare EC car rear-view mirror dimming after strong light from back has been sensed (right) and non-EC rear-view mirror for comparison (left), and (b) Plastic Logic's e-paper, adapted with permission from Plastic Logic, http://www.plasticlogic.com/ . Copyright 2009 Plastic Logic.....	8
Figure 2.2 Fluorescence quenching of an EFC device at different potentials. Reproduced from ref. [47] with permission from The Royal Society of Chemistry.	9
Figure 2.3 Schematic illustrations of (a) a single-layer ECD and (b) a dual-layer (complementary) ECD (side view, not to scale).....	12
Figure 2.4 The smart windows at (a) 'Off' state (colorless) and (b) 'On' state (blue).	13
Figure 2.5 (a) Schematic diagram of the complementary ECD (from top to bottom): ITO glass, PANBS, PDHFA, electrolyte, PEDOT VPP, P3HT, and ITO glass. (b) Transmittance spectra (inset: the photographs of colored state and bleached state), and (c) CIE (Commission Internationale de l'Eclairage) diagram of the ECD (RGBY). Reprinted with permission from ref. [60]. Copyright (2012) American Chemical Society.	15
Figure 2.6 Diagrams of (a) CIE 1931 color space and (b) CIE Lab color space (inset: a^*b^* two dimensional coordinate plane).	17
Figure 2.7 (a) Flexible films of electrochromic aromatic polyamides. Reproduced from ref. [115] with permission from The Royal Society of Chemistry. (b) Electrochromism exhibited by triphenylamine-substituted derivative polyimides. Adapted with permission from ref. [117]. Copyright (2011) American Chemical Society.....	22
Figure 2.8 (a) Spectroelectrochemistry of PEDOT thin film. Adapted with permission from ref. [148]. Copyright (2004) WILEY-VCH Verlag GmbH & Co. KGaA, Weinheim. (b) Structure demonstration of PEDOT:PSS.	28
Figure 2.9 Schematic diagram of an EFC device. Reproduced from ref. [47] with permission from The Royal Society of Chemistry	39
Figure 2.10 Configuration of a three-electrode electrochemical cell (cuvette) for spectroelectrochemical characterization.	41
Figure 3.1 (a) ^1H NMR spectra of P_0 , P_1 , P_3 , P_5 and P_{20} in CDCl_3 (* indicates CDCl_3 , # indicates H_2O). The molar ratios of carbazole to BTB units (P_1 was here taken as an example) were estimated by integration of peak a + b + c + d + e + f (all aromatic protons) to peak g (protons from N- CH_2). (b) ^{13}C NMR spectra of P_0 , P_5 and P_{20} in CDCl_3	50

Figure 3.2 Visible spectra of P ₀ , P ₅ and P ₂₀ dissolved in chloroform (8×10^{-5} M for each solution). The inset shows UV–vis–NIR absorption spectra of the copolymers.....	54
Figure 3.3 Visible spectra of spin-coated (a) P ₀ , (b) P ₁ , (c) P ₃ , (d) P ₅ and (e) P ₂₀ on ITO/PET under different potentials (0, +0.6, +0.8, +1.0, +1.2V) in 0.1 M LiClO ₄ /ACN.	55
Figure 3.4 Cyclic voltammograms of spin-coated (a) P ₀ and (b) P ₅ on ITO/PET in 0.1 M LiClO ₄ /ACN at a scan rate 10 mV/s.	57
Figure 3.5 Absorption–time profiles ($\lambda_{\text{max}} = 550$ nm) of spin-coated P ₀ (dash line) and P ₅ (solid line) on ITO/PET switched between –0.4 and 1.0 V in 0.1 M LiClO ₄ /ACN.	60
Figure 3.6 Visible spectra of spin-coated (a) P ₅ and PEDOT:PSS on ITO/PET in 0.1 M LiClO ₄ /ACN under various potentials, (b) complementary ECD of P ₅ /PEDOT:PSS under different potentials (0, + 0.5, + 1.0, + 1.5 V). The insets show the color of spin-coated films (picture taken after placing the ECD on a white paper background) at (I) neutral state before electrochemical switching; (II) electrochemically oxidized; (III) neutral after electrochemical switching. (c) CIE diagram of the complementary ECD at (▲) bleached state and (■) colored state.	61
Figure 4.1 ¹ H NMR spectra of copolymer EFP _C in CDCl ₃	72
Figure 4.2 Absorption and PL spectra of EFP _C dissolved in CHCl ₃ and spin-coated thin film on plain glass (λ_{exc} : 450 nm for solution and 465 nm for film)...	74
Figure 4.3 Cyclic voltammograms of EFP _C /ITO/PET in 0.1 M LiClO ₄ /ACN at different scan rates (25, 50, 75 and 100 mV/s)	75
Figure 4.4 (a) Absorption spectra under different potentials, (b) absorption–time profiles ($\lambda_{\text{monitor}} = 465$ nm; switching between 1.4 V and –1.0 V), (c) PL intensity changes ($\lambda_{\text{exc}} = 465$ nm) under potentials different potentials and (d) PL intensity–time profiles ($\lambda_{\text{exc}} = 465$ nm, $\lambda_{\text{monitor}} = 580$ nm; switching between 1.2 V and –1.0 V with 80 s per cycle), of EFP _C /ITO/PET in 0.1 M LiClO ₄ /ACN	76
Figure 4.5 Normalized PL intensities ($\lambda_{\text{exc}} = 465$ nm and $\lambda_{\text{monitor}} = 580$ nm) of EFP _C /ITO/PET as a function of potential, E. The curves in (a) were obtained with the reference electrolyte (R) containing different concentrations of TBACN (0, 10^{-6} , 10^{-5} and 10^{-4} M), and that in (b) were obtained from R with 10^{-4} M TBACN as well as R + 10^{-4} M TBACN with/without 8 types of TBA-based anions (OH [–] , F [–] , Cl [–] , Br [–] , I [–] , AcO [–] , NO ₃ [–] and HSO ₄ [–] , 10^{-5} M each).	78
Figure 4.6 PL intensity–time profiles ($\lambda_{\text{exc}} = 465$ nm, $\lambda_{\text{monitor}} = 580$ nm) of (a) EFP _C /ITO/PET switched between 1.0 V and –1.0 V in R + 10^{-4} M TBACN, and (b) EFP _C /ITO/PET that had been taken out from the R + 10^{-4} M TBACN after cycling and washed with ACN before this test. The switching time used was 80 s per cycle.	79

Figure 4.7 Normalized PL intensities ($\lambda_{\text{exc}} = 465 \text{ nm}$ and $\lambda_{\text{monitor}} = 580 \text{ nm}$) of EFP _C /ITO/PET as a function of potential, E. The two curves were obtained using the reference electrolyte (R) as well as R + TBA-based anions (OH ⁻ and F ⁻ , 10 ⁻⁴ M each).	81
Figure 5.1 ¹ H NMR spectra of (a) monomer (HT-C-BTD-C-HT) and (b) electrodeposited copolymer EFP _E , dissolved in CDCl ₃ . Asterisk indicates the peak of CDCl ₃	89
Figure 5.2 Cyclic voltammograms for the electrodeposition on ITO glass. HT-C-BTD-C-HT (0.5 mM) was dissolved in the electrolyte of 0.1 M TBAPF ₆ /PC, and the scan rate was 100 mV/s.	91
Figure 5.3 Absorption spectra of the electrodeposited EFP _E film, and the solution of that polymer and monomer dissolved in chloroform, respectively.	93
Figure 5.4 FESEM images for the surface of EFP _E film electrodeposited using E-PC with magnification of (a) 10k and (b) 50k, and for that using E-ACN with magnification of (c) 10k and (d) 50k. The scan rate was 100 mV/s for the electrodeposition in each electrolyte.	94
Figure 5.5 (a) Cyclic voltammograms of EFP _E film at different scan rates (10, 25, 50, 75 and 100 mV/s), diagram of (b) peak current density versus scan rate and (c) peak current density versus scan rate ^{1/2}	96
Figure 5.6 (a) UV-vis-NIR absorption spectra of EFP _E film in 0.1 M LiClO ₄ /ACN under different potentials and (b) absorption-time profile ($\lambda_{\text{monitor}} = 900 \text{ nm}$) of EFP _E in 0.1 M LiClO ₄ /ACN, switching between +0.9 V and -0.4 V with 20 s per cycle.	97
Figure 5.7 PL intensity ($\lambda_{\text{exc}} = 450 \text{ nm}$) change of EFP _E film with (a) quenching and (b) recovery under different potentials; (c) PL intensity-time profile of switching between +0.7 V and -0.8 V with 80 s per cycle.	99
Figure 5.8 Normalized PL intensities ($\lambda_{\text{monitor}} = 580 \text{ nm}$) of electrodeposited EFP _E film as a function of potential, E. The curves in (a) were obtained with the reference electrolyte (R) containing different concentrations of TBACN (0, 10 ⁻⁶ , 10 ⁻⁵ and 10 ⁻⁴ M), and that in (b) were obtained from R with 10 ⁻⁴ M TBACN as well as R + 10 ⁻⁵ M TBACN with/without 8 types of other TBA-based anions (OH ⁻ , F ⁻ , Cl ⁻ , Br ⁻ , I ⁻ , AcO ⁻ , NO ₃ ⁻ and HSO ₄ ⁻ , 10 ⁻⁵ M each).	100
Figure 5.9 PL intensity-time profiles ($\lambda_{\text{exc}} = 450 \text{ nm}$, $\lambda_{\text{monitor}} = 580 \text{ nm}$; switching between 0.7 V and -0.8 V with 80 s per cycle) of (a) the detection electrode in R + 10 ⁻⁴ M TBACN, and (b) the detection electrode that had been taken out from R + 10 ⁻⁴ M TBACN after cycling and washed with ACN before this switching test.	101
Figure 5.10 (a) Cyclic voltammograms of EFP _E film in the electrolytes R and R + TBACN. The concentrations of TBACN used are 10 ⁻⁶ , 10 ⁻⁵ and 10 ⁻⁴ M, respectively. (b) Plot of normalized intensities of the detection electrode under 0.6 V external potential in the electrolytes containing TBACN, against TBACN	

concentration, and the peak oxidation potentials obtained from the cyclic voltammograms at a scan rate 25mV/s. The electrolytes of R + TBACN were used and the concentrations of TBACN were 0, 10^{-6} , 10^{-5} and 10^{-4} M, respectively. 103	
Figure 5.11 Normalized PL intensities ($\lambda_{\text{monitor}} = 580$ nm) of EFP _E film as a function of potential, E. The curves were obtained using the electrolyte of 0.1 M LiClO ₄ in (a) ACN (R), R + TBACN; (b) ACN/H ₂ O (v/v = 1:1, R ^{1:1}), R ^{1:1} + TBACN; and (c) ACN/H ₂ O (v/v = 1:2, R ^{1:2}), R ^{1:2} + TBACN. The TBACN concentrations used are 10^{-6} , 10^{-5} and 10^{-4} M, respectively.105	
Figure 5.12 (a) Cyclic voltammograms of EFP _E film in the electrolytes R ^{1:2} and R ^{1:2} + TBACN. The concentrations of TBACN used are 10^{-6} , 10^{-5} and 10^{-4} M, respectively. (b) Plot of normalized intensities of the detection electrode under 0.6 V external potential in the electrolytes containing TBACN, against TBACN concentration, and the peak oxidation potentials obtained from the cyclic voltammograms at a scan rate 25mV/s. The electrolytes of R ^{1:2} + TBACN were used and the concentrations of TBACN were 0, 10^{-6} , 10^{-5} and 10^{-4} M, respectively.106	
Figure 5.13 Cyclic voltammograms of EFP _E film in the electrolyte of 0.1 M LiClO ₄ in ACN/H ₂ O with ACN/H ₂ O volume ratio of 1:3 at a scan rate 25mV/s.108	

Scheme 2.1 Repeating units of some common CPs. From right to left: N-alkylcarbazoles, azulene, thiophene and 3,4-ethylenedioxythiophene (EDOT).20	
Scheme 2.2 Four forms of PANI from the fully reduced (leucoemeraldine) to the fully oxidized (pernigraniline) forms. X ⁻ represents the doping anion.23	
Scheme 2.3 An illustration of neutral state, radical cation and dication state of poly(carbazole-co-phenylene).....25	
Scheme 2.4 Some examples of electrochromic D-A CPs: a ¹⁵⁹ , b ^{5, 25} , c ^{148, 171} and d ¹⁶⁴30	
Scheme 2.5 An example of the catalytic cycle for Suzuki coupling reaction of organic halides and organoboranes (using NaOR as the base, e.g., Na ₂ CO ₃).32	
Scheme 2.6 A schematic illustration of the fluorescence process from a conjugated molecule.33	
Scheme 2.7 Switchable dyad systems through (a) electron transfer or (b) energy transfer. Reproduced from ref. [13] with permission from The Royal Society of Chemistry.....36	
Scheme 2.8 Electrochemical switching of the fluorescence. Reproduced from ref. [13] with permission from The Royal Society of Chemistry.....37	
Scheme 3.1 Synthesis route of the terpolymers, P ₁ , P ₃ , P ₅ and P ₂₀ (with P ₀ as reference).49	
Scheme 3.2 Possible redox processes of (a) A-BTD-A and (b) A-C-A.....56	

Scheme 3.3 A proposed redox mechanism for P ₀	58
Scheme 4.1 Structures of compound 1 to 5 and the synthesis route of copolymer EFP _C	72
Scheme 5.1 Synthesis route leading to the copolymer, EFP _E	88
Scheme 6.1 The structure of a proposed carbazole–BTD-based EFC copolymer (containing sulfonate group) which is possibly partially hydrophilic.	114
Table 2.1 Comparison between inorganic EC materials and conjugated EC polymers.....	21
Table 2.2 Coloration of polythiophene and its derivatives ^{2, 143, 144}	26
Table 3.1 Theoretical molar ratios of carbazole to BTD units calculated from feed compositions (x:y) and the corresponding ratios estimated from integrations of ¹ H NMR spectra (x':y') for P ₀ and the terpolymers.....	51
Table 3.2 Molecular weights and polydispersities of P ₀ and the terpolymers.....	52

Abstract

Two electrochemical reaction-induced chromic phenomena, electrochromism and electrofluorochromism, exhibited by some conjugated polymers (CPs) have been attracting much attention from researchers in recent years. Electrochromism is defined as the reversible change in absorption or transmission of a material due to redox processes induced by an external voltage. Electrofluorochromism is known as reversible change in fluorescence emission induced by applying an electric potential. The electrochromic (EC) and electrofluorochromic (EFC) properties are both related to the redox process of CPs induced by external potential, albeit they are two different types of chromic properties in terms of their work mechanism. The motivation of this work is to explore the structure design of CPs to tune their electrochromic and electrofluorochromic properties, and investigate the underlying mechanism.

Firstly, a series of carbazole–2,1,3-benzothiadiazole (BTD)–azulene-based donor–acceptor (D–A) conjugated terpolymers were designed and synthesized. These terpolymers exhibit high EC contrast in high energy band region of the visible spectrum. BTD (A) facilitates electron removal from carbazole and azulene units (D) upon oxidation, leading to a reduction in oxidation potentials of the terpolymers and hence enhanced EC contrasts at relatively low potentials. This enables the terpolymers being used as anodically coloring materials to complement cathodically coloring poly(3,4-ethylenedioxythiophene) doped with

poly(styrenesulfonate) (PEDOT:PSS), which covers low energy band region of the visible spectrum at colored state, in EC devices (ECDs). A black-to-transmissive complementary ECD was successfully demonstrated using such a terpolymer and PEDOT:PSS as the two EC layers .

Secondly, a novel carbazole (C)–BTD–3-hexylthiophene (HT)-based conjugated copolymer **EFP_C** was designed and synthesized, which has alternating structure, -C–BTD–C–HT–C–HT-, and exhibits both EC and EFC properties. A cyanide anion (CN[−]) detection system was designed using **EFP_C** spin-coated on indium tin oxide coated poly(ethylene terephthalate) (**EFP_C** /ITO/PET) as the detection electrode in EFC tests. It is observed that the oxidative quenching-induced reduction in fluorescence intensity is significantly weakened in the presence of CN[−] (as low as 1 μM) and higher CN[−] concentration leads to stronger weakening effect. In addition to high sensitivity, this detection approach also exhibits selectivity towards CN[−] over many other anions, including highly nucleophilic OH[−] and F[−]. The recovered fluorescence intensity induced by CN[−] may be attributed to the partial reduction of **EFP_C** at the oxidized state, which is probably caused by the interaction between the nucleophilic CN[−] and electron-deficient BTD at oxidized state. This interaction is noncovalent and reversible, possibly a type of anion– π interaction. The triple bond of CN[−] may provide electron-rich π system for non-covalent interaction with electron-deficient π system of BTD, leading to charge transfer between CN[−] and BTD ($\pi^- - \pi^+$ interaction) and hence weakening the oxidative quenching.

Thirdly, another carbazole–BTD–HT-based conjugated copolymer **EFP_E** was designed and synthesized via electrochemical polymerization. It has alternating structure, -HT-C-BTD-C-HT-, and also exhibits both EC and EFC properties. The electropolymerization brings **EFP_E** film with nanoporous morphology, and the redox reactions in LiClO₄/acetonitrile (ACN)-based electrolyte are nearly non-diffusion-controlled. Sensitive and selective EFC detection of CN[−] with **EFP_E** is also demonstrated. The EFC detection results were further verified by the change of peak oxidation potentials presenting in cyclic voltammograms with electrolytes of different CN[−] concentrations, showing high reliability of the method. Furthermore, **EFP_E** could be used for detection of CN[−] in partially aqueous media. On one hand, the nanoporous structure of **EFP_E** creates short diffusion distance for H₂O as well as dissolved CN[−] into the film. On the other hand, the formation of radical cations and dications on the conjugated chains at oxidized state may bring some hydrophilicity to **EFP_E**, facilitating the swelling of nanoporous **EFP_E** film to some extent with the help of ACN.

1. Introduction

1.1 Background

Conjugated polymers (CPs) are organic semiconductors that possess the optical and electrical properties of semiconductors in combination with the light-weight, mechanical and processing advantages of organic polymers. This unique combination of properties makes CPs very attractive for modern optoelectronic devices, of which two important categories are electrochromic (EC) and electrofluorochromic (EFC) devices.

EC properties of a material refers to the capability to change its optical absorption/transmission under an applied voltage within the whole or a region of electromagnetic spectrum, such as in ultraviolet–visible (UV–vis), near-infrared (NIR) or mid-infrared region.¹ Nowadays, EC materials have already been used in various industrial products, such as smart windows, anti-glare car rear-view mirror and displays. In comparison with other types of smart windows or displays, a significant advantage of EC devices (ECDs) is that they can be switched at very low potentials and have bistable states with long optical memory (in principle, power is only needed to switch from one state to another), leading to significant energy saving. For example, ECDs have great potential for energy-saving digital displays. The demands for such simple displays promote the studies of “black” EC materials, which could appear black at one redox state and transmissive at

another redox state. The “black” results from the even absorption over the entire visible wavelength range (400–700 nm).

There are many different types of EC materials. The most common ones include Prussian blue, transition metal oxides (TMOs), viologens and CPs. Among these EC materials, CPs have been extensively studied owing to their high contrast, fast switching speed, high coloration efficiency, ease of processability and advantage in color-tuning.^{2,3} Almost all colors have been achieved by tuning molecular structures of CPs. Electrochromic transition metal oxides such as oxides of iridium, molybdenum and nickel, have been studied for black ECDs. However, such metal oxides often exhibit long switching time, low coloration efficiencies and contrast.⁴ In 2008, Reynolds’ group published the first report on a donor–acceptor (D–A) conjugated polymer that exhibits black-to-transmissive electrochromism.⁵ Since then, D–A type of CPs prevail in black ECD applications owing to the facile color tuning as well as fast switching, high contrast and color efficiency.

Besides single-active-layer (single-layer for short) black ECDs fabricated using D–A CPs, complementary ECDs is an alternative approach to black ECDs. In a complementary ECD, two EC layers (one anodically coloring and the other cathodically coloring) on anodic and cathodic electrode, respectively, could be simultaneously switched between colored and transmissive state. Such a dual-active-layer (dual-layer for short) ECD may achieve the broadly absorbing “black” state if the absorption bands of the two EC materials are complementary to each other in covering the entire visible region under a certain potential. In addition to

extending the absorption wavelength range, complementary ECDs may exhibit better long-term switching stability⁶ than single-layer ECDs, as the oxidation of the anodic EC layer would create an internal driving force for the diffusion of dopants towards cathodic EC layer and vice versa, thus reducing the potential required for the redox processes and prolonging cycling life. However, finding a suitable pair of EC materials that fulfill the requirements for both absorption wavelength range and redox potentials for building a complementary black ECD is still a challenge.

Different from electrochromism that is associated with transmission or absorption spectra, electrofluorochromism is a chromic phenomenon associated with fluorescence spectra, i.e., the fluorescence emission from a material undergoes reversible change upon an applied potential. Different from the EC materials that have been intensively studied in the past few decades (since 1969)⁷, electrofluorochromism was rarely studied for very long. Only till 2004, Levillain *et al.* published the first report on the fluorescence quenching and recovery of an intrinsically electroactive fluorophore induced by external potential.⁸ Later on, Audebert's group reported the first example of electrofluorochromic (EFC) device⁹ and this group has published some pioneering works on EFC materials.¹⁰⁻¹³ Commonly studied EFC materials include intrinsically switchable fluorophores, molecular dyads and switchable fluorescent CPs.¹³ Compared with the other two types of EFC materials, the EFC CPs exhibit efficient electronic delocalization and rapid transport of excitons along the π -conjugated chains, offering them the capability of amplifying the sensitivity in response to fluorescence change.¹⁴⁻¹⁷

Some of the EFC CPs can be easily solution-processed or electropolymerized into thin films, and therefore they are good candidates for fabrication of EFC devices. EFC materials have great potentials for various applications, such as chemosensor, bio-analysis, fluorescence imaging and signaling recognition. For example, the detection of a protein (electrochemical) redox state based on the tryptophan fluorescence emission was reported,¹⁸ which provides dual detection of electrochemical and fluorescence signals and could improve the bio-sensing accuracy. However, so far the functionality of EFC CPs has hardly been explored.

1.2 Motivation, Hypotheses and Objectives

The motivation of this work is to explore the structural design of CPs to tune their electrochromic and electrofluorochromic properties for the functions mentioned below, and investigate the underlying mechanism.

Firstly, in a complementary ECD, typically the anodically coloring EC layer covers the high energy-band (short wavelength) region while the cathodically coloring EC layer covers the low energy-band (long wavelength) region. Commercially available PEDOT:PSS is a good candidate for cathodically coloring EC layer because of its good processability, high electrical conductivity and relatively narrow band gap. However, up to now, PEDOT:PSS-based black-to-transmissive complementary ECDs have not been reported due to the lack of suitable complementary EC material. Poly(3,6-carbazole) has been demonstrated to be electrochromic,¹⁹⁻²¹ exhibiting an absorption peak that can potentially complement that of PEDOT:PSS to cover the whole visible region. It however,

has higher oxidation potentials,²² which do not match well with the potential window of PEDOT:PSS. It was hypothesized that the potentials required for the coloration and bleaching of the polycarbazole may be reduced by copolymerizing 3,6-carbazole (electron donor) with 2,1,3-benzothiadiazole (BTD), a commonly used electron acceptor.^{5, 23-25} Thus the first objective of the PhD study was to synthesize and characterize a series of carbazole–BTD-based conjugated copolymers, study the EC properties of the copolymers and explore the possibility to achieve black ECDs using the copolymers as anodic layer and PEDOT:PSS as complementary layer.

Secondly, although EFC CPs have drawn some attention in past few years, the possibilities of utilizing their EFC functions for applications like sensing have not been explored. Nowadays, cyanide detection has attracted much attention because of public health and environment concerns caused by toxicity of cyanide. Various methods that utilize colorimetric and fluorometric techniques have been developed for the detection of cyanide anion (CN^-). Free cyanide anion form complexes with transition metals,²⁶ CdSe quantum dots,²⁷ boronic acid derivatives,²⁸ or gold nanoclusters,²⁹ providing a common approach to chemosensors. Nucleophilic attack of CN^- that possesses strong nucleophilicity to electron-deficient compounds, such as benzothiadiazole,³⁰ pyrylium salt,³¹ oxazine,³² triazene,³³ trifluoroacetophenone,³⁴ dipyrrole carboxamide,³⁵ acridinium,³⁶ salicylaldehyde³⁷ and squaraine,³⁸ offers an alternative approach. Enlightened by the aforementioned cyanide detection methods that utilize the strong nucleophilicity of cyanide, we hypothesized that carbazole–BTD-based

conjugated copolymers may also be used as EFC polymers for detection of CN^- as the electron-deficient BTB unit may interact with CN^- strongly, especially upon oxidation. The use of an EFC conjugated copolymer for cyanide detection allows adjusting electronic structure of the chromophore, and hence may lead to more sensitive detection than that offered by traditional chemosensors. Thus, the second objective of this PhD study was to design and synthesize novel carbazole–BTB-based conjugated copolymers that exhibit EFC properties, explore the possibility of employing these conjugated copolymers for cyanide detection and understand the underlying mechanism.

1.3 Organization of this thesis

After this brief introduction chapter, a literature review on ECDs and applications, ECD performance parameters, EC materials, EFC materials, characterization of electrochemical, EC and EFC properties, will be given in Chapter 2. Synthesis, characterization and EC properties of carbazole–BTB-based donor–acceptor conjugated copolymers, as well as black ECD, are discussed in Chapter 3. Synthesis, characterization and EFC properties of a carbazole–BTB-based conjugated copolymer, as well as its application in cyanide detection, are present in Chapter 4. Chapter 5 shows electropolymerization and characterization of another EFC carbazole–BTB-based conjugated copolymer as well as its application in cyanide detection. The conclusions and recommendations are given in Chapter 6.

2. Literature Review

2.1 Introduction

Electrochromism is commonly defined as a reversible change in absorbance/transmittance or reflectance, resulting from reduction or oxidation induced by an external voltage.^{1, 2, 39, 40} In 1961, Platt suggested the name “electrochromism” to define the electrochromic (EC) effect.⁴¹ Deb *et al.* demonstrated the first example of electrochromic device (ECD) using tungsten trioxide (WO_3) in 1969.⁷ The color change of the EC material is usually between the colored state and the bleached state. Some EC materials possess two or more colored states; such electrochromism is termed as multi-electrochromism.

Nowadays, electrochromic systems are widely used and some examples are given as follows. Smart windows can be switched between opaque and transparent or different colors with potential change, and anti-glare electrochromic car rear-view mirror can adjust the brightness so that strong light from cars at the back will not dazzle the driver’s eyes. Besides, electrochromism has also been industrially applied in displays, printing, and e-paper, etc. Figure 2.1 shows two examples of EC applications: an electrochromic car rear-view mirror and e-paper.



Figure 2.1 (a) Anti-glare EC car rear-view mirror dimming after strong light from back has been sensed (right) and non-EC rear-view mirror for comparison (left), and (b) Plastic Logic's e-paper, adapted with permission from Plastic Logic, <http://www.plasticlogic.com/>. Copyright 2009 Plastic Logic.

Electrofluorochromism, known as the reversible change in fluorescence emission induced by an external electric potential, is similar to electrochromism that corresponds to reversible change in transmission or reflectance upon a potential bias. Electrofluorochromic (EFC) materials, which exhibit electrochemically switchable fluorescence, have attracted much attention over the past few years.^{8-13, 42-52} They are promising candidates for various applications such as displays, sensors and fluorescence imaging. Figure 2.2 shows an example of an EFC device fabricated using an EFC conjugated polymer.⁴⁷ The detailed introduction of ECDs and EC materials will be given in the next two sections, followed by the EFC materials and devices.

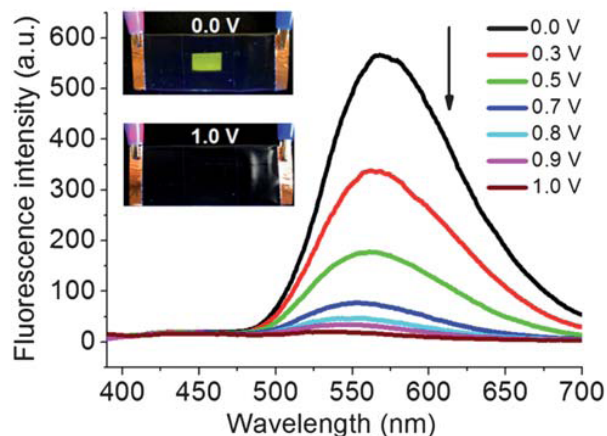


Figure 2.2 Fluorescence quenching of an EFC device at different potentials. Reproduced from ref. [47] with permission from The Royal Society of Chemistry.

2.2 Electrochromic devices

An electrochromic device (ECD) is an electrochemical device with a sandwich structure: the electrochromic electrode (working electrode) and the charge balancing counter electrode are separated by solid (or semi-solid) or liquid (or semi-liquid) electrolyte. The color changes occur in the redox process of the electrochrome, which is induced by positive or negative potentials applied to the electrochemical cell.

2.2.1 Configuration of ECDs

2.2.1.1 Components

Electrochromic layer

Electrochromic layer is the key component that directly determines the performance of the ECD. It is usually formed by the electrochromic material using techniques such as electrodeposition, spin-coating, spraying and dip-coating. The detailed introduction of EC materials will be given in section 2.3.

Transparent electrodes

A true potentiostatic measurement of ECDs requires three electrodes, so an approximation to potentiostatic control with two electrodes is commonly used. The work electrode of ECDs refers to the EC material layer coated on a transparent and conductive substrate, such as ITO glass and ITO/PET). For single-layer ECDs, the counter electrode plays the role of charge balancing. For dual-layer ECDs, the counter electrode is also coated with an EC layer which complements the EC layer on work electrode, leading to different absorption spectra.

Electrolytes

The electrolyte between the electrodes is normally of high ionic conductivity, and it should be electronically an insulator at the same time. Semi-solid organic electrolytes including polymer electrolytes and polyelectrolytes are commonly used. Polymer electrolytes contain neutral macromolecules such as poly(ethylene oxide) (PEO), poly(methyl methacrylate) (PMMA), and poly(ethylene glycol) (PEG). Inert salt such as lithium perchlorate (LiClO_4) is added into such macromolecules, forming the inorganic electrolyte layer. Polyelectrolytes, sometimes called polysalts, are polymers in which each repeating unit bearing an

electrolyte group along the backbone and show similar properties to both electrolytes and polymers. A typical example is poly(2-acrylamido-2-methylpropanesulfonic acid) (poly(AMPS)). Different from semi-solid organic electrolytes, ionic liquids are another type of electrolytes, which usually consist of nitrogen containing organic cations and inorganic anions. As ionic liquids are nonvolatile, nonflammable, highly thermally stable and relatively inexpensive, they are now widely used in ECDs. Two ionic liquids, 1-butyl-3-methylimidazolium cation (BMIM^+) with the tetrafluoroborate (BF_4^-) or hexafluorophosphate (PF_6^-) anion, were reported as electrolytes for ECDs by Lu *et al.*⁵³

2.2.1.2 Transmissive ECDs

Based on the optical transmission, ECDs could be divided into two types: transmissive ECDs and reflective ECDs. The following section will focus on transmissive ECDs. A transmissive ECD switches reversibly between colored state and a transmissive state under external potentials. According to the configuration, transmissive ECDs could be categorized into single-active-layer (single-layer) and dual-active-layer (dual-layer) ECDs. Single-layer ECDs are most commonly used, consisting of only one EC layer, as illustrated in Figure 2.3a. To enhance the coloration performances, dual-layer ECDs, i.e., complementary ECDs, which consist of two EC layers on work electrode and counter electrode, respectively, have been developed, as illustrated in Figure 2.3b. The two EC layers could simultaneously switch between colored to bleached states through opposite redox behavior. Common examples of complementary

ECDs are composed of PANI as primary electrochromic layer and PEDOT as the complementary layer.⁵⁴⁻⁵⁶ In regard to redox stability, the switching of such ECDs can perform well only when the counter electrode is stable within the potential window of both the working electrode and electrolyte. Thus, the pair of complementary EC materials for a complementary ECD must match each other, in not only meeting the color requirements but also balancing the redox processes at both electrodes to enhance its cycle life. In most cases, one EC layer is anodically coloring material while the second is cathodically coloring (on counter electrode). Hence, such an ECD could exhibit simultaneously colored to transmissive switches and vice versa. For some complementary ECDs, only one layer is electrochromic, while the layer of material coated on the other electrode is non-electrochromic yet electroactive, playing the role of charge storage layer that helps to eliminate the contrast limitations for common complementary ECDs and improve the stability.⁵⁷

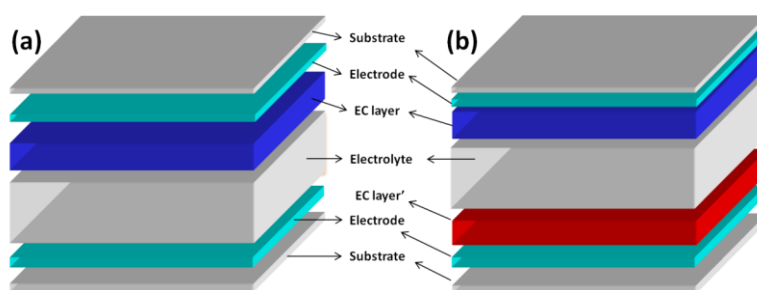


Figure 2.3 Schematic illustrations of (a) a single-layer ECD and (b) a dual-layer (complementary) ECD (side view, not to scale).

2.2.2 Types of ECDs

2.2.2.1 Visible and Vis–NIR ECDs

Most ECDs focus on optical change in visible region, in which the coloration and bleaching could be observed by naked eyes. However, some ECDs have extended the wavelength range of absorption to near infrared (IR) and IR region. An application of this type of ECD is electrochromic smart windows, which could absorb or transmit visible light and infrared heat energy to reduce the energy needed to cool and heat a building while providing good quality day light through adjusting the redox state of the EC layer inside the windows. Figure 2.4 shows an example of smart windows.

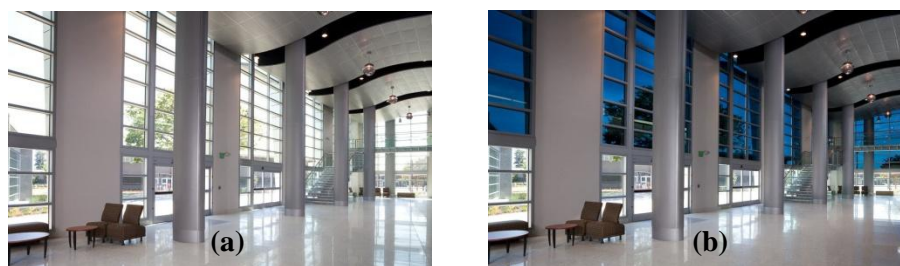


Figure 2.4 The smart windows at (a) ‘Off’ state (colorless) and (b) ‘On’ state (blue).

2.2.2.2 Black ECDs

In the past few years, great interest has been paid to “black ECDs”^{5, 25, 57-62} that appear black color with very low transmittance at one redox state and transmissive at another state. The “black” results from the entire visible region

coverage of the absorption spectrum (400–700 nm). Black ECDs include single-layer black ECDs and dual-layer (complementary) black ECDs. A single-layer black ECD utilizes only one EC material that could switch between black and transmissive states. An example is a D–A conjugated EC copolymer that appears black at neutral state and transmissive upon oxidation, reported by Reynolds *et al.*⁵ However, the molecular design of such conjugated EC polymers is often a challenge. As mentioned previously, D–A approach provides a versatile method for spectral engineering, and such polymers could be obtained via tuning the two absorption bands towards full coverage of visible region by functionalization and changing feed ratio of monomers. For a complementary black ECD, the two EC layers switch simultaneously to achieve an absorption spectrum that extends to the entire visible region from their respective absorption bands. However, this type of ECD was seldom investigated. Kim *et al.* reported a multi-layer complementary black ECD,⁶⁰ as shown in Figure 2.5. PANBS/PDHFA and PEDOT/P3HT EC layer pair are deposited onto the two electrodes (Figure 2.5a), respectively, via either spin-coating or electrochemical polymerization. Figure 2.5b shows the transition from transmissive state to CIE black (Figure 2.5c), which is attributed to the color combination of multiple EC conjugated polymer layers.

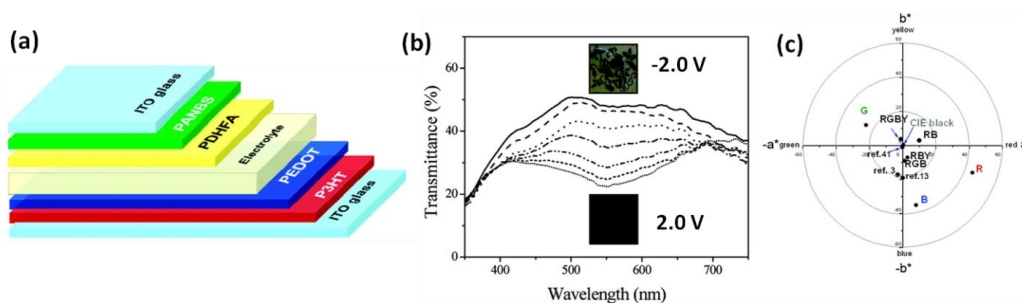


Figure 2.5 (a) Schematic diagram of the complementary ECD (from top to bottom): ITO glass, PANBS, PDHFA, electrolyte, PEDOT VPP, P3HT, and ITO glass. (b) Transmittance spectra (inset: the photographs of colored state and bleached state), and (c) CIE (Commission Internationale de l'Eclairage) diagram of the ECD (RGBY). Reprinted with permission from ref. [60]. Copyright (2012) American Chemical Society.

2.2.3 Key performance parameters

The key parameters for characterizing the performance of ECDs are listed below.

Contrast: An essential parameter to evaluate an EC material. The EC contrast is a quantitative parameter indicating the color intensity change of an ECD. It is often represented using a percent transmittance change ($\Delta\%T$), which is obtained at a specified wavelength where the EC material exhibits the highest change in transmittance. Sometimes, the contrast over a specified wavelength range is also used.

Switching time: Often reported as the response time for an EC material to switch between colored and bleached states. It is a very important characteristic of ECDs, especially for applications that require fast switching speed, such as dynamic displays. The switching time of electrochromic materials depends on factors such as the thickness, morphology and ionic conductivity of the thin EC film, ionic conductivity of the electrolyte, and the magnitude of the loading potential.

Coloration efficiency (η): Used for measuring the power requirements of the EC layer and compare the efficiency of different EC materials. η (cm^2/C) refers to the optical density change (ΔOD) at a certain wavelength (λ) as a function of the amount of injected/ejected charge per unit area (Q), given by Eq. 2.1.

$$\eta = (\Delta\text{OD})/Q = [\log(T_b/T_c)]/Q \quad (\text{Eq. 2.1})$$

T_b and T_c are the transmittance values at bleached state and colored state, respectively. Organic materials generally exhibit higher coloration efficiencies compared with inorganic due to their higher molar absorptions.

Colorimetric coordinates: Precisely defining the color states of an ECD and usually obtained from measuring with a spectrophotometer.³ CIE (Commission Internationale de l'Eclairage) 1931 (Yxy) and CIELab ($L^*a^*b^*$) are two common standards to describe a color state, and Figure 2.6 shows the chromaticity diagrams of the two color spaces. In comparison with CIE 1931 (Y is the luminance and xy are the coordinates defining the hue and saturation), CIELab color space provides more intuitive color coordinates, L^*,a^*,b^* , where L^*

represents the lightness ($L^* = 0$ indicates black, 100 indicates white), a^* ('-': green, '+': red) and b^* ('-': blue, '+': yellow) are the set of two-dimensional coordinates defining a color's hue and saturation. In addition, the coordinates of the two systems could be interconverted.

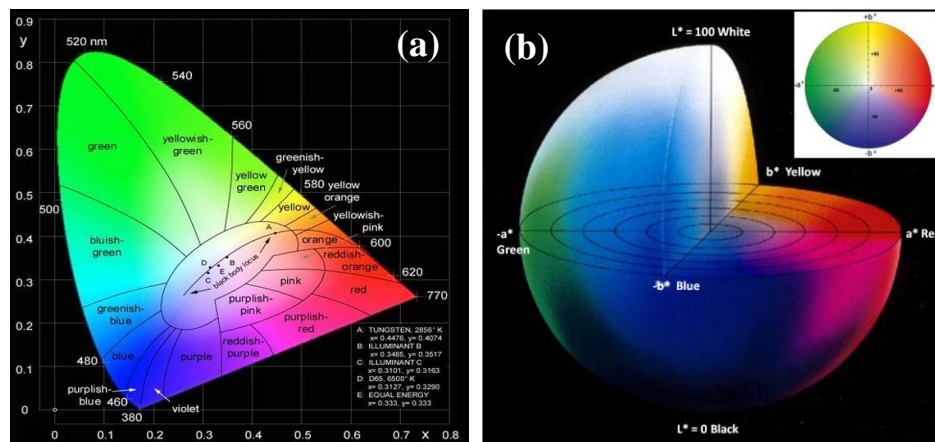


Figure 2.6 Diagrams of (a) CIE 1931 color space and (b) CIE Lab color space (inset: a^*b^* two dimensional coordinate plane).

Stability: Usually associated with electrochemical stability. The degradation of the redox couple of the EC material will lead to reduction in EC contrast and depress its EC performance. In addition, the magnitude of applied potentials and environmental conditions are also responsible the stability of ECDs. However, the inherent stability of the EC material is the most important factor affecting the stability of the device.

Optical memory: Defined as the time for an EC material to retain its colored state with external potential removed. The solution-based ECDs (such as

viologens-based) usually quickly switch to bleached state after current removal as the soluble electrochromes would immediately diffuse away from the working electrode. In solid-state ECDs, the electrochromes are coated on electrodes as solid film, resulting in a much longer optical memory (days or weeks)

2.3 Electrochromic materials

2.3.1 Overview

Electrochromic materials, which are the active components in an ECD, can be categorized into two main groups: inorganic EC materials and organic EC materials. Transition metal oxides (TMOs) are most studied inorganic EC materials, such as oxides of iridium, tungsten, cobalt, manganese, nickel, rhodium, ruthenium, titanium and molybdenum.⁶³⁻⁷⁴ Besides TMOs, other inorganic electrochromic materials such as Prussian blue⁷⁵⁻⁷⁷ have also been studied. Organic EC materials include viologens^{78, 79} which are organic small molecules, and conducting polymers. In the recent years, conducting electrochromic polymers such as polyaniline (PANI)⁸⁰⁻⁸⁴ and PEDOT⁸⁵⁻⁸⁸ have been studied extensively. Based on the conjugation of main chain, conducting polymers could be divided into π -conjugated conducting polymers and non-conjugated conducting polymers. Suzuki coupling as well as Stille coupling reaction is often used for the synthesis of π -conjugated polymers.

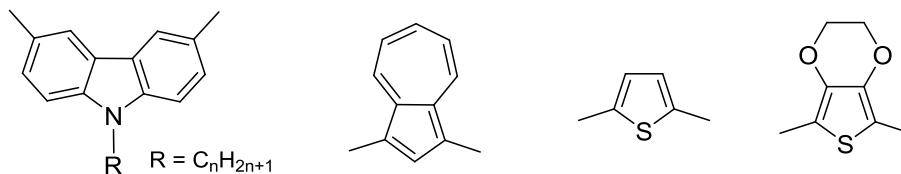
Thin films of TMOs can be switched to a non-stoichiometric state electrochemically, which exhibits an EC absorption band as a result of intervalence charge transfer.^{89, 90} Among the TMOs, tungsten trioxide (WO_3), has

received extensive attention in the past 30 years and become one of the most widely industrially used EC materials nowadays.⁹¹⁻⁹⁴ The tungsten oxides consist of WO_6 octahedra arranged in various corner-sharing or edge-sharing configurations, which create empty space inside the cubes, providing a large number of interstitial sites where the guest ions can be inserted.^{90, 95} Thin film of WO_3 is transparent (appearing pale-yellow color), with all tungsten sites at oxidized state (W^{VI}). Upon electrochemical reduction, some sites of W^{VI} are reduced to W^{V} , which change the color of the film from transparent to blue. The injection and extraction of electrons and metal cations (e.g., Li^+ , Na^+ , H^+ , etc) is generally believed to play the key role in the EC process. As a cathodic ion insertion material, WO_3 's blue coloration can be reversed by electrochemical oxidation. A generalized equation is given as Eq. 2.2, where 'x' indicates the fractional number of sites which are filled in the WO_3 lattice.



Polymerization (chemical or electrochemical) of the organic aromatic molecules, such as aniline, carbazole, azulene, thiophene, pyrrole, furan and indole, produces π -conjugated polymers ("conjugated polymers" for short, CPs for abbreviation). Polyaniline (PANI), polythiophene (PTh), poly(3,4-ethelinedioxythiophene) (PEDOT), polycarbazole (PCz), and their derivatives are among the most widely studied EC CPs. Scheme 2.1 shows repeating units of some common CPs. The electrochromism of such polymers is closely related to the doping processes. For CPs, electrochromism results from redox processes which are accompanied by ion insertion/extraction (doping/dedoping), leading to

color change of the polymers. Most CPs undergo anodic doping with anion insertion (p-doping), while only a few experience n-doping, i.e., cathodic doping with cation insertion. Thus, the following introductions will take p-doping as an example to illustrate the doping process.



Scheme 2.1 Repeating units of some common CPs. From right to left: N-alkylcarbazoles, azulene, thiophene and 3,4-ethylenedioxythiophene (EDOT).

The CPs are “p-doped” with anions upon oxidation and form a delocalized π -electron band structure with lower-energy intraband transitions. Reduction of the “p-doped” CP with concurrent anion extraction removes the π -conjugation and then returns to the “undoped” state (original band structure).^{1, 96} The band gap (E_g) between the valance band and conduction band determines CPs’ intrinsic optical properties. The p-doping (oxidation) forms charge carriers such as polarons and bipolarons, introducing new states into the band gap, which is the work mechanism of EC properties exhibited by CPs.

In the recent years, CPs have attracted much attention in ECD studies, due to their fast response speed, high optical contrast, and ease of processability, in comparison with inorganic EC materials.^{3, 97-100} Besides, color tailorability is another advantage for CPs, which is achieved by monomer functionalization,

copolymerization and polymer blends, laminates, and composites.¹⁰¹⁻¹⁰⁴ Table 2.1 gives the comparison between inorganic EC materials and conjugated EC polymers.² Besides π -CPs, some non-conjugated conducting polymers, such as polyamides and polyimides,¹⁰⁵⁻¹¹⁷ have also been explored in electrochromic area during the recent years. These amide or imide-based non-CPs exhibit high flexibility (thin film form) and multi-electrochromism, and two examples are given in Figure 2.7.

Table 2.1 Comparison between inorganic EC materials and conjugated EC polymers.

	Inorganic materials	Conjugated polymers
Preparation	Sophisticated techniques such as vacuum evaporation, spray pyrolysis, sputtering, etc.	Synthesized via chemical polymerization (film obtained by spin-coating), or electrochemical polymerization (film could be directly used)
Processability	Poor	Good
Cost	High	Low
Color	Limited number of colors	Large number of colors
Contrast	Moderate	High
Switching speed	Low	Fast
Life time	10^3 – 10^5 cycles	10^4 – 10^6 cycles

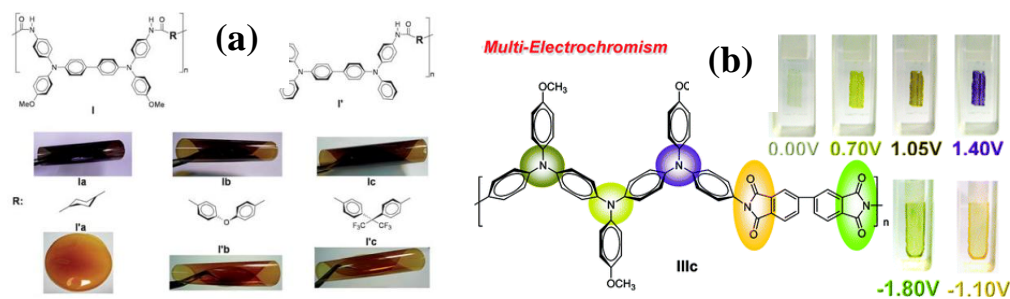


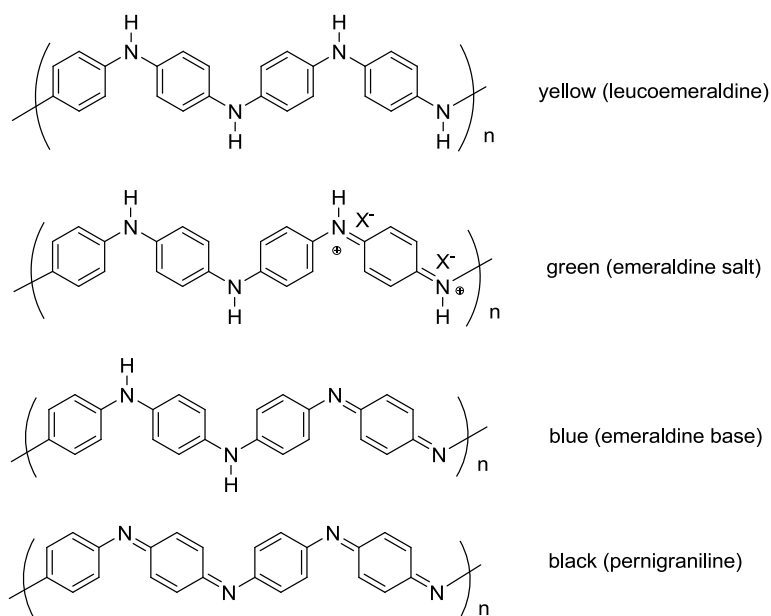
Figure 2.7 (a) Flexible films of electrochromic aromatic polyamides. Reproduced from ref. [115] with permission from The Royal Society of Chemistry. (b) Electrochromism exhibited by triphenylamine-substituted derivative polyimides. Adapted with permission from ref. [117]. Copyright (2011) American Chemical Society.

2.3.2 Anodically coloring conjugated polymers

2.3.2.1 Polyaniline

Polyaniline (PANI) is a most widely studied anodically coloring EC polymer.⁸⁰⁻⁸⁴ As a polyelectrochromic material, PANI can exhibit four different colors (yellow–green–blue–black) during its redox processes. The color transition between yellow and green is repetitive even though the leucoemeraldine form (yellow) is not conjugated. Four types of PANI are shown in Scheme 2.2. Leucoemeraldine (the fully reduced PANI) is an insulator because all rings are in benzenoid form and separated by -NH- or -NH_2^+ groups, which break the conjugation. Emeraldine is either salt (ES) or base (EB) form, with a ratio of one quinoidal ring to three benzenoid rings and electrically conductive. Pernigraniline

(the fully oxidized PANI) has equal proportions of quinoid and benzenoid moieties and exhibits metallic conductivity. Pernigraniline appears intense blue and turns to black at very high positive potentials.



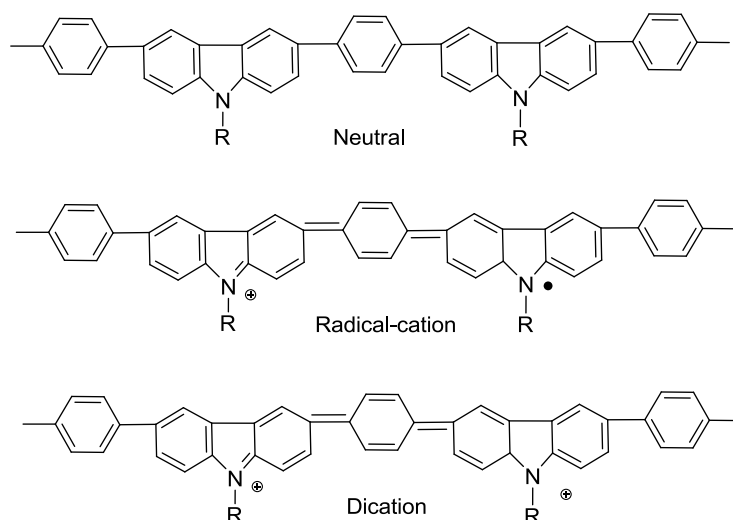
Scheme 2.2 Four forms of PANI from the fully reduced (leucoemeraldine) to the fully oxidized (pernigraniline) forms. X^- represents the doping anion.

2.3.2.2 Carbazole-based conjugated polymers

In the past two decades, carbazole-based conjugated polymers have attracted increasing interests in electrochromic¹¹⁸⁻¹²⁰ and electroluminescence¹²¹⁻¹²⁷ areas due to their good hole-transporting ability and optical properties. Additionally, the nitrogen atom from carbazole is easily functionalized to improve polymer solubility as well as tune the electrical and optical properties.^{128, 129} Mengoli *et al.* first reported electrochromic phenomenon of polycarbazole that was synthesized

through electrochemical polymerization.¹⁹ Verghese *et al.* showed the detailed studies of electrochromic properties of polycarbazole films.^{20, 21} Faid *et al.* investigated electrochromism of poly(N-alkylcarbazoles) and found that these polymers appear colorless at neutral state, and green upon a positive potential over 0.7 V (vs SCE), and subsequently blue over 1.0 V.²²

Based on substituted positions, carbazole could be categorized into 3,6-linked carbazole (3,6-carbazole) and 2,7-linked carbazole (2,7-carbazole). Different from 2,7-carbazole, 3,6-carbazole could play a role of “conjugation break” for the main chain of polymers. Owing to the conjugation breaks, their optical properties or redox processes are not affected by the molecular weights. For 3,6-carbazole-based CPs, radicals would form in the main chain upon oxidation. 3,6-Carbazole units as the conjugation breaks separate the radicals from one another and preventing their combination, leading to a relatively stable radical cation state. Dications will form with further oxidation at higher potentials. Radical cation and dication states are typical redox characteristics of 3,6-carbazole based CPs.¹¹⁹ An example of such redox process is shown in Scheme 2.3.



Scheme 2.3 An illustration of neutral state, radical cation and dication state of poly(carbazole-*co*-phenylene)

2.3.2.3 Azulene-based conjugated polymers

Owing to the unusual electronic character and anomalous spectral behaviors, azulene and its derivatives have received much attention during the past decades. Kihara *et al.* reported the first poly(azulene).¹³⁰ Lai's group reported high molecular-weight poly (1,3-azulene),¹³¹ followed by a series of highly conductive azulene–thiophene CPs.^{132–134} Xu's group reported azulene–fluorene CPs with a remarkably reduced band gap (~ 1.60 eV) compared with that of poly(9,9-dihexylfluorene) (2.86 eV).¹³⁵ Wang *et al.* reported azulene–thiophene based CPs that exhibit electrochromism in near IR region (~ 1500 nm).¹³⁶

Azulene can be regarded as an aromatic 6π electron tropylium cation fused by a 6π electron cyclopentadienyl anion. Due to the electron-rich cyclopentadienyl

anion, azulene can easily undergo electrophilic substitution at C-1 or C-3 in the 5-membered ring and form a very stable aromatic 6π -electron azulenium cation (tropylium cation). Such tropylium cation formation would lead to interesting electrochemical^{137, 138} and EC behaviors¹³⁹⁻¹⁴¹. In addition to the unique properties such as the dipolar structure with dipole moment of around 1.0 D and unusual S_2 - S_0 fluorescence, azulene is more easily oxidized than most common aromatic molecules.¹⁴² Thus, the azulene units in azulene-containing CPs are expected experience a redox reaction towards forming azulenium radical cations and therefore lead to promising EC properties for these CPs.

2.3.2.4 Others

Polythiophene and its derivatives exhibit advantage in the ease of polymer synthesis (via chemical or electrochemical polymerization), processability and environmental stability. Electrochromic properties of those polymers are summarized in table 2.2. Polypyrrole is another anodically coloring EC polymer, which appears yellow-green color at neutral state and blue-violet upon oxidation.

Table 2.2 Coloration of polythiophene and its derivatives^{2, 143, 144}

Monomer	Polymer λ_{\max} and color	
	Oxidized state	Reduced state
Thiophene	730 (blue)	470 (red)
3-Methylthiophene	750 (deep blue)	530 (red)
3-Hexylthiophene	750 (pale blue)	520 (red)
2,2'-Bithiophene	680 (blue-grey)	520 (red-orange)

2.3.3 Cathodically coloring conjugated polymers

2.3.3.1 PEDOT

In the recent years, numerous poly (substituted thiophenes), especially 3,4-dialkoxy substituted, have been synthesized and studied. Different from polythiophenes, the poly (3,4-dialkoxy substituted thiophenes) belong to cathodically coloring EC materials. Among them PXDOTs (where X is an alkylene bridge, such as ethylene and propylene) are typical examples. PEDOT (where X = ethylene) has a lower band gap ($E_g = 1.6\text{-}1.7\text{ V}$) than polythiophene and its alkyl-substituted derivatives, attributed to the two electron-donating oxygen atoms adjacent to the thiophene unit. It appears sky blue at neutral state, and dark blue upon reduction. The spectroelectrochemical behavior of PEDOT is shown in Figure 2.8a. In comparison with other substituted polythiophenes, PEDOT exhibits excellent stability and high conductivity in the doped state.

As PEDOT is not easy for processing due to its insolubility, the water-soluble poly(styrene sulfonate) (PSS) is used as the counter ion to dope PEDOT, yielding the commercially available (Bayer AG) PEDOT:PSS (Figure 2.8b) which could form a dispersion in water and be easily processed (e.g., spin-coating). For PXDOT, changes in nature of the substituents on the alkyl bridge as well as the size of the alkylenedioxy ring may lead to higher EC contrasts, faster switching speed and better processability.^{99, 145-147} It is worth noting that PEDOT and its analogues as cathodically coloring EC materials are quite suitable for fabrication

of dual ECDs complemented with anodically coloring CPs. Further introduction of complementary ECDs will be given in later introductions.

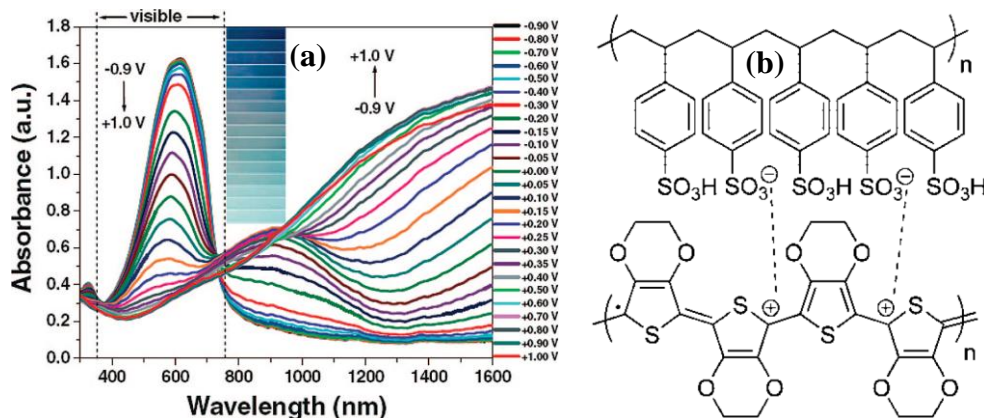


Figure 2.8 (a) Spectroelectrochemistry of PEDOT thin film. Adapted with permission from ref. [148]. Copyright (2004) WILEY-VCH Verlag GmbH & Co. KGaA, Weinheim. (b) Structure demonstration of PEDOT:PSS.

2.3.3.2 Others

Besides PxDOTs, some other poly (3,4-dialkoxy substituted thiophenes) and poly (3 (or 4)-alkoxy substituted thiophenes) have also been studied.¹⁴⁹⁻¹⁵⁴ For example, Leclerc *et al.* reported electrochemical polymers of 3-butoxy-4-methylthiophene and 3-octyloxy-4-methylthiophene, which both could switch from red-violet at neutral state to blue-black upon doping.¹⁵²

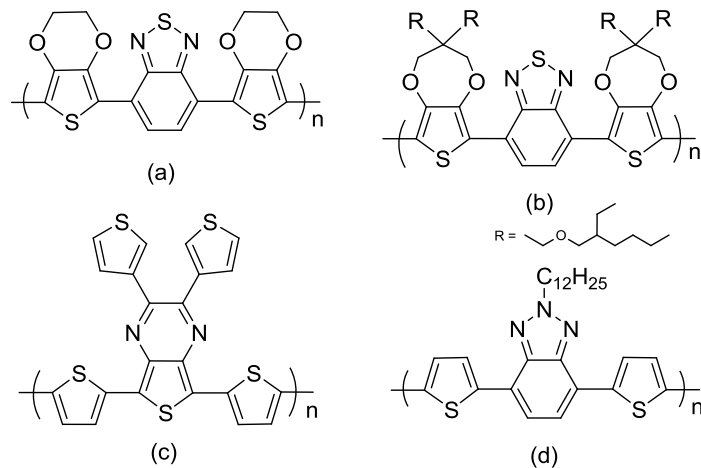
2.3.4 Donor–Acceptor conjugated polymers

Electrochromism of most CPs is dependent on oxidative doping, thus the stability of the doped state is very important to the ECDs. The oxidized

conjugated backbones are often unstable under high potentials, resulting in poor electrochemical stabilities and degradation of polymer chains, and therefore short life cycle of the corresponding ECDs. To address the above issue, recent research on CPs focuses on the engineering of the band gaps to improve their long-term stability in ECDs. Donor–acceptor (D–A) approach prevails these few years.^{5, 23-}

^{25, 97, 148, 155-172} Scheme 2.4 illustrates the chemical structures of some reported D–A CPs. A typical D–A CP consists of alternating electron-rich group (D) and electron-deficient one (A) on the backbone. In comparison with the homopolymers containing either D or A units alone, these D–A type of CPs may exhibit smaller band gaps and wider bandwidths. This is probably attributed to the regular alternation of donor and acceptor groups, which would broaden the valence and conduction bands and hence lead to a reduction in band gap. The lower potentials required for the redox process owing to D–A effect probably reduce the possibility of degradation during the redox switching. Some CP-based ECDs with good long-term stabilities using D–A approach has been demonstrated.

^{97, 165, 167, 171}

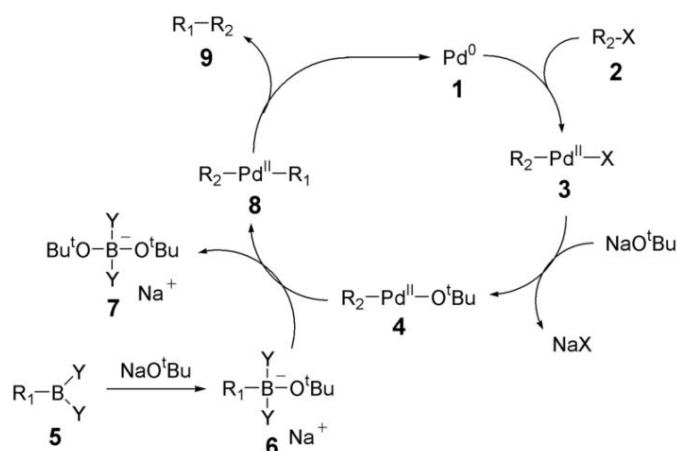


Scheme 2.4 Some examples of electrochromic D–A CPs: a¹⁵⁹, b^{5, 25}, c^{148, 171} and d¹⁶⁴

Spectral engineering of CPs also makes use of D–A approach.^{166, 173} A dual band of absorption in the visible spectrum is often shown by D–A CPs, including a short and a long-wavelength band.¹⁶³ A balance of short- and long-wavelength absorption bands, which can be achieved through modifying of structure or ratio of D and A moieties, may offer a high degree of color tailorability. Wudl *et al.* reported the first neutral green CP that was synthesized via D–A approach.¹⁷¹ D–A type of CPs that could switch between transmissive and saturated colors (such as green and blue) were also reported by Reynolds *et al.*^{23, 24, 165} Toppare *et al.* reported a processable D–A green polymer with a transmissive oxidized state.⁹⁷

2.3.5 Synthesis of conjugated polymers via Suzuki coupling

First reported by Akira Suzuki in 1979,^{174, 175} Suzuki coupling reaction is known as a palladium-catalyzed cross-coupling reaction between organoboron compounds and organic halides or triflates. As a very versatile method for formation of carbon–carbon bonds, Suzuki coupling is widely used in synthesizing poly-olefins, styrenes and substituted biphenyls in the past decades. It is also popularly used in the syntheses of conjugated polymers for EC applications in the recent years.^{119, 120, 135, 136, 172} Stille coupling, which is another versatile coupling method towards carbon–carbon bond generation with palladium as catalyst, is similar to Suzuki coupling but occurs between organotin compounds and organic halides or triflates. Compared with Stille coupling, Suzuki coupling involves less toxic organoboron reagents and is therefore more environmentally friendly. The catalytic cycle for Suzuki coupling reaction mainly includes three steps: oxidative addition, transmetalation and reductive elimination processes,¹⁷⁶ and a schematic illustration is shown in Scheme 2.5. Oxidative addition of palladium catalyst **1** to the halide **2** forms the organopalladium species **3**, which reacts with the base (NaOR) giving the intermediate **4**. Then **4** reacts with the boronate complex **6** (transmetalation), forming the organopalladium species **8**. The following reductive elimination leads to the product **9** while restores the original palladium catalyst **1**.



Scheme 2.5 An example of the catalytic cycle for Suzuki coupling reaction of organic halides and organoboranes (using NaOR as the base, e.g., Na₂CO₃).

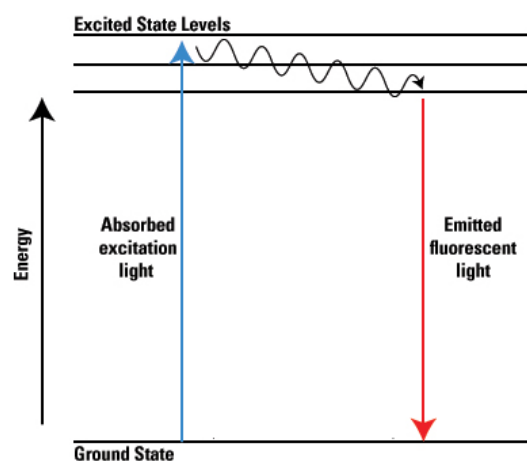
2.4 Electrofluorochromic materials and devices

2.4.1 Fluorescence from conjugated polymers

2.4.1.1 Principles

Upon photo-excitation, a conjugated molecule will be excited from a vibrational level in the electronic ground state to one of the many vibrational levels in the electronic excited state, as shown in Scheme 2.6. The molecule at a higher vibrational level in the excited state will quickly relax to the lowest vibrational level of the excited state, by transferring energy to other molecules through collision. A photon will be emitted when the molecule returns from the excited state to ground state, and such a fluorescence process is also called photoluminescence (PL). This process is also called radiative energy transfer.

There are many other ways for molecules to release absorbed energy non-emissively, so-called non-radiative energy transfer. An example of such a non-radiative energy transfer process is the electrochemical potential induced oxidative quenching of fluorescence, which is the work mechanism of electrofluorochromism.



Scheme 2.6 A schematic illustration of the fluorescence process from a conjugated molecule.

2.4.1.2 Fluorescent conjugated polymers for sensor application and cyanide detection

Fluorescent CPs have the capabilities of converting analyte–receptor interactions into observable (or transducible) responses. CP-based sensors show a significant advantage over small molecule-based ones due to the collective properties of CPs which offer such sensors high sensitivity towards very minor perturbations. Particularly, owing to the transport properties, electrical

conductivity or rate of energy migration, the fluorescent CPs exhibit the ability to produce signal gain in response to interactions with analytes for sensing and thus lead to amplified sensitivity.¹⁵ These fluorescent CPs polymers are often called amplifying fluorescent polymers (AFPs), and this gain is also named “superquenching”.¹⁷⁷ Four common types of CP-based sensors are conductometric, potentiometric, colorimetric and fluorometric sensors.¹⁵ Conductometric sensors provide changes in electrical conductivity in response to the interaction with analyte. Potentiometric sensors show the system’s chemical potential changes induced by analyte. Colorimetric sensors rely on the changes in absorption/transmission upon interaction with analyte. Fluorometric sensors make use of fluorescence change, offering inherent sensitivity, and diverse transduction signals based on the changes in fluorescence intensity, wavelength (excitation and emission), energy transfer and lifetime.

Cyanide exhibits extreme toxicity in physiological systems, and environmental concerns due to its continued and widely industrial use, and thus it has attracted intensive research interests in development of cyanide detection methods. A variety of methods have been used to detect cyanide, employing titrimetry, voltammetry, potentiometry, amperometry, etc. Optical sensors (colorimetric or fluorometric) for CN^- detection have been studied extensively in the past decade due to the ease of operation, low cost and fast detection.¹⁷⁸ As mentioned in Chapter 1, free CN^- forming complexes with compounds such as boronic acid derivatives and nucleophilic attack of nucleophilic CN^- to electron-deficient compounds such as benzothiadiazole, offer two common approaches to

cyanide chemosensors. Compared with the above two types of chemosensors using small molecules, CP-based sensors potentially offer higher (amplified) sensitivity resulting from the collective properties of CPs. Thus, fluorescent CPs have been investigated for applications in optical cyanide sensors in the recent years. Two examples would be given below. Zeng *et al.*¹⁷⁹ reported an imidazole-functionalized polyacetylene and its “turn-on” sensing towards CN^- with high sensitivity and selectivity. Son *et al.*¹⁸⁰ reported a polymer containing benzodiazaborole moieties and sulfonate groups for recognition of CN^- in aqueous solution, which exhibits visible fluorescence quenching (“turn-off”) upon exposure to CN^- concentrations as low as $\sim 2 \mu\text{M}$ and selective detection of CN^- over other anions.

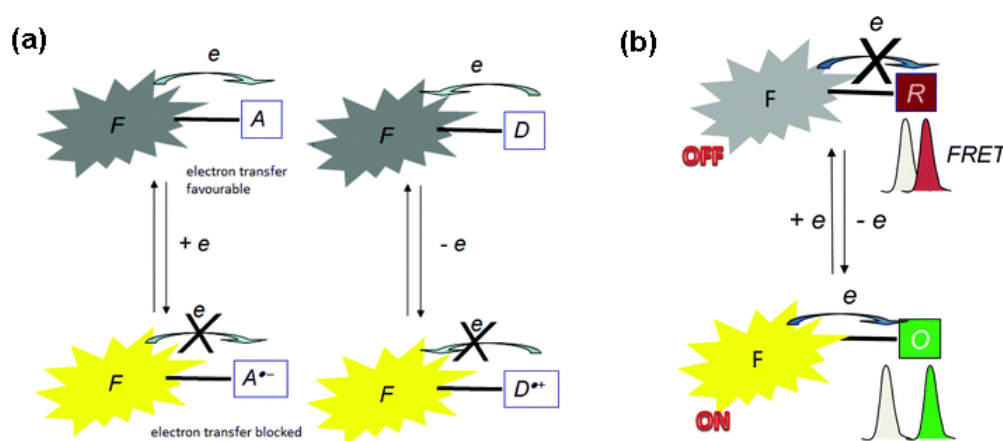
2.4.2 EFC materials

Commonly studied EFC materials could be divided into three groups: switchable molecular dyads, intrinsically switchable fluorophores, and switchable fluorescent CPs, which will be briefly introduced in the following paragraphs.

Switchable molecular dyads

The EFC dyads are made of a fluorophore, linked through a conjugated or a non-conjugated spacer to a redox moiety. The redox moiety provides the electroactive character and the fluorescence switches through photoinduced electron transfer or energy transfer between the excited state of fluorophore and the redox functionality in one state only, as described in Scheme 2.7. According to the oxidizing or reducing character of the fluorophores’ excited state, the

electron transfer is allowed or not, and therefore the fluorescence is switched off when the electron transfer is allowed to produce the quenching species (Scheme 2.7a). Another situation is based on a redox controlled fluorescence resonance energy transfer (FRET) that changes according to the overlap between absorption of the redox part and emission of the fluorophore (Scheme 2.7b). In this case, an electrochromic reaction is responsible for the light emission switch. Kim *et al.*⁴⁵ reported such an example that an intrinsically redox active naphthalimide-tetrazine dyad was demonstrated to exhibit multi-color electrofluorochromism.

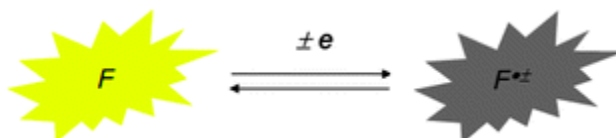


Scheme 2.7 Switchable dyad systems through (a) electron transfer or (b) energy transfer. Reproduced from ref. [13] with permission from The Royal Society of Chemistry.

Intrinsically switchable fluorophores

A very straightforward way to switch on and off the fluorescence is to simply convert the fluorophore to its corresponding ion-radical (as shown in Scheme 2.8).

However, few fluorophores give stable ion-radicals. Although there is a common belief that neutral radicals should be non-fluorescent because of their “open-shell” structure, a few fluorescent radicals are reported.^{181, 182} Very recently, some researchers have begun to study fluorescence in combination with electrochemistry, i.e., monitoring the fluorescence of a thin solution layer near the electrode under electrochemical cycles. This possibly allows a demonstration of the response of an ion-radical, through the appearance of isosbestic points in the recording of fluorescence spectra as a function of applied potential. Audebert’s group investigated the electrofluorochromism of small electroactive fluorophores, providing in-depth analysis of the fluorescence decay of tetrazines, particularly demonstrating the occurrence of self-quenching of the neutral fluorophore through electron transfer with its electrogenerated anion-radical.^{11, 12}



Scheme 2.8 Electrochemical switching of the fluorescence. Reproduced from ref. [13] with permission from The Royal Society of Chemistry.

Switchable fluorescent conjugated polymers

Some CPs are fluorescent in the neutral state, but lose fluorescence (quenched) upon oxidation or reduction. As mentioned in Chapter 1, the CPs exhibit efficient electronic delocalization that offers them the capability of amplifying the

sensitivity in regard to fluorescence change, facilitated by rapid transport of excitons along the π -conjugated chains.¹⁴⁻¹⁷

Furthermore, most of the CPs can be processed into thin films (via electrodeposition or spin-coating) on the electrode, which is an advantage over the solution based materials with regard to the electrochemical redox process. The first report on electrochemically switchable intrinsic electroactive fluorophore appeared in 2004.⁸ A few years later, Montilla *et al.* reported EFC properties of phenylene-vinylene and fluorene-phenylene copolymers.^{10, 42} More recently, dynamically controllable electrofluorochromism of a series of electropolymerized poly(N-alkyl-2,7-di(2-thienyl)carbazole) was demonstrated by Goto *et al.*⁴⁴ Leung *et al.* reported that by blending two EFC CPs in a device, their fluorescence in yellow and blue regions could be simultaneously quenched under a low potential, achieving white–dark state of fluorescence.⁴⁷

2.4.3 EFC devices

The configuration of EFC devices (EFCDs) is a sandwich structure, similar to single layer transmissive ECDs, as introduced in section 2.2.1.2. ITO glass and ITO/PET are often used as the electrode, and polymer gel electrolytes such as LiClO₄/ACN/PC/PMMA are commonly used electrolytes. Epoxy resin is usually used for sealing the device. Figure 2.9 shows a schematic diagram of an EFC device.

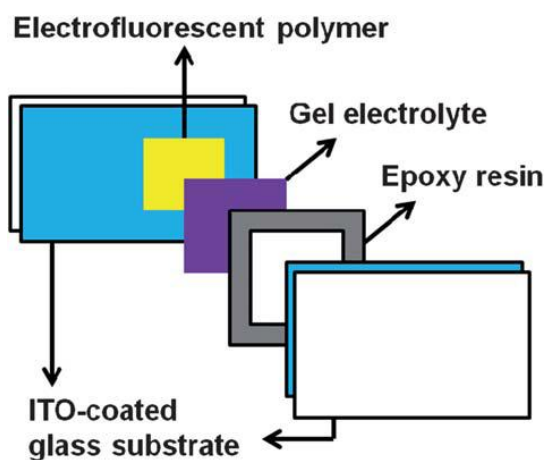


Figure 2.9 Schematic diagram of an EFC device. Reproduced from ref. [47] with permission from The Royal Society of Chemistry

2.4.4 Applications of EFC materials

EFC materials have been investigated actively in the very recent years. However, the applications of EFC materials are still explored and not many have been developed up to today. The current EFC applications are mainly in displays and sensors, and some examples are shown as follows. Kim and Audebert *et al.*^{9, 183} first demonstrated tetrazine-based EFC windows that exhibited switching of emission under UV light during the redox process and they also realized multi-color switching (white–blue–black) for the EFC device.⁴⁵ Such EFC windows are potentially applied in large size display panels. Kobayashi *et al.*⁴⁹ made use of EFC europium(III) complex and viologen derivatives to build a smart dual mode display cell, allowing the user to benefit from reflectance display under bright illumination (like reading outside on a sunny day) and emissive display under

dark illumination. Löffler *et al.*¹⁸⁴ developed an optical pH sensor by coupling Total Internal Reflection Fluorescence (TIRF) microscopy with an electrolysis flow cell, and used it to measure the local pH variations associated with corrosion issues in an occluded electrochemical cell.

2.5 Characterization of electrochemical, EC and EFC properties

2.5.1 Three-electrode electrochemical cell

Other than EC or EFC device, the spectroelectrochemical parameters of EC and EFC materials can also be characterized in a three-electrode electrochemical cell: a quartz cuvette is used as container filled with electrolyte in which the reference electrode (e.g., Ag/AgCl) is inserted,. This three-electrode cell uses the thin film of EC or EFC material (coated on ITO glass or ITO/PET) as the work electrode (WE), a platinum wire as the counter electrode (CE), and a silver wire as the pseudo-reference electrode (RE). The pseudo-RE is usually calibrated by adding into the electrolyte solution a little amount of reversible redox species such as Fc (ferrocene)/Fc⁺ couple (for non-aqueous solutions). Figure 2.10 shows the configuration of a typical three-electrode electrochemical cell. In comparison with the EC or EFC device, such a three electrochemical cell is less complicated and easy to set up, therefore it has been a common tool for spectroelectrochemical characterizations for EC or EFC materials.

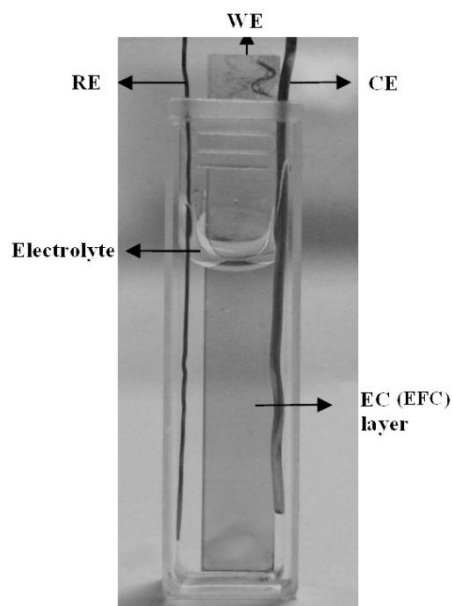


Figure 2.10 Configuration of a three-electrode electrochemical cell (cuvette) for spectroelectrochemical characterization.

2.5.2 Main characterization methods

2.5.2.1 Cyclic voltammetry

Cyclic voltammetry (CV) is a basic tool for studying the electroactivity of CPs. It is often used to identify the potentials at which oxidation and reduction processes take place, the degree of reversibility of the electrode reactions and the potential range in which the electroactive material coated on the electrode is stable. Thus, important parameters obtained from the cyclic voltammograms of electroactive polymers include the potential value of the oxidation and reduction peaks and the peak current densities at different scan rates.

2.5.2.2 Spectroelectrochemistry

Spectroelectrochemistry is a very useful technique that combines the electrochemical and spectroscopic (absorption/transmission and fluorescence) signals, in examining the optical changes induced by the redox processes for an EC or EFC film. This technique can be used to probe structural changes and provide the information about electronic band modifications during the redox processes. Measurements were conducted using a UV-vis-NIR spectrophotometer (for EC study) or fluorescence spectrometer (for EFC study) and a potentiostat. Generally, the EC (or EFC) device or three-electrode electrochemical cell is positioned into a UV-vis-NIR spectrophotometer (or fluorescence spectrometer) and connected to a potentiostat that outputs potentials while the transmission/absorption (or fluorescence) spectra is being monitored and recorded. Common spectroelectrochemical tests include static test and dynamic test. In the static test, waiting time is enough to allow the EC (or EFC) film to achieve its stable redox state at each potential loaded, and the corresponding spectra are then recorded. The dynamic test gives the time-absorption/transmission (or time-fluorescence intensity) profiles of the EC (or EFC) film through periodical switching between two redox potentials. Static tests together with dynamic ones could provide important parameters such as contrast, switching time and stability, which are very important for characterization of both EC and EFC materials.

3. Black-to-Transmissive Electrochromism of Carbazole–Benzothiadiazole–Azulene-Based Donor–Acceptor Conjugated Polymers Complemented by PEDOT:PSS

3.1 Introduction

As introduced in Chapter 2, a complementary ECD is possible to achieve black-to-transmissive electrochromism by switching the two EC materials simultaneously, if the absorption bands of the two EC layers are complementary to each other to cover the whole visible region. The potentials required for the coloration and bleaching of the anodically coloring EC material should match well with those required for the cathodically colored EC material. PEDOT:PSS is a good candidate for cathodically coloring EC layer because of its good processability, high electrical conductivity and relatively narrow band gap. However, anodically coloring CPs that could cover the high-energy end of visible spectrum upon oxidation usually have relatively high oxidation potentials, which do not match well with the potential window of PEDOT:PSS.

Poly(3,6-carbazole) (PCz) has been demonstrated to be electrochromic,¹⁹ exhibiting an absorption band at ~430 nm at neutral state and ~530 nm upon oxidation,²¹ as mentioned in Chapter 2. At oxidized state, PCz covers the high energy band of visible region, so it can be potentially used to fabricate simple dual-active-layer black ECD complemented by PEDOT:PSS which covers the

low energy band upon reduction. However, the oxidation potential of PCz needs to be reduced in order to lessen the gap with the reduction potential of PEDOT:PSS. As a result, 2,1,3-benzothiadiazole (BTD), a commonly used electron acceptor,^{5, 24, 25, 165} was introduced into the system to form D–A type of CPs.

To achieve a better matching PEDOT:PSS in absorption band coverage, the band gap (E_g) of PCz needs to be reduced in order to extend its absorption band towards low energy band by tuning the electronic structure. Azulene has a relatively low oxidation potential and can be more easily oxidized than most common aromatic carbocycles and heterocycles, giving it the potential to reduce the band gap of azulene-containing CPs. In addition, poly(1,3-azulene) film shows absorption bands at around 446 nm at neutral state and 480 nm upon oxidation in visible region, which is close to the absorption band of PCz.¹⁸⁵ Thus, azulene is incorporated to reduce band gap of PCz in this work.

It was expected that, the copolymerization of carbazole, BTD and azulene potentially leads to a CP with relatively low oxidation potential and band gap, which could cover the high energy region of the visible spectrum at oxidized state, and potentially complement PEDOT:PSS to form a black ECD. In this chapter, the synthesis and structures of the carbazole–BTD–azulene copolymers are reported. The effects of the D–A approach on electrochemical and electrochromic properties of the copolymers are illustrated, and a black-to-transmissive complementary ECD is demonstrated.

3.2 Experimental

3.2.1 Materials

Azulene, 3,6-dibromocarbazole, n-butyl lithium, 2-isopropoxy-4,4,5,5-tetramethyl-1,3,2-dioxaborolane, 2,1,3-benzothiadiazole-4,7-bis(boronic acid pinacol ester), Aliquat[®] 336, *p*-xylene, lithium perchlorate (LiClO₄), acetonitrile (ACN, anhydrous), polypropylene carbonate (PC), poly(methyl methacrylate) (PMMA, $M_w = 120,000$ g/mol), PEDOT:PSS and ferrocene (98%) were purchased from Aldrich and used as received. Tetrakis(triphenylphosphine)palladium(0) (Pd(PPh₃)₄) was purchased from Strem Chemical Inc. and used as received. 1-Bromooctane was purchased from Lancaster and used as received. 1,3-Dibromoazulene¹⁸⁶ and 3,6-bis(4,4,5,5-tetramethyl-1,3,2-dioxaborolan-2-yl)-9-octylcarbazole^{123, 125} were synthesized according to the literatures.

3.2.2 Chemical characterization

¹H and ¹³C nuclear magnetic resonance (NMR) spectra were recorded on a Bruker DRX 400-MHz NMR spectrometer in deuterated chloroform (CDCl₃) at room temperature using tetramethylsilane (TMS) as an internal standard. Operating frequencies of the NMR spectrometer were 400.13 MHz (¹H) and 100.61 MHz (¹³C). Size exclusion chromatography (SEC) analyses were carried out on a Waters 2690 system using THF as eluent and polystyrene standards. UV–vis absorption spectra of the copolymers dissolved in chloroform were measured using an Agilent Cary 5000 UV–vis–NIR spectrophotometer. Differential

scanning calorimetry (DSC) thermograms of the copolymers were recorded on a TA Instruments DSC Q10 using N₂ as a purge gas at a heating rate 10 °C min⁻¹.

3.2.3 Synthesis of copolymers

Poly[(3,6-(9-octylcarbazol))-(1',3'-azulenyl)] (P₀)

To a dissolved mixture of 1,3-dibromoazulene (286.0 mg, 1.00 mmol), 3,6-bis(4,4,5,5-tetramethyl-1,3,2-dioxaborolan-2-yl)-9-octylcarbazole (531.3 mg, 1.00 mmol), Aliquat[®] 336 (0.11 g) in dry toluene (10 mL) were added and degassed, followed by a degassed Na₂CO₃ solution (aq. 2 M, 8 mL). Then, Pd(PPh₃)₄ (5.8 mg, 0.005 mmol) was added. After further degassing, the mixture was stirred and refluxed under N₂ at 123 °C for 4 days. The mixture was separated and the organic layer was then poured into excess methanol (200 mL) with vigorous stirring. The obtained precipitate was filtered, washed with water, and dried under vacuum. The crude product was dissolved in chloroform and filtered. The green filtrate was evaporated to dryness, and was dissolved in a minimum volume of toluene. Sufficient methanol was then added to re-precipitate the product. The green precipitate was finally washed with acetone using a Soxhlet extractor for 2 days and dried in a vacuum oven at 40 °C for 2 days. Then the final product was obtained. ¹H NMR: δ = 8.60 (m, 2H), 8.42 (m, 2H), 8.32 (m, 1H), 7.80 (m, 2H), 7.54 (m, 3H), 7.05 (m, 2H), 4.39 (m, 2H), 1.97 (m, 2H), 1.05-1.45 (m, 13H) ppm. ¹³C NMR: δ = 140.3, 139.2, 138.1, 136.9, 136.7, 131.9, 128.6, 123.8, 123.2, 122.0, 109.4, 43.8, 32.2, 29.8, 29.6, 27.8, 23.0, 14.4 ppm.

Poly[(3,6-(9-octylcarbazol)_{0.99, 0.97, 0.95, 0.80})-(1',3'-azulenyl)-(2,1,3-benzothiadiazol)_{0.01, 0.03, 0.05, 0.20}] (P₁, P₃, P₅, P₂₀)

The synthesis route of **P₁**, **P₃**, **P₅**, and **P₂₀** is similar to **P₀**. The feed ratio of 1,3-dibromoazulene was set as 100 mol%, while that of 3,6-bis(4,4,5,5-tetramethyl-1,3,2-dioxaborolan-2-yl)-9-octylcarbazole and 2,1,3-benzothiadiazole-4,7-bis(boronic acid pinacol ester) varied from 99 mol% and 1 mol%, 97 mol% and 3 mol%, 95 mol% and 5 mol%, and 80 mol% and 20 mol%, for **P₁** to **P₂₀**, respectively. ¹H and ¹³C NMR spectra of the terpolymers are listed below. **P₁**: ¹H NMR: δ = 8.60, 8.45, 8.32, 7.79, 7.54, 7.04, 4.38, 1.97, 1.05-1.45 ppm. ¹³C NMR: δ = 140.3, 139.1, 138.5, 137.8, 137.5, 137.0, 136.7, 136.3, 131.9, 128.6, 128.5, 123.9, 123.2, 122.0, 117.7, 109.4, 43.8, 32.2, 29.8, 29.6, 27.8, 26.7, 23.0, 14.5 ppm. **P₃**: ¹H NMR: δ = 8.62, 8.43, 8.33, 7.80, 7.56, 7.05, 4.40, 1.97, 1.05-1.45 ppm. ¹³C NMR: δ = 140.3, 139.1, 138.5, 138.1, 137.8, 137.5, 137.0, 136.9, 136.7, 136.3, 131.9, 128.6, 126.0, 123.9, 123.2, 123.0, 122.0, 117.7, 109.4, 43.8, 32.2, 30.1, 29.8, 29.6, 27.8, 23.0, 14.5 ppm. **P₅**: ¹H NMR: δ = 8.61, 8.42, 8.33, 7.80, 7.55, 7.03, 4.38, 1.97, 1.05-1.45 ppm. ¹³C NMR: δ = 155.8, 141.9, 140.3, 139.2, 138.5, 138.1, 137.8, 137.5, 137.0, 136.9, 136.7, 136.3, 131.9, 128.6, 126.0, 123.9, 123.2, 123.0, 122.0, 117.7, 109.4, 43.8, 32.2, 30.1, 29.9, 29.6, 27.8, 23.0, 14.4 ppm. **P₂₀**: ¹H NMR: δ = 8.63, 8.44, 8.35, 7.81, 7.58, 7.06, 4.41, 1.98, 1.05-1.45 ppm. ¹³C NMR: δ = 155.8, 141.9, 140.3, 139.7, 139.5, 139.2, 138.5, 138.1, 137.8, 137.5, 136.9, 136.7, 136.3, 135.7, 132.8, 131.9, 128.8, 128.6, 126.1, 124.4, 123.9, 123.2, 122.0, 117.7, 109.4, 43.8, 32.2, 30.1, 29.8, 29.6, 27.8, 23.0, 14.4 ppm.

3.2.4 Cyclic voltammetry and spectroelectrochemical characterization

The solutions of polymers in *p*-xylene (20 mg/mL) were spin-coated (1000 rpm) onto indium tin oxide (ITO) electrodes laminated on poly(ethylene terephthalate) (PET) substrates (ITO/PET, 100 Ω /sq) to form electrochromic polymer layer (ECP) on ITO/PET (ECP/ITO/PET). The thickness of the spin-coated film was controlled at ~150 nm, which was measured by Alpha-Step IQ surface profiler. The cyclic voltammetry of ECP/ITO/PET was carried out in a three-electrode cell, with platinum (Pt) foil as counter electrode, silver (Ag) wire as reference electrode, and 0.1 M LiClO₄/ACN as electrolyte using an Autolab PGSTAT302 electrochemical workstation, respectively. For spectroelectrochemical characterization, ECP/ITO/PET was placed in a three-electrode cell using Pt wire as counter and silver wire as reference electrode, respectively, and 0.1 M LiClO₄/ACN as electrolyte in a cuvette, and tested using the same Autolab electrochemical workstation and a Shimadzu UV-vis 2501 spectrophotometer. For both electrochemical and spectroelectrochemical characterization, the pseudo-reference silver wire was calibrated vs. Fc/Fc⁺ by dissolving ferrocene in the electrolyte solution and determining the E_{1/2} of the Fc/Fc⁺ against the silver wire.

3.2.5 ECD fabrication and characterization

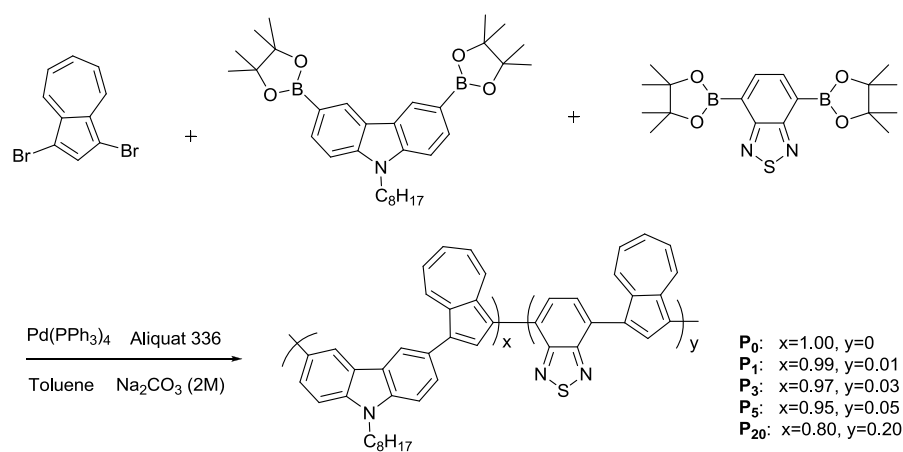
The gel electrolyte was prepared by mixing poly(methyl methacrylate) (PMMA, M_w = 120,000 g/mol), LiClO₄ and PC in dry ACN according to the literature.¹⁸⁷ ECDs with a sandwich structure of PET/ITO/ECL/gel polyelectrolyte/PEDOT:PSS/ITO/PET were then fabricated, where ECL refers to

spin-coated thin film of **P**₀ or **P**₅. The in situ spectroelectrochemical properties of the ECDs were also tested using the same Autolab electrochemical workstation and Shimadzu UV-vis 2501 spectrophotometer. Colorimetry of the complementary ECD was measured using a color reader CS-100A (Konica Minolta).

3.3 Results and discussion

3.3.1 Synthesis and structure verification

The synthesis route of carbazole–azulene alternating copolymer (**P**₀) and carbazole–BTD–azulene terpolymers (**P**₁, **P**₃, **P**₅ and **P**₂₀) is shown in Scheme 3.1.



Scheme 3.1 Synthesis route of the terpolymers, **P**₁, **P**₃, **P**₅ and **P**₂₀ (with **P**₀ as reference).

¹H NMR spectra of **P**₀ and the terpolymers are given in Figure 3.1a. As revealed by Figure 3.1a, the interactions between neighboring azulene and

carbazole units in **P**₀ lead to shift and overlapping of H peaks, compared with the ¹H NMR spectra of the monomers 1,3-dibromoazulene¹⁸⁶ and 3,6-bis(4,4,5,5-tetramethyl-1,3,2-dioxaborolan-2-yl)-9-octylcarbazole.^{123, 125} This verifies the formation of the carbazole–azulene alternating copolymer. As expected, **P**₀ is very soluble in common solvents such as chloroform, toluene, xylene, etc.

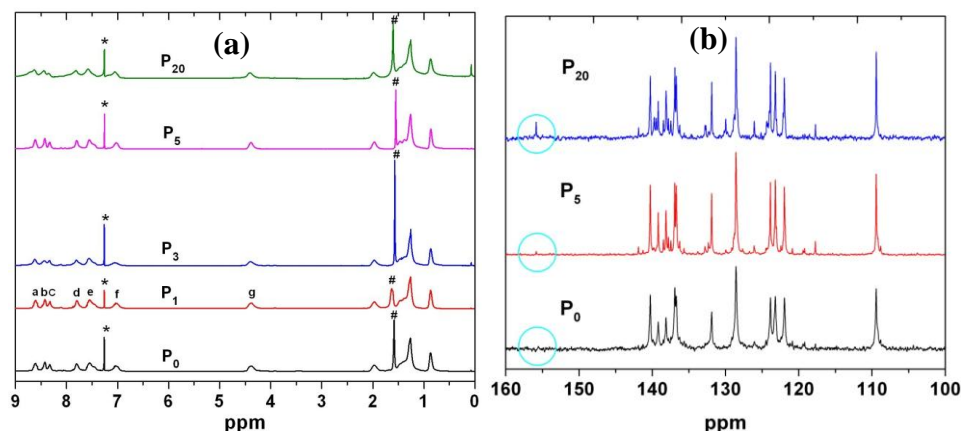


Figure 3.1 (a) ¹H NMR spectra of **P**₀, **P**₁, **P**₃, **P**₅ and **P**₂₀ in CDCl₃ (* indicates CDCl₃, # indicates H₂O). The molar ratios of carbazole to BTB units (**P**₁ was here taken as an example) were estimated by integration of peak a + b + c + d + e + f (all aromatic protons) to peak g (protons from N-CH₂). (b) ¹³C NMR spectra of **P**₀, **P**₅ and **P**₂₀ in CDCl₃.

Different from **P**₀ that has a regular conjugated structure composed of alternating azulene and carbazole units, **P**₁, **P**₃, **P**₅ and **P**₂₀ are terpolymers that contain 1, 3, 5 and 20 mol% BTB units (ratio obtained from BTB over azulene that is set as 100 mol%), respectively. In comparison with **P**₀, several new peaks appear in aromatic region of the ¹³C NMR spectra for these terpolymers, such as

the ones at 140.9, 138.5, 137.8, 137.5, 136.3, and 117.7 ppm, indicating the existence of BTB moieties in the chains. In particular, a new peak can be seen at 155.8 ppm for **P₅** and obviously for **P₂₀** (as circled in Figure 3.1b), which is attributed to the C atoms that are bonded to N atoms (C=N) in BTB. The other new peaks are difficult to be assigned to various carbons of BTB due to random distribution of BTB units along the terpolymer chains.

Table 3.1 shows the theoretical molar ratios of carbazole to BTB units calculated based on feed compositions and the ratios estimated from integrations of ¹H NMR spectra of **P₀** and the terpolymers. It is noticed that the estimated ratio (x':y') obtained from integration of the ¹H NMR peaks decreases as the BTB feed content increases, which is consistent with the trend of theoretical ratios (x:y) obtained from the feed compositions of the terpolymers. This further proves the inclusion of BTB units into the copolymer backbone.

Table 3.1 Theoretical molar ratios of carbazole to BTB units calculated from feed compositions (x:y) and the corresponding ratios estimated from integrations of ¹H NMR spectra (x':y') for **P₀** and the terpolymers.

Polymer	Theoretical ratio (x:y)	Estimated ratio (x':y')
P₀	1.00:0.00	1.00:0.00
P₁	0.99:0.01	0.99:0.01
P₃	0.97:0.03	0.97:0.03
P₅	0.95:0.05	0.93:0.07
P₂₀	0.80:0.20	0.75:0.25

Table 3.2 shows the apparent molecular weights of the copolymers measured using SEC. It is noticed that the molecular weights decrease with increasing feed ratio of BTD for the copolymers. BTD content couple with azulene units and form BTD–azulene moieties in the copolymer backbone. However, BTD–azulene moieties have no side chains. As a result, with increasing feed ratio of BTD, the more BTD–azulene moieties formed lead to reduction in solubility of the copolymer chains in the reaction medium (mixture of toluene and 2 M $\text{Na}_2\text{CO}_3/\text{H}_2\text{O}$). The lower solubility would limit the growth of copolymer chains and therefore result in copolymers with reduced molecular weights. Nevertheless, it is estimated that each terpolymer chain contains on average about thirty aromatic rings on the backbone, based on the apparent number-average molecular weights. Indeed, the molecular weights are high enough for making good-quality thin films for electrochemical and electrochromic characterizations.

Table 3.2 Molecular weights and polydispersities of **P₀** and the terpolymers.

Polymer	M_n	M_w	M_w/M_n
P₀	5200	7200	1.38
P₁	4400	5900	1.34
P₃	4000	5300	1.33
P₅	4000	4600	1.15
P₂₀	3700	4200	1.14

From the DSC thermograms of **P₀**, **P₁**, **P₃**, **P₅** and **P₂₀** (page 135–137 in Appendix), it is observed there are some indications of melting peak (for example,

at $\sim 180^\circ\text{C}$ for **P**₀). However, they are not obvious. It may suggest that most of these copolymers (**P**₀-**P**₂₀) are largely amorphous. Crystallization of polymers is affected by their chemical structures, including structure regularity and chain conformation. **P**₁, **P**₃, **P**₅ and **P**₂₀ are random polymers containing 1, 3, 5 and 20% of BTB-containing repeat units, respectively. The random sequence distribution of the backbone leads to their amorphous structures. **P**₀ is a regular alternating copolymer but it is likely to have highly kinked conformation owing to the combination of the 3,6-linkage of carbazole and 1,3-linkage of azulene moieties. This probably hinders close packing of the main chains and hence makes it amorphous. From the DSC thermograms, it is observed that the glass transition temperatures (T_g) of these copolymers are all higher than 100°C . High rigidity of their conjugated main chains should be the reason for the high T_g .

Figure 3.2 shows the visible spectra of **P**₀, **P**₅ and **P**₂₀ (dissolved in chloroform, 8×10^{-5} M each). It is observed that **P**₀ shows a weak shoulder band at about 470 nm while **P**₅ exhibits a stronger absorption band at about 480 nm and **P**₂₀ gives a distinctive strong band at 506 nm. The red shift from 470 nm for **P**₀ to 480 nm for **P**₅ and 506 nm for **P**₂₀ clearly indicates the effect of the inclusion of BTB units into and thus again verifies the formation of the terpolymers. This also implies the donor-acceptor interactions between acceptor BTB and neighboring azulene and carbazole donor units. It is noticed that the weak absorption band at around 650 nm is reduced from **P**₀ to **P**₂₀. This band is probably from carbazole units¹⁹ and the intensity reduction is consistent with the increase of BTB content, i.e., the

decrease of carbazole content in the backbone, which further verifies the inclusion of BTD units in the copolymers.

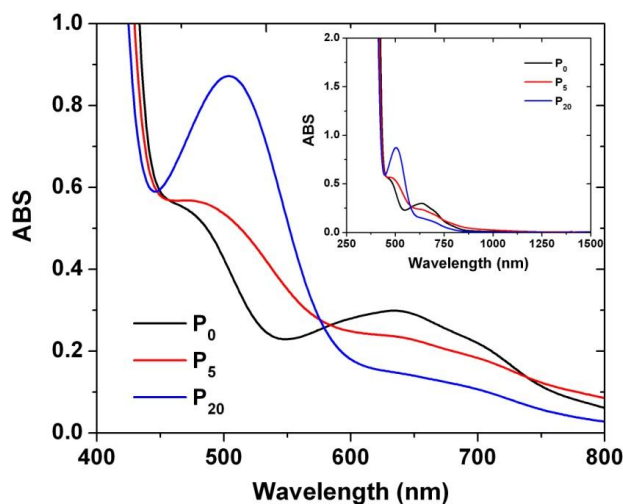


Figure 3.2 Visible spectra of **P₀**, **P₅** and **P₂₀** dissolved in chloroform (8×10^{-5} M for each solution). The inset shows UV-vis-NIR absorption spectra of the copolymers.

Spectroelectrochemical studies reveal that **P₅** exhibits highest EC contrast among the carbazole-BTD-azulene terpolymers (Figure 3.3). The EC contrast is highly influenced by redox charge density.¹⁸⁸ At very low BTD content (**P₁**, **P₃** and **P₅**), the increasing BTD content leads to higher EC contrast due to the D-A effect. However, too high a BTD content (**P₂₀**) would reduce the optical contrast. In this circumstance, more azulene-BTD-azulene (A-BTD-A) and less azulene-carbazole-azulene (A-C-A) units form with increasing BTD content in the polymer chains, while A-BTD-A units are likely to possess lower redox charge density than A-C-A units (Scheme 3.2) and thus would lead to decreased EC

contrast. Hence, the discussion in the following sections will focus on \mathbf{P}_5 , with \mathbf{P}_0 as the reference, to illustrate the effect of the D–A approach on electrochemical and electrochromic properties of the copolymers.

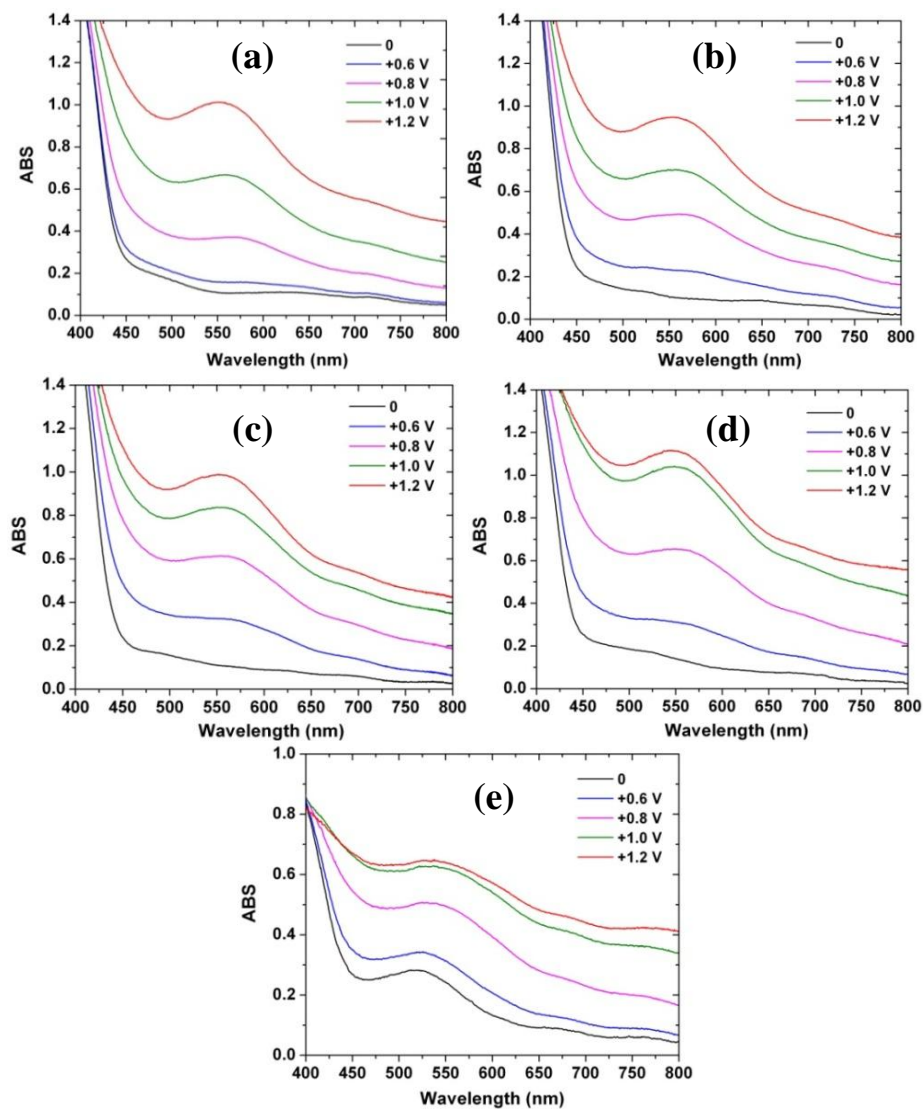
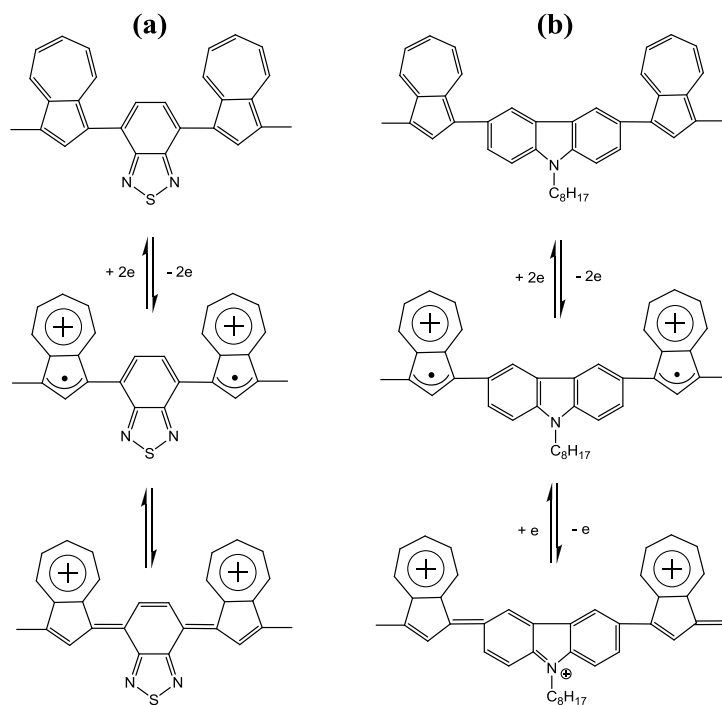


Figure 3.3 Visible spectra of spin-coated (a) \mathbf{P}_0 , (b) \mathbf{P}_1 , (c) \mathbf{P}_3 , (d) \mathbf{P}_5 and (e) \mathbf{P}_{20} on ITO/PET under different potentials (0, +0.6, +0.8, +1.0, +1.2V) in 0.1 M $\text{LiClO}_4/\text{ACN}$.



Scheme 3.2 Possible redox processes of (a) A-BTD-A and (b) A-C-A.

3.3.2 Cyclic voltammetry

Voltammetry sweeps of **P₀** and **P₅** are compared in Figure 3.4. **P₀** exhibits a distinct peak at 1.03 V and a shoulder at around 0.75 V. In typical cyclic voltammograms of 3,6-Polycarbazole (including N-alkyl substituted ones), two pairs of redox peaks usually appear, corresponding to radical cation and dication states, respectively.¹¹⁹ However, the oxidation potential of polyazulene is reported to be at around 0.6 V (vs. Fc/Fc⁺).¹⁸⁵ Thus, the peak attributed to the oxidation of azulene units (Scheme 3.3) from **P₀** is probably partially overlapped with the shoulder peak from the carbazole units. A possible redox mechanism for **P₀** is proposed in Scheme 3.3.

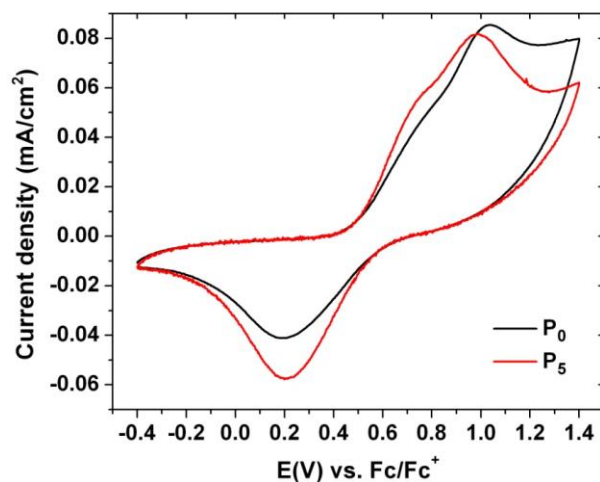
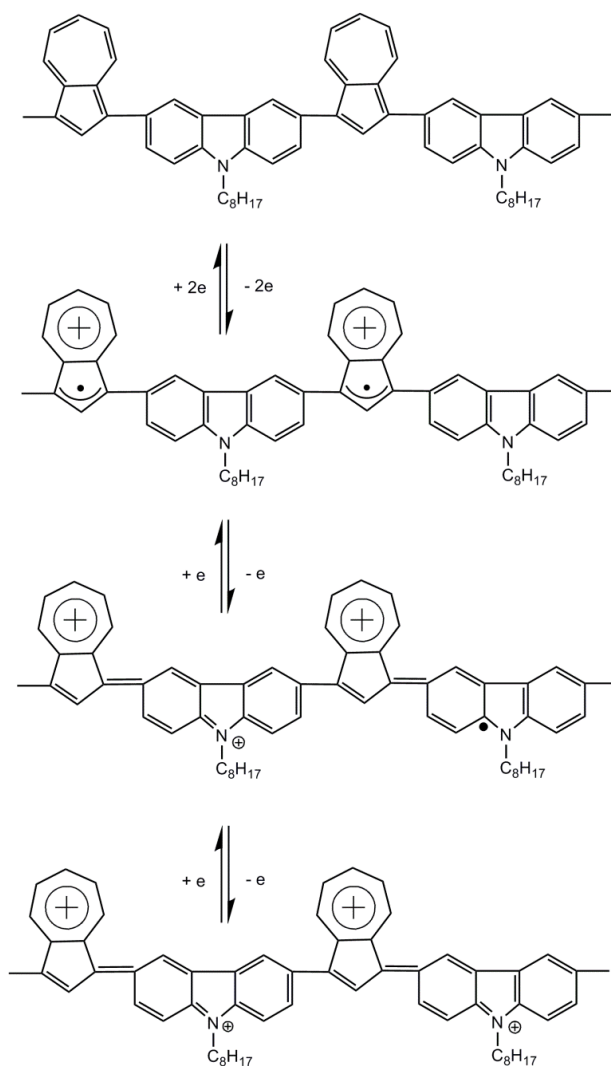


Figure 3.4 Cyclic voltammograms of spin-coated (a) **P₀** and (b) **P₅** on ITO/PET in 0.1 M LiClO₄/ACN at a scan rate 10 mV/s.

Initially, the electron removal is likely to occur at the electron-rich cyclopentadiene part of the azulene ring to form a cationic radical, which probably further rearranges to form a closed shell structure. Then an electron is removed from the carbazole unit and the radical cation is formed upon further oxidation. In most cases, these radicals are unstable and would combine to give dications. However, as the conjugation breaks present due to the 3,6-carbazole units, the radical cations separate from each other and do not combine. With higher potentials, another electron is removed from carbazole units upon further oxidation, leading to dications.

P₅ also shows a main oxidation peak and a shoulder, which is similar to **P₀**. However, the shoulder peak becomes more distinct, and the main peak appears at 0.98 V, which is 0.05 V lower than that of **P₀**, implying easier formation of the

radical cation and dication for **P**₅, in comparison with **P**₀. The lower oxidation potential for the main peak and more distinct shoulder peak could be attributed to the electronic interactions between the units of carbazole, azulene and BTD, i.e., the electron loss of carbazole and azulene units is facilitated by the strong electron-withdrawing effect of BTD units.



Scheme 3.3 A proposed redox mechanism for **P**₀.

3.3.3 Spectroelectrochemical behavior

Figure 3.3a and d show the visible spectra of **P₀** and **P₅** thin film under various potentials. It is observed that **P₀** appears transmissive green at neutral state while it turns to grey upon oxidation. Slightly different from **P₀**, **P₅** shows yellow–green at neutral state. It is striking to see that with a small amount of BTB units, **P₅** exhibits much higher absorption than **P₀** at relatively low positive potentials. For example, from 0 V to 1.0 V, **P₅** gives a total change in absorbance (ΔA) of 0.90 at its λ_{\max} (550 nm), while the ΔA for **P₀** is only 0.56 at its λ_{\max} (550 nm), i.e., the optical contrast (ΔA) of **P₅** is 61% higher than that of **P₀**. It can be attributed to the lower oxidation potentials of **P₅** induced by the BTB units. When the applied potential reaches 1.2 V, well above the second oxidation potential of both **P₀** and **P₅** (0.98 V and 1.03 V, respectively, obtained the previous cyclic voltammograms), their difference in optical contrast diminishes, confirming that the significant enhancement in EC contrast at lower potentials is indeed due to the reduced oxidation potentials, albeit the reduction is small. The reduced oxidation potential could help **P₅** to reduce the possibility of over-oxidation when it is switched simultaneously with PEDOT:PSS in a complementary ECD.

The optical switching behaviors of the films are examined at wavelengths corresponding to their maximum change in absorbance ($\lambda_{\max} = 550$ nm) using a UV–vis spectrophotometer with the applied potential stepped between -0.4 V and 1.0 V at 80 s per cycle. The dynamic switching curves of the electrochromic films are shown in Figure 3.5. It is observed that **P₅** exhibits slightly faster switching kinetics for both the coloration and bleaching than **P₀**. The faster switching

kinetics of \mathbf{P}_5 is likely to be caused by its lower oxidation potential because under the same potential more azulene and carbazole units can be quickly oxidized in \mathbf{P}_5 than in \mathbf{P}_0 . In addition, the conformational change of the polymer backbone caused by the random inclusion of BTD units may also play a role in facilitating motion of ions due to the slight larger inter-chain distances at some locations. For the same reasons, \mathbf{P}_5 also exhibits higher dynamic EC contrast than \mathbf{P}_0 .

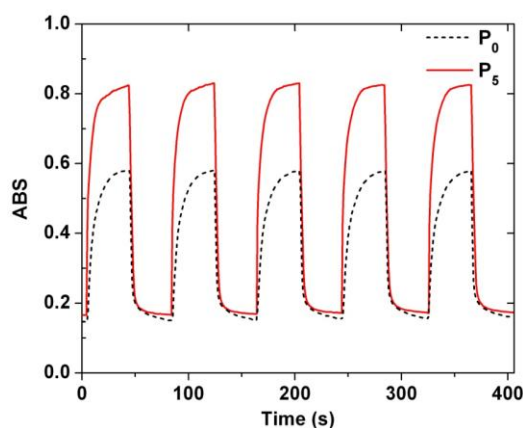


Figure 3.5 Absorption–time profiles ($\lambda_{\text{max}} = 550 \text{ nm}$) of spin-coated \mathbf{P}_0 (dash line) and \mathbf{P}_5 (solid line) on ITO/PET switched between -0.4 and 1.0 V in $0.1 \text{ M LiClO}_4/\text{ACN}$.

3.3.4 Black-to-transmissive ECD

PEDOT:PSS exhibits cathodic coloration from transmissive sky blue to dark blue, while \mathbf{P}_5 exhibits anodic coloration from transmissive yellow–green to grey. As shown by the visible absorption spectra in Figure 3.6a, the absorption band of PEDOT:PSS covers $550\text{--}700 \text{ nm}$ of the visible region upon reduction, while that of \mathbf{P}_5 covers $400\text{--}600 \text{ nm}$ upon oxidation. As shown in Figure 3.6b, using \mathbf{P}_5 as

working electrode and PEDOT:PSS as counter electrode, the complementary ECD exhibits transmissive light green–yellow at bleached state with transmittance of about 65% at 600 nm, while it exhibits transmittance of less than 10% for almost the whole visible spectrum during coloration. It indicates that PEDOT:PSS and P_5 could be simultaneously switched between oxidized state and reduced state for coloration and bleaching with external potentials applied. In addition, the complementary ECD exhibits near CIE black at colored state with L^* , a^* , and b^* values of 22.0, 6.3, and 7.5, respectively; while at bleached state the values of L^* , a^* and b^* are 76.0, -3.0 and 30.2, respectively (Figure 3.6c).

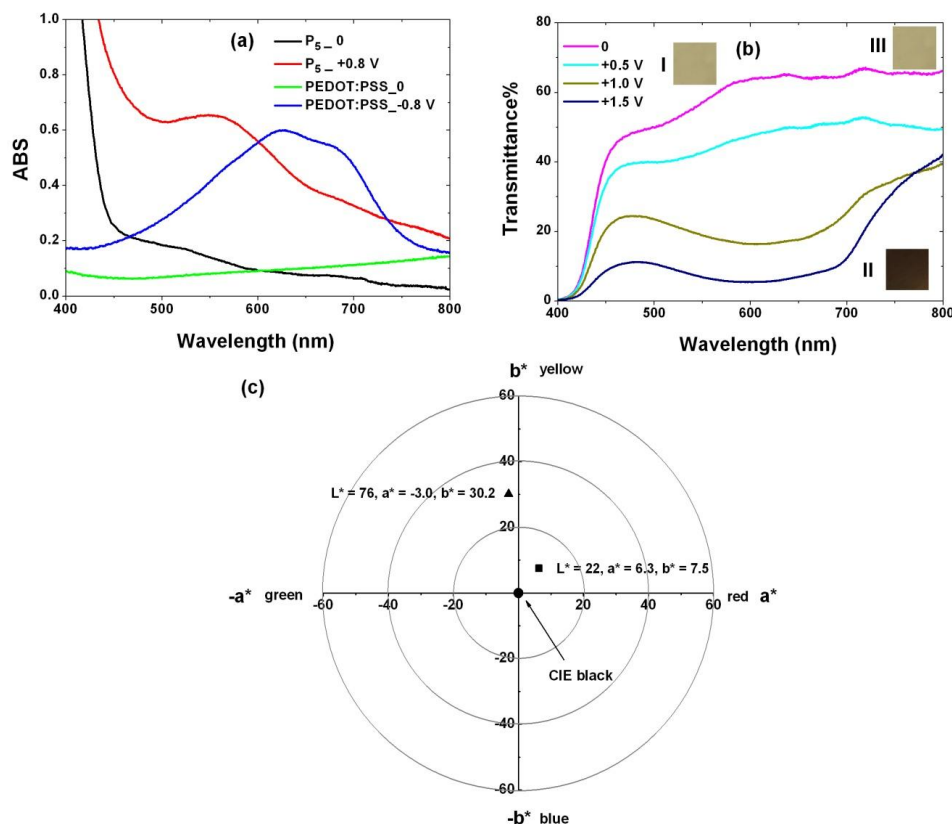


Figure 3.6 Visible spectra of spin-coated (a) P_5 and PEDOT:PSS on ITO/PET in 0.1 M $\text{LiClO}_4/\text{ACN}$ under various potentials, (b) complementary ECD of

P₅/PEDOT:PSS under different potentials (0, + 0.5, + 1.0, + 1.5 V). The insets show the color of spin-coated films (picture taken after placing the ECD on a white paper background) at (I) neutral state before electrochemical switching; (II) electrochemically oxidized; (III) neutral after electrochemical switching. (c) CIE diagram of the complementary ECD at (▲) bleached state and (■) colored state.

3.4 Conclusions

A series of carbazole–BTD–azulene copolymers with BTD molar ratio from 0 to 20mol% were synthesized via Suzuki coupling reactions. These polymers exhibit relatively high EC contrasts and wide absorption in the visible region. As electron acceptor, BTD facilitates electron removal from azulene and carbazole units upon oxidation due to D–A effect and thus leads slightly lower oxidation potentials of the copolymers than that of the carbazole–azulene alternating copolymer. The reduced oxidation potential leads to enhanced EC contrasts at relatively low potentials. In addition, the switching speed of the terpolymer **P₅** is also faster than that of the alternating copolymer **P₀**, which is possibly due to the conformational change of polymer backbone attributed to the random inclusion of BTD. A complementary ECD was fabricated using **P₅** as anodic coloring layer and PEDOT:PSS as cathodic coloring layer, exhibits black-to-transmissive electrochromism, as well as high contrast.

4. Electrofluorochromic Detection of Cyanide Anion Using A Benzothiadiazole-Containing Conjugated Copolymer

4.1 Introduction

As introduced in Chapter 1 and 2, the EFC conjugated polymers allow adjusting the fluorophores' electronic structure through redox reactions induced by electrochemical potential. Thus, the EFC CPs are good candidates for sensors, in which active component (receptor) mediates with an analyte, such as a specific type of ions, giving responses that indicate the presence of the analyte as well as its concentration. By adjusting electronic structures of the fluorophores, the responses may be magnified to achieve more sensitive detection.

Due to the extreme toxicity of cyanide anion (CN^-), CN^- detection has attracted much attention and varieties of detection methods have been developed, including titrimetric,¹⁸⁹ electrochemical (potentiometric and amperometric),¹⁹⁰⁻¹⁹² optical (colorimetric and fluorometric) methods,¹⁹³ etc. Among them, optical methods, which monitor the change in color (absorption intensity or wavelength, colorimetric method) and/or fluorescence intensity (or emission wavelength, fluorometric method), have been studied actively due to the ease and low cost. For these conventional cyanide sensors, the detection results are obtained via chemical reaction or interaction of receptor with CN^- . The hypothesis is to design an EFC detection method which combines both optical and electrochemical

methods, and thus provides dual signals that may provide more accurate and reliable results. Hence, a possible approach is to make use of EFC CPs as receptor for EFC detection of cyanide.

As mentioned in the Chapter 1, the nucleophilic attack of CN^- to electron-deficient compounds, such as benzothiadiazole,³⁰ offers an effective detection approach that makes use of the strong nucleophilicity of CN^- . Enlightened by the CN^- detection method utilizing electron-deficient compounds, as well as promising sensing ability of EFC CPs, in this work, we designed and synthesized a novel conjugated copolymer (**EFP_C**) that contains benzothiadiazole (BTD) as receptor. The EFC properties of **EFP_C** and its capability for sensitive yet selective detection of CN^- were demonstrated. To the best of our knowledge, this is the first demonstration of EFC detection of CN^- , and EFC detection of other chemicals was also rarely reported.

4.2 Experimental

4.2.1 Materials

3-Bromocarbazole were purchased from TCI and used as received. 3-Hexylthiophene-2-boronic acid pinacol ester, [1,1'-Bis(diphenylphosphino)ferrocene]dichloropalladium(II) ($\text{Pd}(\text{dppf})\text{Cl}_2$), and bis(pinacolato)diborane were purchased from Aldrich and used as received. The other chemicals are the same as that reported in the previous chapter. 3-Bromo-9-octylcarbazole¹⁹⁴ was synthesized according to literature.

4.2.2 Chemical characterization

NMR spectra (^1H and ^{13}C) and size exclusion chromatography (SEC) results were obtained using the same equipment and conditions as reported in the previous chapter. Mass spectroscopy of the compounds was measured by Finnigan LCQ Mass Spectrometer. Elemental analysis of the polymer was conducted on an Elementar Vario Micro Cube for C, H, N and S determination. Absorption (ABS) spectra of the polymer were measured using a Shimadzu UV-3600 UV-vis-NIR spectrophotometer. Photoluminescence (PL) spectra of the polymer were recorded using a Perkin Elmer LS-55 fluorescence spectrometer. Differential scanning calorimetry (DSC) thermogram of the copolymer was recorded on a TA Instruments DSC Q10 using N_2 as a purge gas at a heating rate $10\text{ }^\circ\text{C min}^{-1}$.

4.2.3 Synthesis

Compound **1**. To a 50 mL Schlenk tube 3-bromo-9-octylcarbazole (716.6 mg, 2.00 mmol), 2,1,3-benzothiadiazole-4,7-bis(boronic acid pinacol ester) (388.1 mg, 1.00 mmol), Aliquat[®] 336 (0.15 g) and toluene (8 mL) were added. After all the monomers were dissolved, Na_2CO_3 aqueous solution (2 M, 6 mL) was added. Followed by degassing of the mixture, $\text{Pd}(\text{PPh}_3)_4$ (11.6 mg, 0.01 mmol) was added and then the tube was sealed using a rubber stopper bound by a cable stripper. The mixture was stirred and refluxed at $110\text{ }^\circ\text{C}$ for 24 h. After reaction, the organic layer was separated and then the solvent was removed under reduced pressure. The crude product was purified over silica gel column chromatography

using hexane/dichloromethane (DCM) (v/v, 3:2) as eluent. The final product was obtained as brightly orange solid (95%). ^1H NMR (ppm): δ = 8.72 (s, 2H), 8.21 (d, 2H), 8.15 (d, 2H), 7.93 (s, 2H), 7.58 (d, 2H), 7.51 (t, 2H), 7.46 (d, 2H), 7.28 (t, 2H), 4.37 (t, 4H), 1.94 (m, 4H), 1.27-1.46 (m, 20H), 0.88 (t, 6H). ^{13}C NMR (ppm): δ = 155.1, 141.4, 140.9, 133.8, 128.9, 128.3, 127.5, 126.2, 123.7, 123.6, 121.6, 121.0, 119.4, 109.3, 109.1, 43.7, 32.2, 30.1, 29.8, 29.6, 29.4, 27.7, 23.0, 14.4. MS (ESI) m/z for $\text{C}_{46}\text{H}_{50}\text{N}_4\text{S}$: calcd, 690.4; found, 690.4.

Compound **2**. NBS (373.8 mg, 2.1 mmol) was added into the solution of compound **1** (689.0 mg, 1.00 mmol) dissolved in DCM (20 mL), and the mixture was stirred overnight at room temperature. After reaction, the solvent was removed under reduced pressure and the crude product was purified over silica gel column chromatography using hexane/DCM (3:2) as eluent. The final product was obtained as brightly orange solid (85%). ^1H NMR (ppm): δ = 8.67 (s, 2H), 8.31 (s, 2H), 8.16 (d, 2H), 7.91 (s, 2H), 7.57 (d, 4H), 7.32 (d, 2H), 4.33 (t, 4H), 1.91 (m, 4H), 1.27-1.46 (m, 20H), 0.87 (t, 6H). ^{13}C NMR (ppm): δ = 155.0, 141.1, 140.0, 133.6, 129.3, 128.9, 128.3, 128.2, 125.3, 123.7, 122.7, 121.8, 112.3, 110.7, 109.4, 43.8, 32.2, 30.1, 29.7, 29.5, 29.4, 27.8, 23.0, 14.4. MS (ESI) m/z for $\text{C}_{46}\text{H}_{48}\text{N}_4\text{SBr}_2$: calcd, 848.2; found, 848.2.

Compound **3**. A mixture of compound **2** (848.8 mg, 1.00 mmol), bis(pinacolato)diborane (533.3 mg, 2.10 mmol), potassium acetate (KOAc) (588.8 mg, 6.00 mmol), and Pd(dppf)Cl_2 (73.2 mg, 0.10 mmol) in degassed DMF (20 mL) was stirred overnight at 80 °C under nitrogen atmosphere. After cooled to room temperature, water and chloroform (CHCl_3) were added to the mixture, and

the separated organic layer was washed with brine and water and dried over anhydrous MgSO_4 . After the removal of the solvent under reduced pressure, the residue was purified over silica gel column chromatography using hexane/DCM (v/v, 3:2) as eluent to give compound **3** as a brightly orange solid (65%). ^1H NMR (ppm): δ = 8.82 (s, 2H), 8.73 (s, 2H), 8.18 (d, 2H), 7.97 (d, 2H), 7.92 (s, 2H), 7.57 (d, 2H), 7.44 (d, 2H), 4.36 (t, 4H), 1.93 (m, 4H), 1.27-1.47 (m, 44H), 0.88 (t, 6H). ^{13}C NMR (ppm): δ = 155.0, 143.5, 140.9, 133.7, 132.8, 129.4, 128.4, 128.3, 127.6, 125.9, 124.0, 123.3, 121.9, 109.2, 108.7, 43.7, 32.2, 30.1, 29.8, 29.6, 29.4, 27.7, 25.3, 23.0, 14.4. MS (ESI) m/z for $\text{C}_{58}\text{H}_{72}\text{N}_4\text{SO}_4\text{B}_2$: calcd, 942.5; found, 942.5.

Compound 4. To a 50 mL Schlenk tube 3,6-dibromo-9-octylcarbazole (437.2 mg, 1.00 mmol), 3-hexylthiophene-2-boronic acid pinacol ester (588.5 mg, 2.00 mmol), Aliquat[®] 336 (0.15 g) and toluene (8 mL) were added. After all the monomers were dissolved, Na_2CO_3 aqueous solution (2 M, 6 mL) was added. Followed by degassing of the mixture, $\text{Pd}(\text{PPh}_3)_4$ (11.6 mg, 0.01 mmol) was added and then the tube was sealed using a rubber stopper bound by a cable stripper. The mixture was stirred and refluxed at 110 °C for 24 h. After reaction, the organic layer was separated and then the solvent was removed under reduced pressure. The crude product was purified over silica gel column chromatography using hexane as eluent. The final product was obtained as colorless oil (92%). ^1H NMR (ppm): δ = 8.10 (d, 2H), 7.45 (s, 2H), 7.32 (d, 2H), 7.27 (d, 2H), 7.03 (d, 2H), 4.31 (t, 2H), 2.75 (t, 4H), 1.90 (m, 2H), 1.68 (m, 4H), 1.26-1.43 (m, 22H), 0.85 (t, 9H). ^{13}C NMR (ppm): δ = 141.4, 139.4, 139.0, 132.8, 130.0, 123.9, 122.3,

121.3, 120.6, 110.0, 43.7, 32.2, 32.1, 31.5, 30.1, 29.8, 29.7, 29.6, 29.4, 29.3, 27.8, 27.3, 23.0, 14.4. MS (ESI) m/z for $C_{40}H_{53}NS_2$: calcd, 611.4; found, 611.3.

Compound **5**. NBS (373.8 mg, 2.1 mmol) was added in portions to the solution of compound **4** (612.0 mg, 1.00 mmol) in $CHCl_3$ /acetic acid (5 mL / 5 mL) at 0 °C in 1 h. The mixture was then stirred at 0 °C for 1 more hour and then at room temperature overnight. Then water and $CHCl_3$ was added into the mixture. The organic layer were separated and washed with NaOH aqueous solution, and then dried over magnesium sulfate. After the solvent was removed under reduced pressure, the crude product was purified over silica gel column chromatography using hexane as eluent. The final product was obtained as colorless oil (72%). 1H NMR (ppm): δ = 8.06 (s, 2H), 7.48 (d, 2H), 7.42 (d, 2H), 6.97 (s, 2H), 7.32 (t, 2H), 2.63 (t, 4H), 1.91 (m, 2H), 1.62 (m, 4H), 1.25-1.44 (m, 22H), 0.86 (t, 9H). ^{13}C NMR (ppm): δ = 140.8, 140.7, 139.3, 132.4, 128.0, 125.0, 123.2, 121.8, 109.9, 109.3, 43.8, 32.2, 32.0, 31.3, 30.1, 29.7, 29.6, 29.5, 29.4, 29.0, 27.7, 27.3, 23.0, 14.4. MS (ESI) m/z for $C_{40}H_{51}NS_2Br_2$: calcd, 769.2; found, 769.2.

Polymer **EFP_C**. To a 25 mL Schlenk tube compound **3** (471.5 mg, 0.50 mmol), compound **5** (384.9 mg, 0.50 mmol), Aliquat[®] 336 (0.10 g) and toluene (4 mL) were added. After all the monomers were dissolved, Na_2CO_3 aqueous solution (2 M, 3 mL) was added. Followed by degassing of the mixture, $Pd(PPh_3)_4$ (5.8 mg, 0.005 mmol) was added and then the tube was sealed using a rubber stopper bound by a cable stripper. The mixture was stirred and refluxed at 110 °C for 72 h. After reaction, the organic layer was separated and then the solvent was removed under reduced pressure. The crude product was dissolved in a very small amount

of chloroform and then dropped into excess methanol (100 mL) for precipitation. The obtained precipitate was filtered and dried under vacuum. The precipitate was finally washed with acetone using a Soxhlet extractor for 2 days and dried in a vacuum oven at 40 °C for 2 days. Then the final product (**EFP_C**) was obtained as orange solid (87%). ¹H NMR: δ = 8.77 (m, 2H), 8.45 (m, 2H), 8.26 (m, 2H), 8.17 (m, 2H), 7.91 (m, 2H), 7.81 (m, 2H), 7.33-7.64 (m, 10H), 4.32 (m, 6H), 2.79 (m, 4H), 1.92 (m, 6H), 1.61 (m, 4H), 1.29 (m, 42H), 0.89 (m, 15H) ppm. ¹³C NMR: δ = 143.2, 141.3, 140.8, 140.5, 139.5, 133.7, 129.7, 129.2, 128.4, 127.9, 126.7, 126.3, 125.9, 125.0, 124.6, 124.0, 123.7, 123.4, 121.8, 121.6, 118.0, 109.5, 109.3, 109.1, 43.8, 32.2, 32.1, 31.5, 29.8, 29.7, 29.6, 29.5, 29.1, 27.7, 23.0, 14.4 ppm. Anal Calcd for C₈₆H₉₉N₅S₃: C, 79.5; H, 7.7; N, 5.4; S, 7.4. Found: C, 78.8; H, 7.4; N, 5.3; S, 7.4.

4.2.4 Cyclic voltammetry and spectroelectrochemical characterization

Polymer **EFP_C** was dissolved in *p*-xylene (20 mg/mL) and then spin-coated (1000 rpm) onto indium tin oxide (ITO) electrodes laminated on poly(ethylene terephthalate) (PET) substrates (ITO/PET, 100 Ω/sq) to form **EFP_C/ITO/PET**. The thickness of the spin-coated film was controlled at around 100 nm, which was measured using an Alpha-Step IQ surface profiler. The cyclic voltammetry (CV) of **EFP_C/ITO/PET** was carried out in a three-electrode cell, with platinum (Pt) wire as counter electrode, silver (Ag) wire as reference electrode, and 0.1 M LiClO₄/ACN as electrolyte, respectively, using an Autolab PGSTAT302 electrochemical workstation. In spectroelectrochemical characterization, the **EFP_C/ITO/PET** was placed in a three-electrode cell using Pt wire as counter and

Ag wire as reference electrode, respectively, and 0.1 M LiClO₄/ACN as electrolyte in a quartz cuvette. With the same Autolab electrochemical workstation, the Shimadzu UV-3600 UV–vis–NIR spectrophotometer was used to acquire absorption spectra, and the Perkin Elmer LS-55 fluorescence spectrometer to acquire PL spectra. For both electrochemical and spectroelectrochemical characterization, the pseudo-reference silver wire was calibrated vs. Fc/Fc⁺ by dissolving ferrocene in the electrolyte solution.

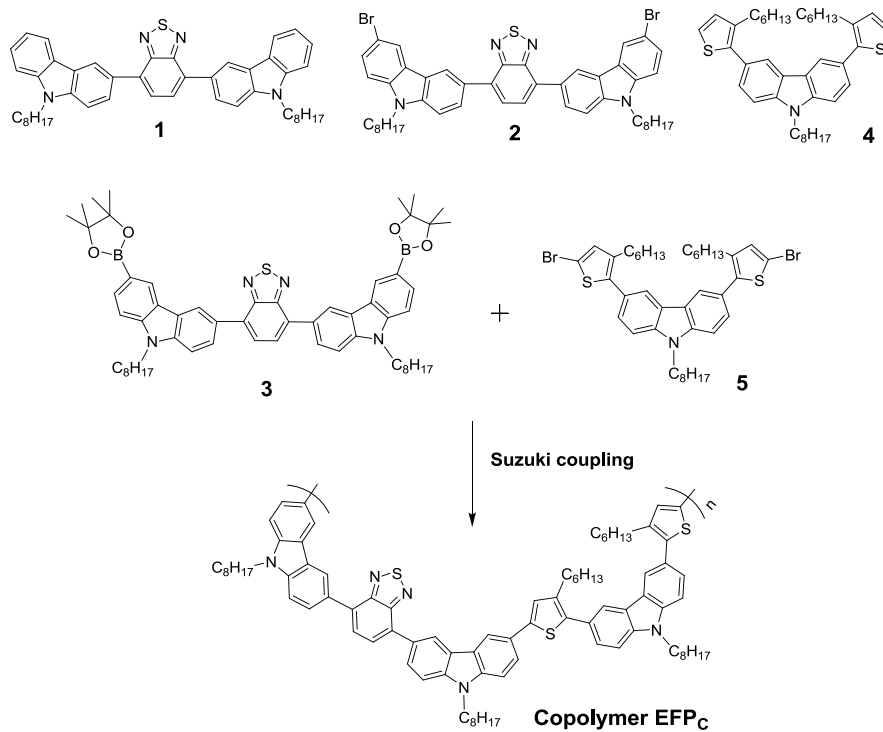
4.3 Results and discussion

4.3.1 Synthesis and structural characterization

Scheme 4.1 shows the chemical structure of compounds **1** to **5** and the synthesis route of copolymer **EFP_C**. It can be seen that besides BTd, **EFP_C** also contains N-octyl-3,6-carbazole (C) and 3-hexylthiophene (HT) units. Carbazole is a common electron donor, which is often used as a fluorophore in conjugated copolymers due to its ease in functionalization on N position for improving solubility as well as its good hole-transport ability.^{125, 128} 3-Hexylthiophene is incorporated to act as fluorophore separator and to enhance solubility as well. Both monomers are of A–B–A type and thus give an alternating copolymer, poly(C-BTD-C-co-HT-C-HT), via Suzuki coupling. The structures of the compounds were verified by NMR and mass spectroscopy. The structure of **EFP_C** was characterized by NMR spectroscopy and elemental analysis. In the ¹H NMR spectrum of **EFP_C** (Figure 4.1), the peak at 4.32 ppm corresponds to the H atoms that are bonded to N atom in carbazole (N–CH₂), while the peak at 2.79 ppm

corresponds to the H atoms from CH₂ that is directly bonded to the thiophene ring (C–CH₂). The integration ratio of the two peaks is 3/2, which is highly consistent with that calculated from the repeating unit structure of **EFP_C**, confirming the successful synthesis of the copolymer.

SEC measurement of **EFP_C** gives the apparent number-average molecular weight $M_n = 13,400$ Da, with polydispersity index (PDI) of 1.10. Thus, based on the calculated repeating unit weight (~1,300 Da), each polymer chain contains ca. 10 repeating units. **EFP_C** shows good solubility in common solvents such as chloroform, DCM, toluene and *p*-xylene, which is attributed to the alkyl side chains from carbazole and thiophene units. An obvious melting peak at around 135 °C is observed in the DSC thermogram of **EFP_C** (see page 137 in Appendix), indicating it is semi-crystalline. The semi-crystalline nature of the copolymer can be attributed to its regular alternating structure. The T_g of **EFP_C** is around 100 °C as obtained from the DSC thermogram. Thus, the work temperature of this copolymer (room temperature) is well below T_g during the electrofluorochromic detection of CN[−].



Scheme 4.1 Structures of compound **1** to **5** and the synthesis route of copolymer **EFP_C**.

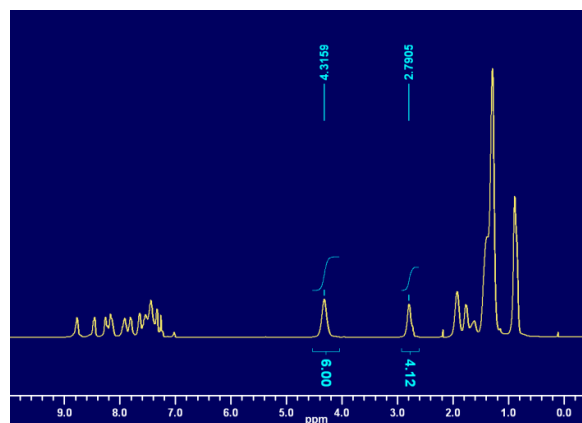


Figure 4.1 ¹H NMR spectra of copolymer **EFP_C** in CDCl₃

4.3.2 Optical and electrochemical properties

Figure 4.2 shows UV-vis absorption and photoluminescence (PL) spectra of **EFP_C** in solution and thin film form, respectively. The solution of **EFP_C** exhibits an absorption band at 315 nm, a shoulder at 350 nm and another band at 450 nm. Similarly, the **EFP_C** thin film shows a slightly weaker absorption band at 315 nm and a shoulder at 350 nm. The band at 450 nm for the solution is, however, red shifted to 465 nm for the thin film, which is probably due to inter-chain π - π stacking in the thin film caused by its more densely packed structure. The absorption band at 315 nm corresponds to carbazole segments for both thin film and solution, while the band at 465 nm for thin film (450 nm for solution) can probably be attributed to π - π^* transition of C-BTD-C moiety.^{125, 195} The shoulder at 350 nm possibly arises due to the interactions between HT and carbazole units. Despite the slight red shift for the absorption band corresponding to BTD, the PL peaks obtained by exciting at 450 nm for the solution and 465 nm for the film are at the same wavelength of 580 nm. It is worth noting that the thin film is still highly fluorescent, i.e., the quenching caused by inter-chain interactions is insignificant. As mentioned previously, HT units play the role of separators for fluorophores, which not only separate C-BTD-C moieties in the main chain, but also prevent π - π stacking between adjacent chains using its alkyl side chains. Furthermore, the alkyl side chains from carbazole units also help to reduce the chance of inter-chain π - π stacking.

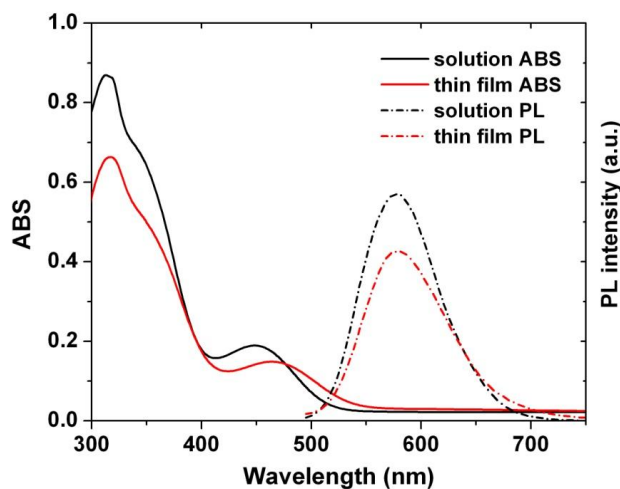


Figure 4.2 Absorption and PL spectra of **EFP_C** dissolved in CHCl₃ and spin-coated thin film on plain glass (λ_{exc} : 450 nm for solution and 465 nm for film).

Cyclic voltammograms of the **EFP_C** thin film spin-coated on ITO/PET (**EFP_C/ITO/PET**) in 0.1 M LiClO₄/acetonitrile (ACN) are shown in Figure 4.3. It is observed that **EFP_C** shows an oxidation peak at 0.94 V and a shoulder peak at 1.10 V, and two reduction peaks at 0.52 and 0.80 V, respectively. Two pairs of redox peaks are typical in cyclic voltammograms of CPs containing N-alkyl substituted 3,6-carbazole, corresponding to the radical cation and dication states, respectively.¹¹⁹ It is interesting to note that the two oxidation (shoulder) peaks are fairly close to each other, indicating a relatively easy transition from the state of radical cation to dication. This phenomenon can be attributed to the electron-deficient BTB that plays the role of electron acceptor, facilitating electron removal from electron-rich carbazole and reducing its oxidation potential.³⁶

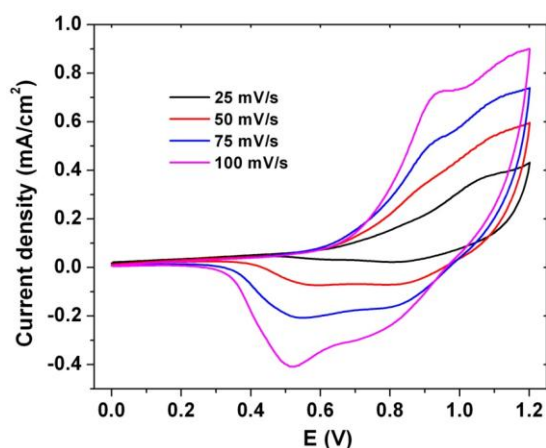


Figure 4.3 Cyclic voltammograms of **EFP_C**/ITO/PET in 0.1 M LiClO₄/ACN at different scan rates (25, 50, 75 and 100 mV/s)

4.3.3 Electrochromic and electrofluorochromic properties

EFP_C exhibits both electrochromism and electrofluorochromism. The intensity of the absorption peak at 465 nm increases with positive potential owing to oxidation (Figure 4.4a), and it can be repeatedly switched by applying an oscillating potential (Figure 4.4b). Upon increasing positive potential, the PL intensity of **EFP_C** is gradually reduced due to oxidative quenching, as shown in Figure 4.4c. The PL intensity starts to reduce at 0.6 V, and falls to as low as about 20% of the maximum value at 1.0 V. This is consistent with previously discussed CV results that the oxidation becomes significant when the potential exceeds the first oxidation peak at 0.94 V. The fluorescence could recover when a negative potential is applied, and the switching is repeatable (Figure 4.4d). The fluorescence quenching of **EFP_C** is due to electrochemical oxidation as when

photo-excited, the oxidized chains would undergo non-radiative exciton decay, rather than energy relaxation via a radiative pathway.⁸ By exciting at 465 nm, the C–BTD–C moiety is likely to be the main fluorophore that determines the fluorescence intensity at different states, whereas the carbazole unit located between the two HT units is believed to play the role of fluorophore separator (together with the two HT units) rather than a fluorophore in the EFC process.

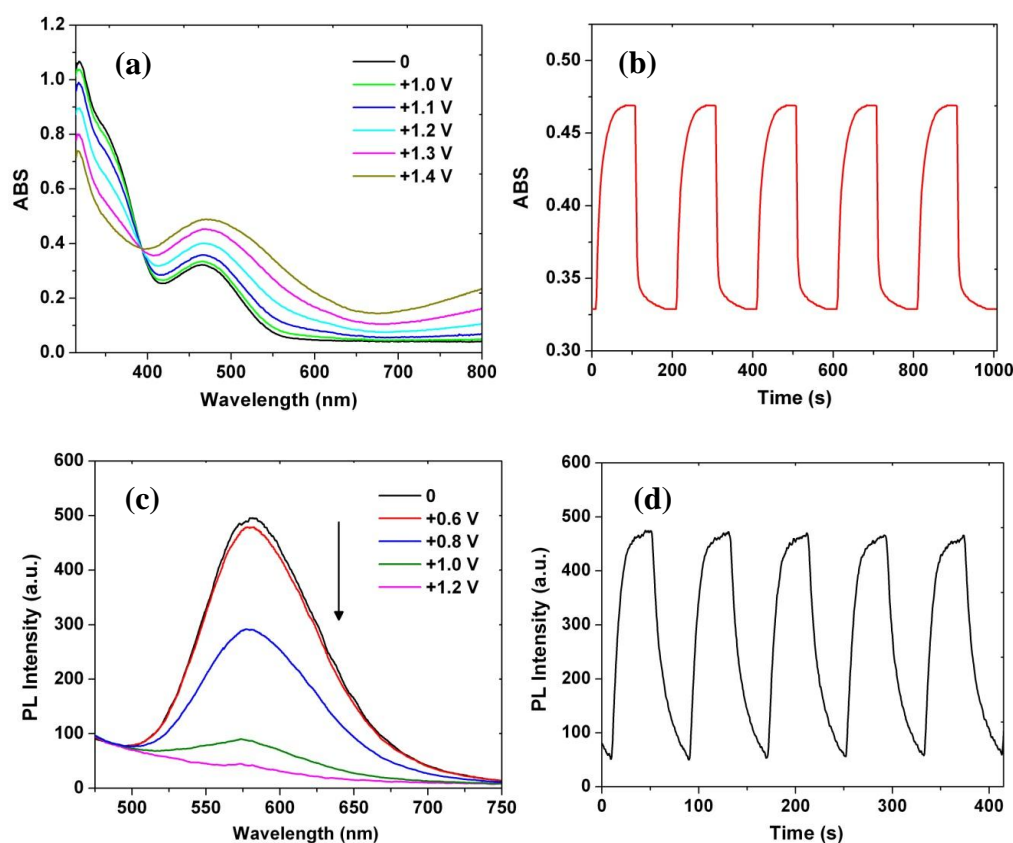


Figure 4.4 (a) Absorption spectra under different potentials, (b) absorption–time profiles ($\lambda_{\text{monitor}} = 465$ nm; switching between 1.4 V and -1.0 V), (c) PL intensity changes ($\lambda_{\text{exc}} = 465$ nm) under potentials different potentials and (d) PL intensity–

time profiles ($\lambda_{\text{exc}} = 465 \text{ nm}$, $\lambda_{\text{monitor}} = 580 \text{ nm}$; switching between 1.2 V and -1.0 V with 80 s per cycle), of **EFP**_C/ITO/PET in 0.1 M LiClO₄/ACN

4.3.4 Cyanide detection

Detection of CN⁻ by fluorescent polymers is commonly conducted in solutions. In this work, we developed a different cyanide detection approach. Firstly, an **EFP**_C/ITO/PET electrode was inserted into a three-electrode electrochemical cell: a quartz cuvette filled with 0.1 M LiClO₄/ACN (reference electrolyte, **R**) with Pt wire as counter electrode and Ag wire as reference electrode, and a fluorescence spectrometer (Perkin Elmer LS-55) was used to record PL intensities ($\lambda_{\text{exc}} = 465 \text{ nm}$, $\lambda_{\text{monitor}} = 580 \text{ nm}$) under a series of positive potentials provided by an electrochemical workstation (Autolab PGSTAT302). When the system reached equilibrium state at zero potential, the stabilized PL intensity was recorded as I_0 . For a certain potential, the ratio of the PL intensity detected at equilibrium state, I , to I_0 is defined as normalized intensity. I/I_0 obtained at different potentials were plotted against potential, E , as shown by the black curve (■) in Figure 4.5a. Then the **EFP**_C/ITO/PET electrode was inserted into another cell that contained **R** with a certain concentration of tetrabutylammonium cyanide (TBACN), and the stabilized PL intensities were recorded under the same series of potentials. The normalized intensities were calculated and plotted against E again. Three I/I_0 - E curves corresponding to cyanide concentrations of 10^{-6} , 10^{-5} and 10^{-4} M , respectively, are shown in Figure 4.5a.

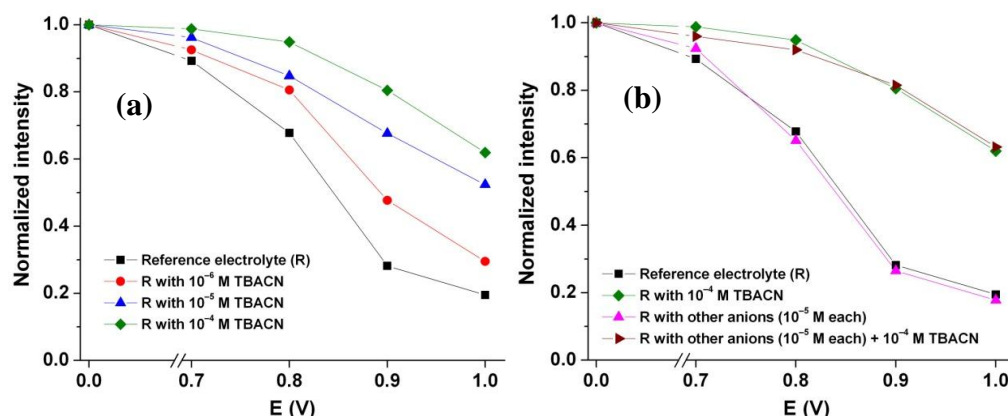


Figure 4.5 Normalized PL intensities ($\lambda_{\text{exc}} = 465$ nm and $\lambda_{\text{monitor}} = 580$ nm) of **EFP_C**/ITO/PET as a function of potential, E. The curves in (a) were obtained with the reference electrolyte (**R**) containing different concentrations of TBACN (0, 10^{-6} , 10^{-5} and 10^{-4} M), and that in (b) were obtained from **R** with 10^{-4} M TBACN as well as **R** + 10^{-4} M TBACN with/without 8 types of TBA-based anions (OH^- , F^- , Cl^- , Br^- , I^- , AcO^- , NO_3^- and HSO_4^- , 10^{-5} M each).

It can be seen that with **R** only, the normalized intensity decreases with increasing positive potential due to oxidative quenching. However, with **R** + TBACN, the normalized intensities are higher than that without TBACN at all positive potentials (0.7 to 1.0 V), indicating that the oxidative quenching is significantly weakened in the presence of TBACN. In particular, it is striking to see that when the potential is above 0.9 V, even 1 μM TBACN can induce a significant change in normalized PL intensity. This phenomenon probably results from the partial reduction of **EFP_C** owing to the interaction between nucleophilic CN^- and electron deficient BTD. From Figure 4.5a it is also observed that the

higher the TBACN concentration, the higher the normalized PL intensity, i.e., the effect of oxidative quenching is weakened more at higher TBACN concentration. Thus, the I/I_0 -E curves corresponding to different cyanide concentrations may be used as calibration curves to determine cyanide concentrations of various analytes. Like in the reference electrolyte, the PL intensity of **EFP_C** in the electrolytes containing TBACN could also be completely recovered under negative potentials (Figure 4.6a). In addition, after cycling in the electrolyte containing TBACN (10^{-4} M), the **EFP_C**/ITO/PET electrode was washed in ACN, and then put into the reference electrolyte again. It could exhibit the original EFC switching curve corresponding to reference electrolyte (Figure 4.6b), indicating that CN^- can be easily removed from the electrode and the interaction between cyanide and BTD is a physical interaction.

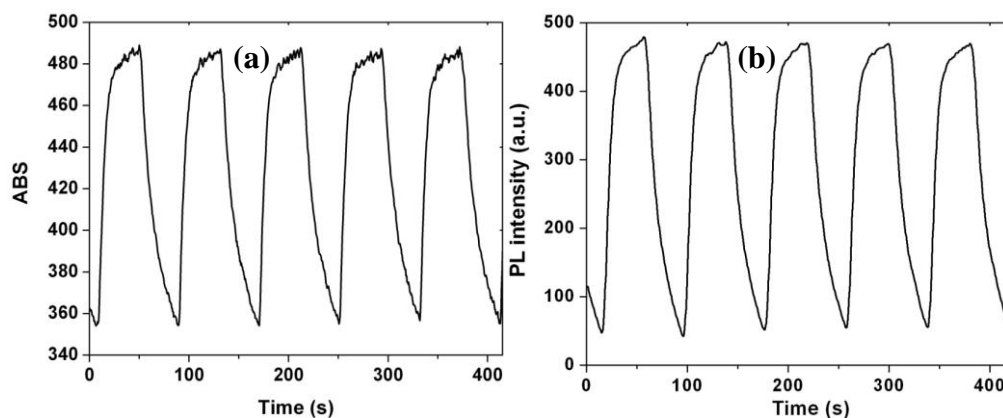


Figure 4.6 PL intensity–time profiles ($\lambda_{\text{exc}} = 465$ nm, $\lambda_{\text{monitor}} = 580$ nm) of (a) **EFP_C**/ITO/PET switched between 1.0 V and –1.0 V in **R** + 10^{-4} M TBACN, and (b) **EFP_C**/ITO/PET that had been taken out from the **R** + 10^{-4} M TBACN after

cycling and washed with ACN before this test. The switching time used was 80 s per cycle.

To check whether CN^- could be selectively detected by this system, other anions including tetrabutylammonium (TBA)-based hydroxide (OH^-), fluoride (F^-), chloride (Cl^-), bromide (Br^-), iodide (I^-), acetate (AcO^-), nitrate (NO_3^-) and bisulfate (HSO_4^-) (10^{-5} M for each type of anion) were added together into the reference electrolyte. As shown in Fig. 4.5b, the PL intensity changes upon oxidative quenching are almost the same for the electrolytes with and without these anions. This confirms that it is CN^- , rather than TBA cation, that dominates the PL intensity of **EFP_C** upon oxidative quenching. Furthermore, by adding higher concentrations of OH^- and F^- (10^{-4} M for each) into **R**, still no significant change in I/I_0 -E curves could be observed (Figure 4.7). This demonstrates that the detection is selective towards CN^- over other common nucleophilic anions. To further verify cyanide selectivity of the system, TBACN (10^{-4} M) was added into the electrolyte containing the eight types of other anions. It is observed that in this electrolyte, the normalized PL intensities of **EFP_C** under various potentials are similar to that in the reference electrolyte containing 10^{-4} M TBACN, further confirming the selectivity of the system towards CN^- . The specific interaction of CN^- with **EFP_C** is probably a type of anion- π interactions. Such energetically favorable non-covalent interactions could exist between an electropositive aromatic ring and a nucleophilic anion.^{196, 197} At oxidized state, BTB ring would be highly electron-deficient. Although OH^- and F^- are also very nucleophilic, only CN^- undergoes significant interaction with oxidized **EFP_C** based on our

results. This may be attributed to the stronger nucleophilicity of CN^- and its triple bond. The triple bond may provide electron-rich π system for non-covalent interaction with electron-deficient π system of BTB, leading to charge transfer between CN^- and BTB ($\pi^- - \pi^+$ interaction) and hence weakening the oxidative quenching.

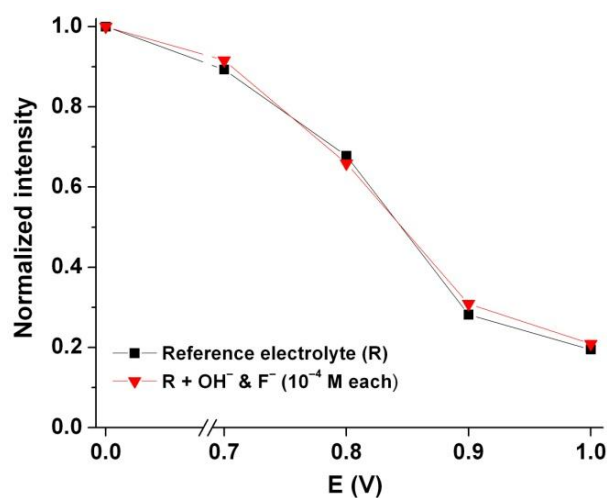


Figure 4.7 Normalized PL intensities ($\lambda_{\text{exc}} = 465 \text{ nm}$ and $\lambda_{\text{monitor}} = 580 \text{ nm}$) of **EFP_c**/ITO/PET as a function of potential, E. The two curves were obtained using the reference electrolyte (**R**) as well as **R** + TBA-based anions (OH^- and F^- , 10^{-4} M each).

4.4 Conclusions

In summary, we have synthesized a new conjugated copolymer that exhibits electrochromic and electrofluorochromic properties. Electrochemical oxidation of the copolymer induces severe fluorescence quenching when the potential is above

0.9 V. Moreover, the fluorescence intensity reduction caused by oxidative quenching becomes significantly smaller when TBACN is added into the electrolyte owing to the strong interactions between nucleophilic CN^- and electron deficient BTB. The detection of CN^- using this system is sensitive and selective, offering a promising route for CN^- sensing. The approach may also be extended to other CPs for detection of other ions or molecules.

5. Nanoporous Carbazole–Benzothiadiazole-Based Copolymer Electrode for Electrofluorochromic Detection of Cyanide Anion

5.1 Introduction

Conjugated polymers (CPs) have been extensively investigated in the past twenty years. Compared with chemical synthetic methods, electrochemical polymerization (electropolymerization) is a relatively easy method towards the preparation of thin films of CPs. As a noncatalytic reaction, electropolymerization offers good reproducibility as the electrodeposition process can be conveniently controlled by the current, potential, CV scan rate, and accumulated charge across the work electrode as well. For electrochemical polymerization, no modification for chemical structure of monomers is required to produce reactive sites, such as halogen (-Cl, -Br, -I), organotin (-SnR₃), and organoboronic acid or ester (-B(OR)₂). In addition, the electropolymerized polymer requires no further purification process and could be directly under electrochemical and spectroelectrochemical characterization. Other than convenient synthesis and processing, electropolymerization leads to various morphologies of the polymer thin film, either compact or loose structure, depending on the electrodeposition condition such as scan rates and electrolyte formulations used, whereas solution processed polymer thin films, such as casted or spin-coated films, usually exhibit flat surface and compact structure. For CPs, loosely packed structure possibly

facilitates ions insertion and extraction during redox processes and thus may enhance the response speed upon external potential loaded.

As introduced previously, cyanide is highly toxic for physiological systems and brings serious environmental concerns. Cyanide containing salts are widespread chemicals found in surface water, not only from industrial waste but also from biological sources. Thus, free CN^- existing in aqueous solutions is the most common state for cyanide pollutants. To make the detection more useful and effective, the cyanide sensors should be designed to work in aqueous environment. In Chapter 4, we reported a carbazole–BTD based EFC conjugated polymer that was demonstrated for use in CN^- detection utilizing its EFC properties. The detection was conducted in electrolytes composed of organic solvent (0.1 M $\text{LiClO}_4/\text{ACN}$) and the detection system offers high sensitivity and selectivity towards CN^- over other anions. However, this EFC polymer does not swell in water due to its high hydrophobicity, and thus limits its cyanide sensing application in aqueous solutions.

To address this issue, in this chapter, we reported another carbazole–BTD based conjugated copolymer that was synthesized via electropolymerization. This copolymer was designed for sensing towards CN^- in partially aqueous solution, as electropolymerization of CPs may lead to nanoporous morphology that shortens the diffusion distance for water (and dissolved CN^-) diffusing into the polymer film with the help of ACN that could swell the polymer. Furthermore, at oxidized state, the polymer may contain radical cations and dications along the backbone, which could help to pull the nucleophilic CN^- into the polymer. The EFC

properties of this electrodeposited polymer were studied and its capability for sensitive and selective detection of CN^- was demonstrated, in the electrolytes using organic solvent (ACN) and mixed solvent ACN/ H_2O (in different volume ratios).

5.2. Experimental

5.2.1 Materials

Tetrabutylammonium hexafluorophosphate (TBAPF_6 , 99%) was purchased from Aldrich and used as received. The other chemicals and solvent used are the same as reported in the previous chapters. 4,7-Bis(6-bromo-9-octylcarbazol-3-yl)-2,1,3-benzothiadiazole (Br-C-BTD-C-Br) was synthesized using the same procedure as reported in Chapter 4.

5.2.2 Chemical and morphological characterization

^1H and ^{13}C NMR spectra were recorded using the same Bruker NMR spectrometer and the same conditions as reported in Chapter 4. High Resolution Mass Spectroscopy (HRMS) of the monomer was measured by Finnigan LCQ Mass Spectrometer. Size exclusion chromatography (SEC) analyses were carried out on a Waters 2690 system using THF as eluent and polystyrene standards. Absorption (ABS) and photoluminescence (PL) spectra of the polymer were measured using Agilent Cary 5000 UV-vis-NIR spectrophotometer and Perkin Elmer LS-55 fluorescence spectrometer, respectively. Surface morphology of the electrodeposited polymer thin film was examined using a Jeol JSM-6340F field-emission scanning electron microscope (FESEM).

5.2.3 Monomer synthesis

To a 50 mL Schlenk tube, Br-C-BTD-C-Br (848.8 mg, 1.00 mmol), 3-hexylthiophene-2-boronic acid pinacol ester (588.5 mg, 2.00 mmol), Aliquat[®] 336 (0.15 g) and toluene (8 mL) were added. After all the compounds were dissolved, Na₂CO₃ aqueous solution (2 M, 6 mL) was added. Followed by degassing of the mixture, Pd(PPh₃)₄ (11.6 mg, 0.01 mmol) was added and then the tube was sealed using a rubber stopper bound by a cable stripper. The mixture was stirred and refluxed at 110 °C for 24 h. After reaction, the organic layer was separated and then the solvent was removed under reduced pressure. The crude product was purified over silica gel column chromatography using hexane/DCM (v/v, 3:2) as eluent. Then monomer (HT-C-BTD-C-HT) was obtained as orange solid (94%). ¹H NMR (ppm): δ = 8.72 (s, 2H), 8.24 (s, 2H), 8.16 (d, 2H), 7.93 (s, 2H), 7.57 (t, 4H), 7.47 (d, 2H), 7.24 (d, 2H), 7.02 (d, 2H), 4.39 (t, 4H), 2.73 (t, 4H), 1.96 (m, 4H), 1.66 (m, 4H), 1.24-1.30 (m, 32H), 0.88 (t, 6H), 0.81 (t, 6H). ¹³C NMR (ppm): δ = 155.1, 141.2, 140.7, 139.3, 138.6, 133.7, 129.7, 129.1, 128.4, 128.0, 127.8, 126.1, 123.6, 123.5, 122.0, 121.8, 109.3, 109.1, 43.8, 32.2, 32.1, 31.5, 29.8, 29.6, 29.1, 27.8, 23.0, 14.5. HRMS (ESI) m/z for C₆₆H₇₈N₄S₃: calcd, 1022.5389; found, 1022.5388.

5.2.4 Electropolymerization, cyclic voltammetry and spectroelectrochemical characterization

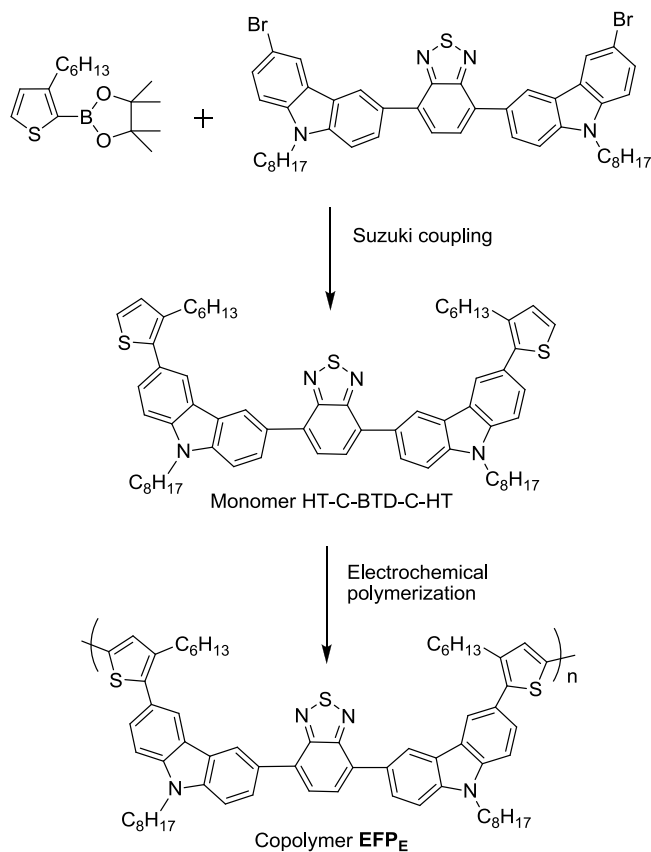
The electrochemical polymerization was carried out in a three-electrode cell: a beaker filled with 0.1 M tetrabutylammonium hexafluorophosphate

(TBAPF₆)/propylene carbonate (PC) as electrolyte (with a small amount of chloroform for fully dissolving the monomer), using indium tin oxide coated glass (ITO glass, 7 Ω /sq) as work electrode, Pt foil as counter electrode, Ag wire as reference, and an Autolab PGSTAT302 as potentiostat. The monomer (HT–C–BTD–C–HT) was dissolved in the electrolyte at a concentration of 0.5 mM, and then electropolymerized via CV method. The CV scan was between 0 and 1.1 V for 50 cycles at the scan rate 100 mV/s. Cyclic voltammograms of the electrodeposited polymer film was then conducted in a three-electrode cell using 0.1 M LiClO₄ dissolved in ACN (and ACN/H₂O in different volume ratios) as electrolyte, the same counter and reference electrodes as used for electropolymerization, and the same potentiostat. The set-up for spectroelectrochemical characterization is similar to that for CV tests except that a quartz cuvette and Pt wire were used to replace the baker and Pt foil, respectively. Absorption and PL spectra were recorded using the same Agilent Cary 5000 UV–vis–NIR spectrophotometer and Perkin Elmer LS-55 fluorescence spectrometer, respectively, under varying potentials provided by the same potentiostat. For both electrochemical and spectroelectrochemical characterization, the pseudo-reference silver wire was calibrated vs. Fc/Fc⁺ by dissolving ferrocene in the electrolyte solution.

5.3. Results and discussion

5.3.1 Synthesis and structural verification

The monomer HT-C-BTD-C-HT was obtained via Suzuki coupling reaction, as shown in Scheme 5.1.



Scheme 5.1 Synthesis route leading to the copolymer, **EFP_E**.

The structure of the monomer has been verified by ^1H MNR spectrum and HRMS. In the ^1H NMR spectrum (Figure 5.1a), the peak at 4.38 ppm corresponds to the H atoms that are bonded to N atom in carbazole (N-CH₂), while the peak at 2.73 ppm corresponds to the H atoms from CH₂ that is directly bonded to the thiophene ring (C-CH₂). The integration ratio of the two peaks is 1:1, which coincides with the ratio calculated from the molecular structure of HT-C-BTD-

C-HT, proving that the compound obtained is the monomer needed. In addition, the HRMS result (as shown in section 5.2.3) further confirms the successful synthesis. This compound shows good solubility in common organic solvents such as chloroform, DCM and toluene. However, its solubility in PC and ACN is not good. Thus, chloroform was added into the electrolyte (0.1 M TBAPF₆/PC) at a certain volume ratio to completely dissolve the monomer for electropolymerization.

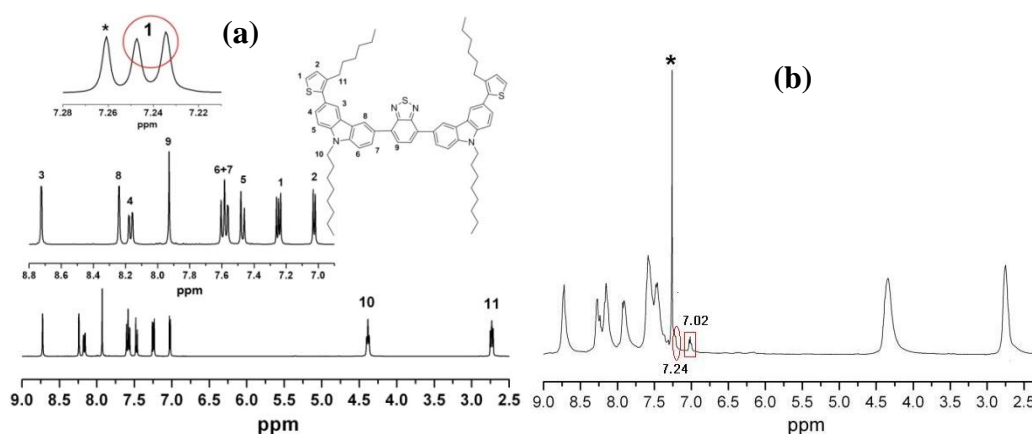


Figure 5.1 ¹H NMR spectra of (a) monomer (HT-C-BTD-C-HT) and (b) electrodeposited copolymer **EFP_E**, dissolved in CDCl₃. Asterisk indicates the peak of CDCl₃.

The electrochemical oxidative coupling reaction between the monomers creates linkages at 5-position between thiophene rings, leading to a conjugated copolymer, **EFP_E**, which is composed of -HT-C-BTD-C-HT- repeating units, as shown in Scheme 5.1. Broadened proton peaks in ¹H NMR spectrum of **EFP_E** (Figure 5.1b), rather than sharp ones of monomer (Figure 5.1a), supports the

successful coupling between monomer units as the broadened peaks are characteristics of polymers. Figure 5.2 shows cyclic voltammograms of the electropolymerization. For the first cycle, the oxidation peak appear at around 0.95 V corresponds to the oxidation of HT-C-BTD-C-HT at 5-position of 3-hexylthiophene units. In the subsequent cycles, increasing current densities indicate the oxidative polymerization progress of the monomers that were coupled to form π -conjugated copolymers on the ITO glass. Reduction of the oxidation and reduction current densities onsets with increasing number of cycles reveals the extension of effective conjugation length in the polymer backbone.⁴⁴ It is observed from the inset of Figure 5.2a that a shoulder peak at about 0.85 V emerges since the second cycle. This shoulder should correspond to the radical cation of the newly formed oligomer/polymer as it agrees with characteristic of conjugated polymers containing 3,6-carbazole¹¹⁹ and thus further confirms the successful coupling of monomers. Attributed to the side alkyl chains from carbazole and HT units, the electropolymerized copolymer **EFP_E** can be dissolved in organic solvents such as chloroform, DCM, and toluene.

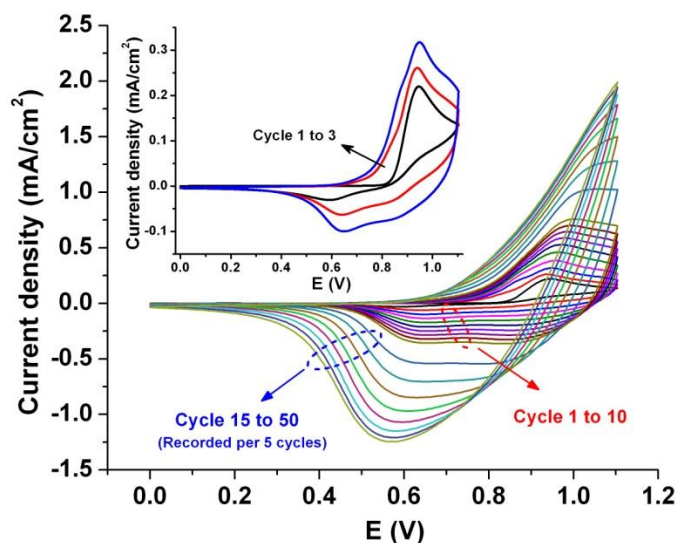


Figure 5.2 Cyclic voltammograms for the electrodeposition on ITO glass. HT-C-BTD-C-HT (0.5 mM) was dissolved in the electrolyte of 0.1 M TBAPF₆/PC, and the scan rate was 100 mV/s.

It is important to note that the peak at 7.24 ppm (doublet, circled in Figure 5.1a) that corresponds to H atom from 5-position of 3-hexylthiophene is weakened to one with very low intensity (as indicated by the ellipse in Figure 5.1b) for the electrodeposited film. This directly indicates the successful coupling of monomers, i.e., linkages are created at 5-position between 3-hexylthiophene rings. However, it is worth noting that the peak at 7.02 ppm (as indicated by the rectangle in Figure 5.1b) that corresponds to 4-position of 3-hexylthiophene is strongly weakened, in comparison with the corresponding one in Figure 5.1a. This phenomenon implies the electrochemical polymerization is achieved via α (5-position)- β (4-position) coupling, rather than exclusively α - α coupling, which may

lead to crosslinked polymer chains.^{198, 199} SEC measurement of the electrodeposited copolymer gives the apparent number-average molecular weight $M_n = 7,000$ Da, with polydispersity index (PDI) 1.38. The SEC results reveal that on average a polymer chain contains around seven repeating units.

Figure 5.3 shows UV-vis absorption (ABS) spectra of **EFPE** (solution and thin film) and monomer (HT-C-NSN-C-HT) solution. The polymer solution exhibits a strong absorption band at 310 nm, a shoulder at 365 nm and another band at 440 nm. For the monomer solution, two absorption bands present at 310 nm and 440 nm, respectively. Also, the emergence of two absorption bands at 350 nm and 365 nm, respectively, is observed, albeit very weak. As discussed in Chapter 4, the band at 350 nm is possibly due to the carbazole-HT interaction, for both monomer and polymer solutions. And the band at 365 nm may also be attributed to HT units, as this band for **EFPE** is very strong, probably attributed to HT-HT interaction where the HT units from the monomer, HT-C-BTD-C-HT, are bonded to one another. This further confirms the successful electropolymerization of **EFPE**.

Similarly, the thin film of **EFPE** shows an absorption band at 315 nm, a shoulder at 365 nm and another band at 450 nm. The absorption bands at 315 nm for the thin film and 310 nm for the solutions of polymer and monomer correspond to carbazole segments, while the bands at 450 nm for the film and 440 nm for solutions are probably attributed to π - π^* transition of C-BTD-C moiety.¹²⁵ The shoulder at 365 nm for thin film possibly arises because of the interactions between HT and carbazole units, as discussed in the last paragraph.

The thin film exhibits an obvious 10 nm red-shift for the band at 450 nm from 440 nm (for the solution) to, in comparison with the band at 440 nm for the solution, probably due to the inter-chain π - π stacking of C-BTD-C moiety caused by the denser packing of polymer chains in the thin film.

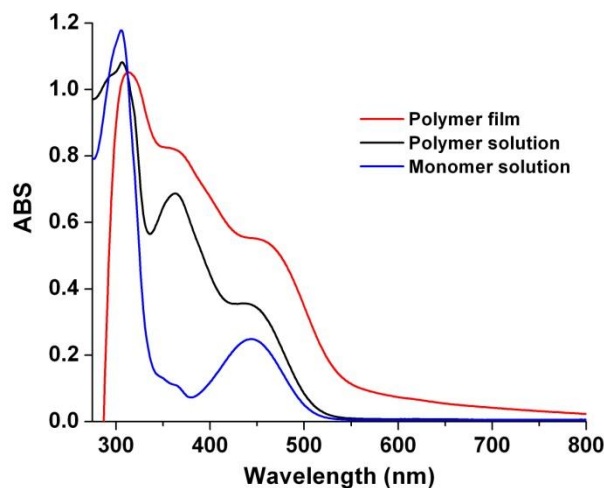


Figure 5.3 Absorption spectra of the electrodeposited **EFP_E** film, and the solution of that polymer and monomer dissolved in chloroform, respectively.

5.3.2 Effect of morphology on electrochemical properties

The surface morphology of the copolymer films electrodeposited on ITO glass electrode was observed using FESEM. As shown in Figure 5.4a and b, the obtained polymer film exhibits granular and porous surface morphology. The surface morphology is possibly affected by the electrolyte solvent. To study the effect of electrolyte to electropolymerization, 0.1 M TBAPF₆/ACN (with a very small amount of chloroform, E-ACN) was prepared and used to compare with 0.1 M TBAPF₆/PC (with a very small amount of chloroform, E-PC) and FESEM

images (Figure 5.4c and d) shows the surface morphology of the corresponding polymer film obtained using this electrolyte. In Figure 5.4, it is observed that the electrodeposited polymer film obtained from E-PC exhibits smoother surface with more uniform granules of smaller size (ca.150–250 nm), compared with that obtained from E-ACN (granule size: ca. 300–500 nm). Thus, this result proves that the surface morphology of the electrodeposited polymer film could be affected by the electrolyte solvents. As the granule formation is due to the nucleation growth of polymer chains, the larger granule size for E-ACN indicates that ACN is likely more favorable for polymer chain nucleation and growth than PC.

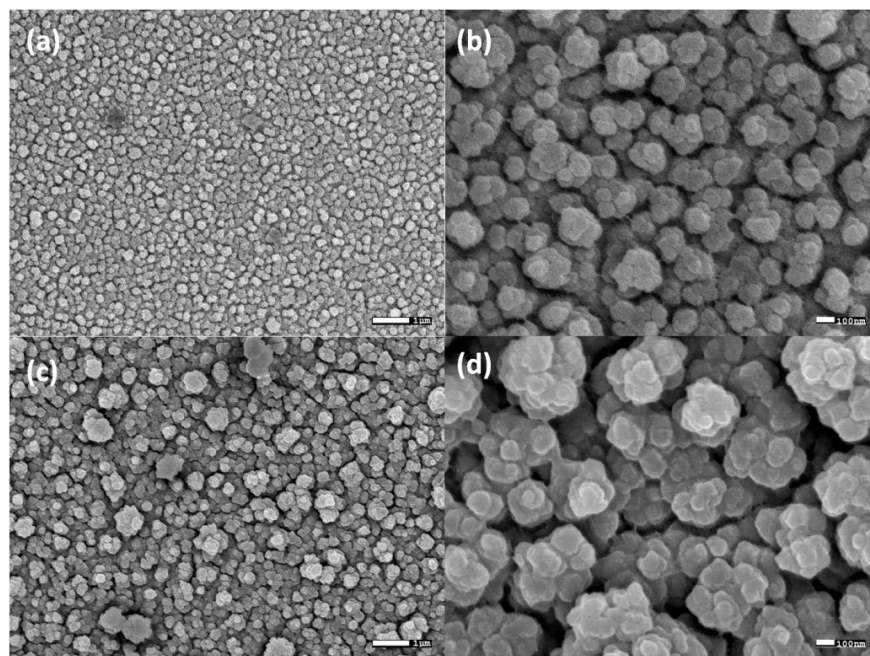


Figure 5.4 FESEM images for the surface of **EFP_E** film electrodeposited using E-PC with magnification of (a) 10k and (b) 50k, and for that using E-ACN with

magnification of (c) 10k and (d) 50k. The scan rate was 100 mV/s for the electrodeposition in each electrolyte.

Such nanoporous structure potentially facilitates insertion and extraction of ions across the polymer film, in particular, during the redox process. However, in the electrochemical test, the electrodeposited polymer film obtained from E-ACN could easily swell in the electrolyte (e.g., LiClO₄/ACN), followed by cleavage and peeling off from the ITO glass after a short time. The instability makes such film not suitable for sensing applications. This is the reason why E-PC was chosen for electrodeposition instead of E-ACN. Furthermore, too large granule would lead to a small surface to volume ratio, and therefore possibly reduce its surface contact with analyte for cyanide detection. As a result, the sensitivity of cyanide detection would be reduced.

Cyclic voltammograms of the polymer thin film electrodeposited on ITO glass are shown in Figure 5.5a. It is observed that **EFP_E** shows an oxidation peak at 0.88 V, a weak shoulder at 0.76 V, and a reduction peak at 0.60 V. Two pairs of redox peaks corresponding to the radical cation and dication states, respectively, usually present in cyclic voltammograms of CPs containing N-alkyl substituted 3,6-carbazole.¹¹⁹ For **EFP_E**, only one pair of two redox peaks is obvious, while the other pair is not, the second oxidation peak appears as a weak shoulder and another reduction peak could not be observed which is probably too weak and therefore overlapped by the main one. The shoulder oxidation peak is ~0.12 V lower than the main one. This very small difference indicates an easy transition from radical cation to dication state. It could be attributed to the electron acceptor

BTD which is between two carbazole units and facilitates electron removal from electron-rich carbazole and thus reduces the oxidation potential.²⁰⁰ The anodic and cathodic peak current densities against the scan rate and square root of scan rate are extracted and plotted as Figure 5.5b and c, respectively. The nearly linear relationship between the peak current densities and scan rate, and non-linear relationship between the peak current densities and square root of scan rate, indicate that the redox behavior of the polymer is close to a non-diffusion-controlled process. This is possibly attributed to the nanoporous structure (as revealed by Figure 5.4) that probably facilitates mobility of ions across the surface of **EFP_E** film.

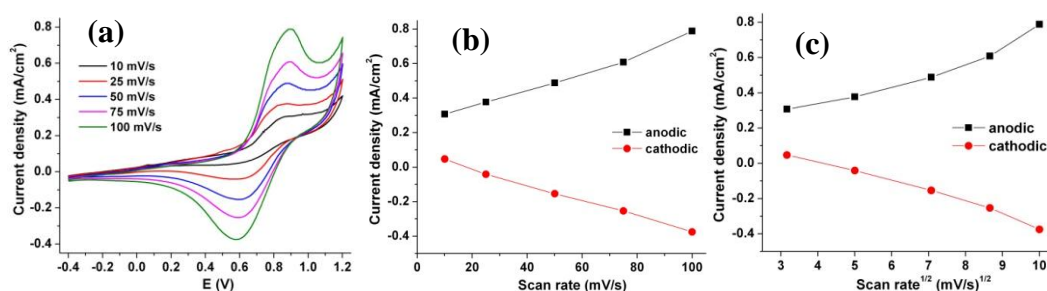


Figure 5.5 (a) Cyclic voltammograms of **EFP_E** film at different scan rates (10, 25, 50, 75 and 100 mV/s), diagram of (b) peak current density versus scan rate and (c) peak current density versus scan rate^{1/2}.

5.3.3 Electrochromic and electrofluorochromic properties

Figure 5.6 shows the UV-vis-NIR absorption spectra of the polymer under various potentials and absorption-time profile of **EFP_E** switched between two

redox potentials. Upon oxidation, the absorption bands at 315 nm and 365 nm are reduced, while the band at 450 nm remains almost the same intensity. Meanwhile, two new bands arise at 660 nm and 900 nm, respectively. The dynamic absorption spectrum (Figure 5.6b) reveals fast coloration (~ 4 s) and bleaching (~ 1 s) in the redox process. This fast switching may result from the nanoporous structure of **EFP_E** film (Figure 5.4), as such structure could facilitate ions insertion into and extraction from the film and thus enhance the switching response.

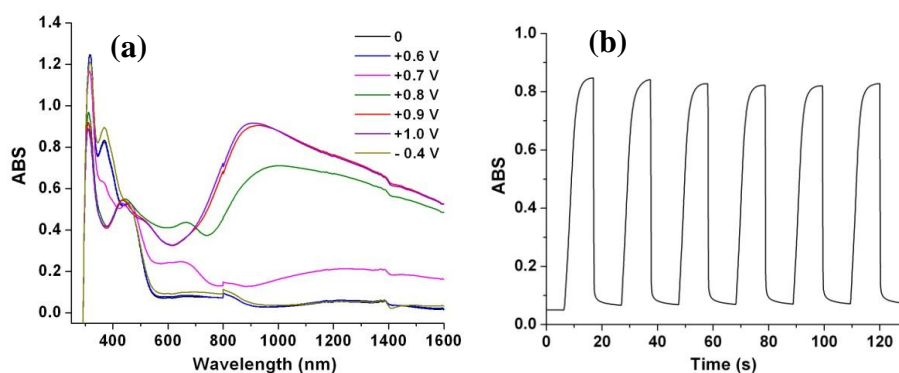


Figure 5.6 (a) UV-vis-NIR absorption spectra of **EFP_E** film in 0.1 M LiClO₄/ACN under different potentials and (b) absorption-time profile ($\lambda_{\text{monitor}} = 900$ nm) of **EFP_E** in 0.1 M LiClO₄/ACN, switching between +0.9 V and -0.4 V with 20 s per cycle.

EFP_E is highly fluorescent, and the PL peak obtained by exciting at 450 nm for thin film is located at 580 nm (at neutral state, as presented by the black curve in Figure 5.7a). C-BTD-C moieties are believed to play the role of fluorophores, while HT units act as separators between these segments. And the side alkyl chains from carbazole and HT units probably help to reduce the chance of inter-

chain π - π stacking. Figure 5.7a and b show the PL intensities of the polymer film under increasing positive potential and decreasing negative potentials, respectively, as well as the dynamic switching fluorescence spectra. The PL intensity of **EFP_E** is gradually reduced with increasing positive potential (Figure 5.7a). This reduction starts at 0.4 V, and reaches the maximum at 0.7 V. It is consistent with the CV results (Figure 5.5a) that the oxidation becomes obvious when the potential is over the onset oxidation potential at ~0.6 V. The fluorescence could recover when negative potentials are loaded (Figure 5.7b), indicating the oxidative quenching is reversible. Additionally, Figure 5.7c shows the repeatability of the quenching and recovery of fluorescence. As interpreted in Chapter 4, the fluorescence quenching of this polymer owes to the electrochemical oxidation induced by external positive potential. Upon oxidation, the photo-excited polymer chains undergo non-radiative exciton decay, which is attributed to the formation of radical cation and dication in the conjugated main chain, rather than radiative energy relaxation, leading to the depression of PL intensity.

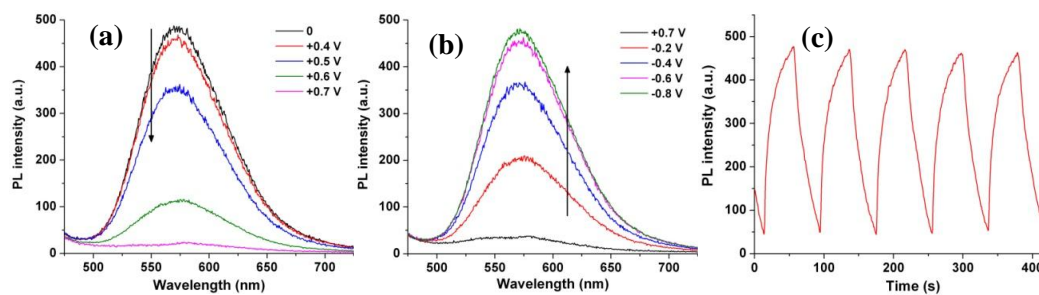


Figure 5.7 PL intensity ($\lambda_{\text{exc}} = 450 \text{ nm}$) change of **EFP_E** film with (a) quenching and (b) recovery under different potentials; (c) PL intensity–time profile of switching between +0.7 V and –0.8 V with 80 s per cycle.

5.3.4 Cyanide detection and possible mechanism

The cyanide sensing tests were performed with the same approach as that used in Chapter 4. The set-up of the detection system is the same as that used in the previous chapter except the detection electrode. In this work, the as-electrodeposited **EFP_E** film on ITO glass was used as detection electrode and 0.1 M LiClO₄/ACN was still used as reference electrolyte (**R**). The experiment procedure of the cyanide detection test as well as the rule of plotting normalized intensity against potential can be referred to section 4.3.4 in Chapter 4. In Figure 5.8a, four normalized intensity (I/I_0)–potential (E) curves (symbols: ■, ●, ▲ and ▼) are obtained using reference electrolyte (**R**) and **R** with different concentrations of CN[–], 10^{–6}, 10^{–5} and 10^{–4} M, respectively.

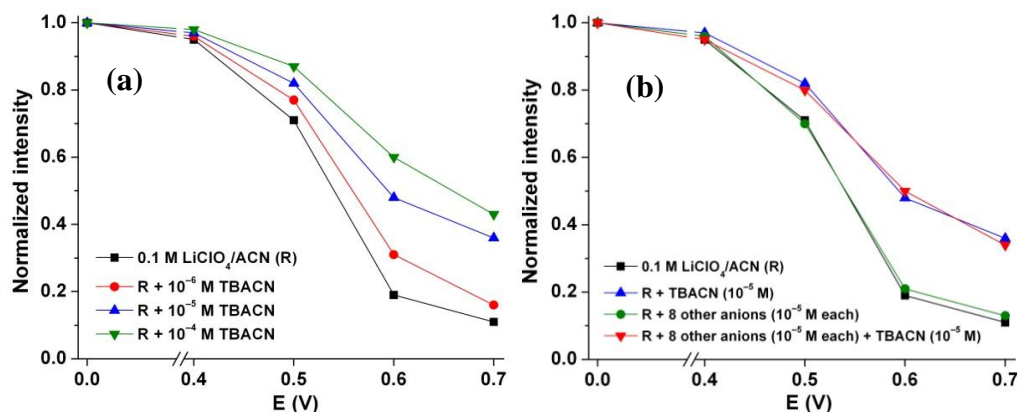


Figure 5.8 Normalized PL intensities ($\lambda_{\text{monitor}} = 580 \text{ nm}$) of electrodeposited EFP_E film as a function of potential, E . The curves in (a) were obtained with the reference electrolyte (**R**) containing different concentrations of TBACN (0 , 10^{-6} , 10^{-5} and 10^{-4} M), and that in (b) were obtained from **R** with 10^{-4} M TBACN as well as **R** + 10^{-5} M TBACN with/without 8 types of other TBA-based anions (OH^- , F^- , Cl^- , Br^- , I^- , AcO^- , NO_3^- and HSO_4^- , 10^{-5} M each).

From Figure 5.8a, it can be seen that using reference electrolyte (**R**) only, the normalized intensity decreases with increasing positive potential due to oxidative quenching. However, with **R** + TBACN, the normalized intensities are higher than that without TBACN at all positive potentials (0.4 , 0.5 , 0.6 and 0.7 V), indicating that the oxidative quenching is significantly weakened in the presence of TBACN. When the potential is above 0.6 V , as low as $1 \mu\text{M}$ TBACN could induce an obvious reduction in normalized PL intensity. As discussed in Chapter 4, it probably results from the partial reduction caused by the interaction between nucleophilic CN^- and electron deficient BTB. It is also observed that the

normalized PL intensity is higher at higher TBACN concentration for the same positive potential, i.e., higher concentration of TBACN leads to stronger weakening effect towards the oxidative quenching. Hence, these I/I_0 -E curves corresponding to different cyanide concentrations can be used as calibrations to determine cyanide concentrations of other analytes. Similar to polymer **EFP_C**, the PL intensity of **EFP_E** film in the electrolytes containing TBACN could also be completely recovered under negative potentials (Figure 5.9a). Also, taken out from **R** + TBACN (10^{-4} M) after cycling, washed in ACN, and inserted into **R** again, the detection electrode exhibited very similar dynamic PL spectra (Figure 5.9b) to that obtained initially using **R**. It indicates that the CN^- could be easily removed from the detection electrode and the interaction between cyanide and BTD is a noncovalent (physical) and reversible process.

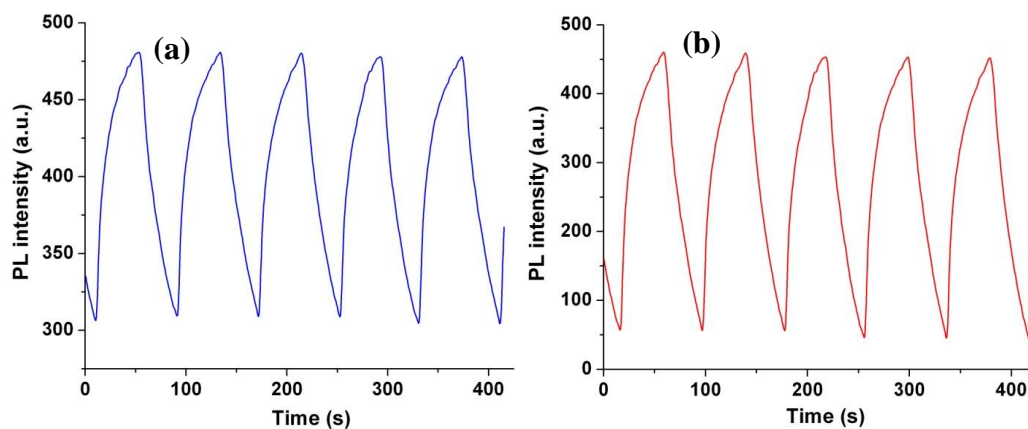


Figure 5.9 PL intensity–time profiles ($\lambda_{\text{exc}} = 450$ nm, $\lambda_{\text{monitor}} = 580$ nm; switching between 0.7 V and -0.8 V with 80 s per cycle) of (a) the detection electrode in **R**

+ 10^{-4} M TBACN, and (b) the detection electrode that had been taken out from **R** + 10^{-4} M TBACN after cycling and washed with ACN before this switching test.

As explained in Chapter 4, the cyanide detection performed by this system is possibly attributed to the cyanide–BTD interaction that is believed to be a noncovalent (physical) and reversible process which are confirmed by experiments. Thus, this interaction is probably a type of anion– π interactions, i.e., energetically favorable non-covalent interaction could exist between an electropositive aromatic ring (BTD) and a nucleophilic anion (CN^-). The selective detection towards cyanide may be attributed to the strong nucleophilicity of CN^- and its triple bond (compared with other anions such as F^- and OH^-). The triple bond may provide electron-rich π system for non-covalent interaction with electron-deficient π system of BTD, leading to charge transfer between CN^- and BTD (π^- – π^+ interaction) and hence weakening the oxidative quenching.

To verify the above mechanism proposed, cyclic voltammetry of **EFPE** film (Figure 5.10) was measured in the electrolytes used for cyanide detection. As illustrated in Figure 5.10a, the peak oxidation potential increases with the cyanide concentration. The oxidation potential of **EFPE** increases with the concentration of cyanide, probably due to the partial reduction induced by CN^- – π interactions during the oxidation. It is consistent with the fact that higher TBACN concentration leads to higher PL intensity as previously discussed, providing some indirect evidence to support the proposed mechanism.

The diagram combining the polymer's normalized intensities obtained under loaded potential at 0.6 V as well as peak oxidation potentials (extracted from cyclic voltammograms), as a function of cyanide concentrations in **R** + TBACN, is shown as Figure 5.10b. It can be clearly seen that at the same oxidation potential (0.6 V) used for cyanide detection, higher cyanide concentration gives higher normalized intensity. Also, the peak oxidation potential obtained from the cyclic voltammogram also increases with cyanide concentration. Thus, in addition to the EFC signals, CV offers another signal to indicate the concentration of CN^- . This could help to further improve reliability of the CN^- detection system.

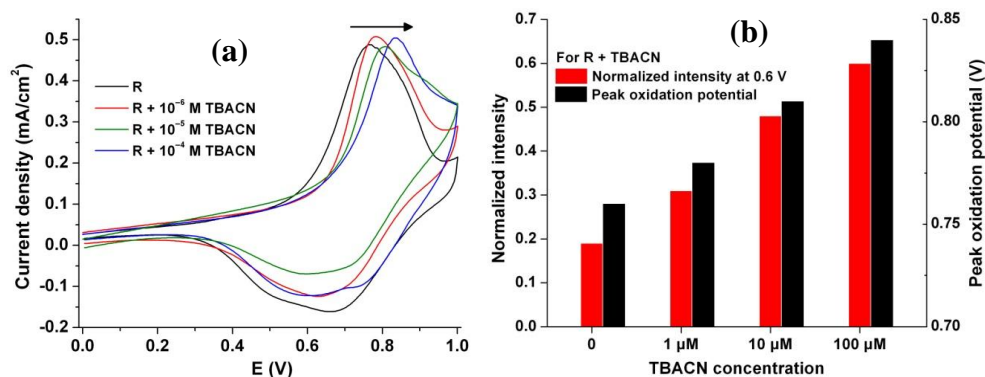


Figure 5.10 (a) Cyclic voltammograms of EFP_E film in the electrolytes **R** and **R** + TBACN. The concentrations of TBACN used are 10^{-6} , 10^{-5} and 10^{-4} M, respectively. (b) Plot of normalized intensities of the detection electrode under 0.6 V external potential in the electrolytes containing TBACN, against TBACN concentration, and the peak oxidation potentials obtained from the cyclic voltammograms at a scan rate 25mV/s. The electrolytes of **R** + TBACN were

used and the concentrations of TBACN were 0, 10^{-6} , 10^{-5} and 10^{-4} M, respectively.

5.3.5 Detection of cyanide in partially aqueous media

Since the EFC copolymer has hydrophobic molecular structure, its thin film does not swell in pure water at neutral state. As a result, it is unable to be electrochemically switched to different redox states owing to the poor ionic conductivity of the film. In addition, the CN^- also could not diffuse into the copolymer film and interact with the fluorophore when **EFP_E** film is inserted into an aqueous electrolyte. The polymer thus cannot be used for cyanide detection in fully aqueous media. However, at oxidized state, the formation of radical cation and dication on the conjugated chains may provide the copolymer with some hydrophilicity, facilitating the swelling of the film to some extent. Thus, unlike common hydrophobic CPs that can only be used for fluorescent detection of cyanide in organic solvents, this EFC conjugated polymer **EFP_E** may provide the possibility to detect cyanide in partially aqueous solutions.

To verify this hypothesis, the electrolytes with mixed ACN and H_2O , which are miscible in whole concentration range, were attempted for cyanide detection. The electrolyte was prepared by dissolving 0.1 M LiClO_4 in ACN/ H_2O with ACN/ H_2O volume ratios of 1:1 and 1:2, respectively, and the corresponding electrolytes denoted as **R^{1:1}** and **R^{1:2}**. **R**, **R^{1:1}** and **R^{1:2}** were compared in the detection tests and the results are shown in Figure 5.11. It can be seen that at a certain cyanide concentration, similar PL intensities were detected when using different

electrolytes, implying that **R**, **R**^{1:1} and **R**^{1:2} could swell the polymer film to almost the same extent. It is believed that ACN in the mixed electrolyte swells the polymer and thus facilitates CN[−] diffuse into the polymer film, while the oxidation state of the polymer also help to pull CN[−] inside. Additionally, the nanoporous structure of the polymer film may create short diffusion distance for H₂O as well as dissolved CN[−], as discussed in section 5.3.2. The above results indicate that the concentration of cyanide from an aqueous analyte can be determined by mixing that analyte with a certain amount of reference electrolyte and then using the mixed solution as the electrolyte in EFC tests. Since the amount of ACN required is relatively small (as revealed by Figure 5.11 as well as the previous discussion), the detection limit would not be significantly affected. Although the polymer still cannot be used for cyanide detection in fully aqueous solution, it could perform the cyanide sensing in 67% aqueous solution (in the presence of a small amount of ACN).

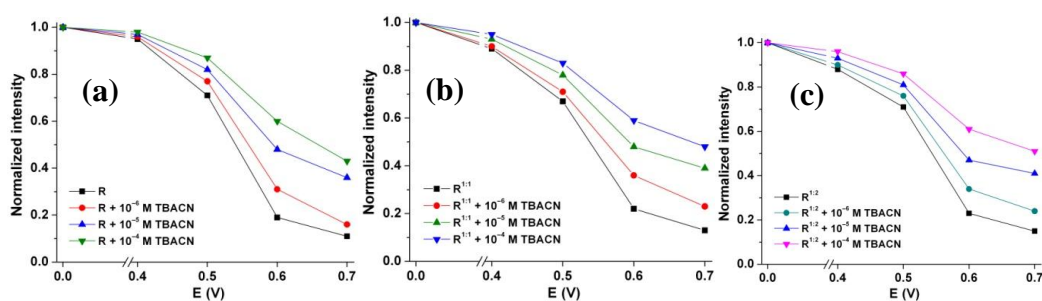


Figure 5.11 Normalized PL intensities ($\lambda_{\text{monitor}} = 580 \text{ nm}$) of **EFP_E** film as a function of potential, E. The curves were obtained using the electrolyte of 0.1 M LiClO₄ in (a) ACN (**R**), **R** + TBACN; (b) ACN/H₂O (v/v = 1:1, **R**^{1:1}), **R**^{1:1} +

TBACN; and (c) ACN/H₂O (v/v = 1:2, **R**^{1:2}), **R**^{1:2} + TBACN. The TBACN concentrations used are 10⁻⁶, 10⁻⁵ and 10⁻⁴ M, respectively.

The cyclic voltammograms of the detection electrode in the mixed electrolyte **R**^{1:2} with different concentrations of TBACN were also measured (Figure 5.12a). Figure 5.12a shows that the peak oxidation potential increases with cyanide concentration, which is similar to the phenomenon observed in **R** + TBACN (Figure 5.10) and also revealed in Figure 5.13b. Figure 5.13b also illustrates the polymer's normalized intensities obtained under loaded potential at 0.6 V against cyanide concentrations in **R**^{1:2} + TBACN. As previously discussed, the oxidation potential of **EPP** increases with the cyanide concentration, which is probably due to the partial reduction induced by BTDC–cyanide interaction occurring during the oxidation.

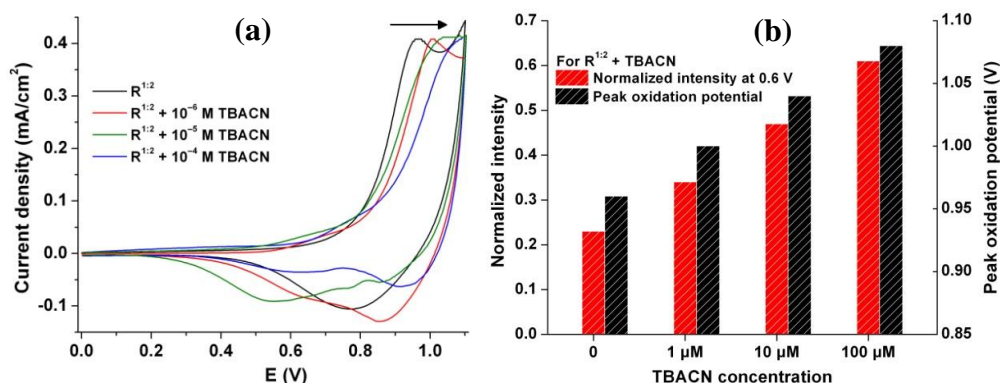


Figure 5.12 (a) Cyclic voltammograms of **EFP**_E film in the electrolytes **R**^{1:2} and **R**^{1:2} + TBACN. The concentrations of TBACN used are 10⁻⁶, 10⁻⁵ and 10⁻⁴ M, respectively. (b) Plot of normalized intensities of the detection electrode under 0.6

V external potential in the electrolytes containing TBACN, against TBACN concentration, and the peak oxidation potentials obtained from the cyclic voltammograms at a scan rate 25mV/s. The electrolytes of $\mathbf{R}^{1:2} + \text{TBACN}$ were used and the concentrations of TBACN were 0, 10^{-6} , 10^{-5} and 10^{-4} M, respectively.

To examine the limit of volume ratio of H_2O in the partially aqueous electrolyte, the electrochemical properties of \mathbf{EFP}_E in the electrolyte prepared by dissolving 0.1 M LiClO_4 in ACN/ H_2O with ACN/ H_2O volume ratio of 1:3 was also characterized. The results show that the potential needed for the oxidizing \mathbf{EFP}_E is very high, as revealed by the cyclic voltammogram in Figure 5.13. It may be attributed to the much reduced ionic conductivity of the \mathbf{EFP}_E film, which possibly results from the depressed swelling effect caused by the lower volume ratio of ACN. Thus, this detection system would not perform well towards CN^- detection. The higher oxidation potential may also lead to over-oxidation and subsequent degradation of \mathbf{EFP}_E .

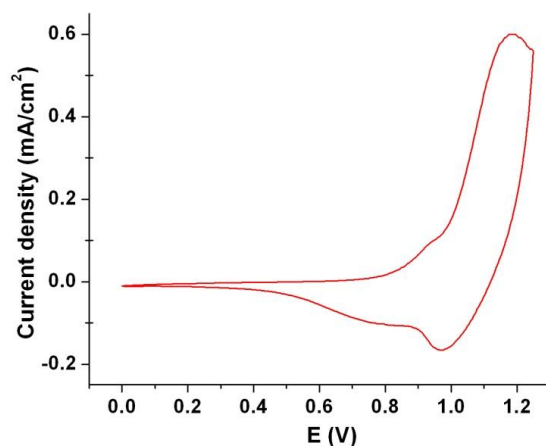


Figure 5.13 Cyclic voltammograms of **EFP_E** film in the electrolyte of 0.1 M LiClO₄ in ACN/H₂O with ACN/H₂O volume ratio of 1:3 at a scan rate 25mV/s.

5.4. Conclusions

In summary, we have synthesized a novel conjugated copolymer via electrochemical polymerization and this polymer shows both electrochromic and electrofluorochromic properties. It exhibits high EC contrast at 900 nm, as well as fast switching speed. Electrochemical oxidation of the polymer leads to significant fluorescence quenching when the potential is above 0.6 V. The reduction in PL intensity caused by oxidative quenching is weakened by CN⁻ added into the electrolyte, which is probably due to the strong interactions between nucleophilic CN⁻ and electron deficient BTB. Using our designed CN⁻ detection system, fluorescence intensities and quenching potentials provide dual signals, further supported by the change of peak oxidation potentials (obtained from cyclic voltammograms), offering high sensitivity, selectivity and reliability.

More importantly, this electrodeposited polymer could be used for detection of CN^- in largely aqueous media. On one hand, it can be attributed to the **EFP_E** film's nanoporous structure, which may create short diffusion distance for H_2O (and dissolved CN^-). On the other hand, and the formation of radical cation and dication at oxidized state on the conjugated chains that may provide the copolymer some hydrophilicity, facilitating the swelling of **EFP_E** film to some extent with the help of ACN.

6. Conclusions and Recommendations

6.1 Conclusions

In this work, three systems of novel carbazole-benzothiadiazole-based conjugated copolymers were synthesized with structures verified. The electrochemical, EC and EFC properties of the copolymers were examined and correlated to their structures. In addition, cyanide detection using the EFC copolymers as the electrodes were demonstrated and the underlying mechanism was investigated. In this chapter, the major findings of this work, as well as the important contributions that this work has made in the field of electrochromism and electrofluorochromism of conjugated polymers will be reviewed.

6.1.1 Dual-active-layer complementary black ECD

The carbazole-azulene-BTD conjugated terpolymers synthesized via Suzuki coupling are found to exhibit high EC contrast in high energy band region of the visible spectrum. Electron deficient BTD facilitates electron removal from polymer chain upon oxidation due to D–A effect and thus results in slightly lower oxidation potentials. The reduced oxidation potential leads to enhanced electrochromic contrasts at relatively low potentials. A complementary black-to-transmissive ECD fabricated using one of the terpolymers (**P**₅) as the anodic coloring layer and PEDOT:PSS as the cathodic coloring layer could achieve CIE black (CIELab coordinates: $L^* = 22.0$, $a^* = 6.3$, $b^* = 7.5$) upon oxidation.

As far as we know, this is the first reported dual-active-layer complementary black ECD. Moreover, the work may be extended to other electrochromic CPs towards the fabrication of simple black ECDs.

6.1.2 Electrofluorochromic sensor towards cyanide detection

The carbazole–BTD-based conjugated copolymer, **EFP_C**, synthesized via Suzuki coupling is found to exhibit both EC and EFC properties. **EFP_C** was used as the active component in EFC detection of CN^- in the electrolyte of 0.1 M $\text{LiClO}_4/\text{ACN}$. The presence of CN^- (as low as 1 μM) in the electrolyte significantly weakens oxidative fluorescence quenching and a higher CN^- concentration leads to stronger weakening effect. In addition to high sensitivity, **EFP_C** also exhibits selectivity towards CN^- over other anions such as OH^- and F^- . Although OH^- and F^- are also fairly nucleophilic, only CN^- has significant interaction with oxidized **EFP_C**, based on our results. This may be attributed to the stronger nucleophilicity of CN^- and its triple bond.

A mechanism is proposed for this cyanide detection system. The recovered fluorescence intensity induced by CN^- may be attributed to the partial reduction of **EFP_C** at the oxidized state, which is probably caused by the interaction between the nucleophilic CN^- and electro-deficient BTD. This interaction is noncovalent and reversible, possibly a type of π –anion interaction. Furthermore, the triple bond of CN^- may provide electron-rich π system for non-covalent interaction with electron-deficient π system of BTD, leading to charge transfer between CN^- and BTD (π^- – π^+ interaction) and hence weakening the oxidative quenching.

To the best of our knowledge, this is the first demonstration of CN^- detection employing the EFC properties of a conjugated polymer. EFC detection allows the detection to be conducted at different redox states of the CP, and hence has the potential to achieve higher sensitivity than that offered by traditional chemosensors. Thus, this EFC sensing approach offers a promising route for CN^- detection. Moreover, it may also be extended to other CPs for detection of other ions or molecules.

6.1.3 Electrofluorochromic cyanide detection in partially aqueous media

Another EFC carbazole–BTD-based conjugated copolymer (**EFPE**) synthesized via electropolymerization is found to exhibit good EC properties, such as high contrast (at $\lambda = 900$ nm) and fast switching. Like **EFPC**, **EFPE** was also used as detection electrode for cyanide detection in the same non-aqueous media (0.1 M $\text{LiClO}_4/\text{ACN}$) and exhibits high sensitivity as well as CN^- selectivity. In addition to dual EFC signals, the detection results are further verified by the cyclic voltammograms which present the change of peak oxidation potentials correlated to different concentrations of CN^- .

Different from **EFPC**, the electrodeposited **EFPE** could perform CN^- detection well in partially aqueous media, 0.1 M LiClO_4 dissolved in $\text{H}_2\text{O}/\text{ACN}$ (up to 2:1, v/v). This may be attributed to the nanoporous structure of polymer film brought by electrodeposition, creating short diffusion distance for H_2O and dissolved CN^- . In addition, the formation of radical cations and dications along the conjugated chains of **EFPE** upon oxidation may bring some hydrophilicity and hence also

facilitate swelling of the **EFP_E** film to some extent, leading to more interactions between **EFP_E** and CN^- .

This demonstration of EFC CN^- detection has been extended from the one in non-aqueous medium to partially aqueous media with high fraction of water, offering the possibility to determine CN^- concentration in fully aqueous media.

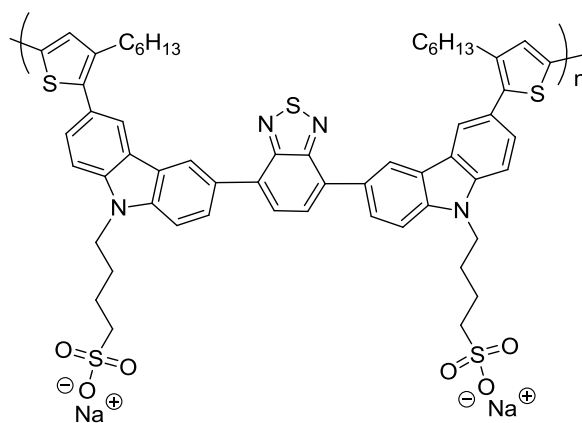
6.2 Recommendations for further research

Nowadays, fluorescent CPs are commonly used for sensing. However, mostly the detection is conducted in polymer solutions. The substance containing a specific kind of ion is added and dissolved in the polymer solution and then this ion would interact or react with the polymer, resulting in a certain change in fluorescence intensity that signifies a certain concentration of that anion. This thesis has demonstrated a new detection method (for CN^-) that combines fluorescence signals and electrochemical signals and could signify a certain concentration of ion to be detected, offering a more convenient and reliable approach. I believe that this detection approach could also be extended to other electrofluorochromic CPs for detection of other ions or molecules. Some recommendations for future research are present as follows:

(1) To investigate whether the introduction of hydrophilic groups into the polymer could help the sensing of CN^- in aqueous media.

The two EFC copolymers discussed in this thesis, which were achieved via either chemical or electrochemical polymerization, are both hydrophobic. The presence of ACN in the electrolyte would swell the polymer thin film and

facilitate ions insertion and extraction during redox process. However, the polymers do not work well for cyanide detection in pure aqueous environment, as H_2O could not swell it due to its high hydrophobicity. Our results show that the detection process of CN^- could only be performed when the volume ratio of ACN/water is higher than 1:2 in the mixed solution of ACN and H_2O . As a result, a possible approach is to synthesize an EFC copolymer that contains some hydrophilic groups such as sulfonate ($-\text{SO}_3^-$), which could facilitate swelling of the polymer in H_2O . At the same time, the number of hydrophilic groups should be controlled relatively small. Otherwise, the polymer may dissolve or partially dissolve in H_2O , and thus lose the sensing capability. Scheme 6.1 demonstrates a possible example of such EFC copolymer.



Scheme 6.1 The structure of a proposed carbazole–BTD-based EFC copolymer (containing sulfonate group) which is possibly partially hydrophilic.

(2) To explore novel EFC CPs with incorporation of other types of fluorophores and their functionalities.

The functional fluorescent molecules which show specific interactions with some certain ions, molecules, or bio-molecules, could be incorporated to form novel EFC conjugated copolymers to extend the EFC detection approach to the many other areas. In other words, the EFC detection system would amplify the sensitivity of fluorescent small molecules (often used in chemosensors), provide both electrochemical and fluorometric signals, and thus lead to more sensitive and reliable sensing.

For example, benzo-[1,2-*c*;4,5-*c'*]bis[1,2,5]thiadiazole (BBT) as a strong electron acceptor, is often used to synthesize D–A CPs that usually exhibit fluorescence in NIR region. Therefore, BBT can be used to synthesize CPs that exhibit electrofluorochromism in NIR region.^{169, 193, 201-206} With very similar structure to BTB, BBT units in conjugated polymer chains are believed to be able to interact with CN^- as well and hence provide these CPs potential in EFC cyanide detection in NIR region.

Furthermore, most of the reported fluorometric chemosensors operate in the visible region and few examples work in the NIR region.^{193, 207} The fluorometric sensor with NIR response are probably useful in systems containing biological species,²⁰⁸ as the NIR electromagnetic waves may be less harmful to some biomolecules in comparison with UV or visible light due to its lower energy. Thus, such BBT-containing CPs that exhibit EFC properties in NIR region would be promising materials for various applications, such as ion detection and biosensors.

References

1. Thakur, V. K.; Ding, G.; Ma, J.; Lee, P. S.; Lu, X., *Adv. Mater.* **2012**, *24*, 4071-4096.
2. Somani, P. R.; Radhakrishnan, S., *Mater. Chem. Phys.* **2003**, *77*, 117-133.
3. Beaujuge, P. M.; Reynolds, J. R., *Chem. Rev.* **2010**, *110*, 268-320.
4. Monk, P. M. S.; Mortimer, R.; Rosseinsky, D., *Electrochromism and electrochromic devices*. Cambridge University Press: 2007.
5. Beaujuge, P.; Ellinger, S.; Reynolds, J., *Nature Mater.* **2008**, *7*, 795-799.
6. Sapp, S. A.; Sotzing, G. A.; Reynolds, J. R., *Chem. Mater.* **1998**, *10*, 2101-2108.
7. Deb, S. K., *Appl. Opt. Suppl.* **1969**, *3*, 192-195.
8. Dias, M.; Hudhomme, P.; Levillain, E.; Perrin, L.; Sahin, Y.; Sauvage, F.-X.; Wartelle, C., *Electrochem. Commun.* **2004**, *6*, 325-330.
9. Kim, Y.; Kim, E.; Clavier, G.; Audebert, P., *Chem. Commun.* **2006**, 3612-3614.
10. Miomandre, F.; Meallet-Renault, R.; Vachon, J.-J.; Pansu, R. B.; Audebert, P., *Chem. Commun.* **2008**, 1913-1915.
11. Miomandre, F.; Allain, C.; Clavier, G.; Audibert, J.-F.; Pansu, R. B.; Audebert, P.; Hartl, F., *Electrochem. Commun.* **2011**, *13*, 574-577.
12. Miomandre, F.; Lépicier, E.; Munteanu, S.; Galangau, O.; Audibert, J. F.; Méallet-Renault, R.; Audebert, P.; Pansu, R. B., *ACS Appl. Mater. Interfaces* **2011**, *3*, 690-696.
13. Audebert, P.; Miomandre, F., *Chem. Sci.* **2013**, *4*, 575-584.
14. Zhou, Q.; Swager, T. M., *J. Am. Chem. Soc.* **1995**, *117*, 7017-7018.
15. Swager, T. M., *Acc. Chem. Res.* **1998**, *31*, 201-207.
16. Yang, J.-S.; Swager, T. M., *J. Am. Chem. Soc.* **1998**, *120*, 5321-5322.
17. Wang, S.; Gaylord, B. S.; Bazan, G. C., *J. Am. Chem. Soc.* **2004**, *126*, 5446-5451.

-
18. Voicescu, M.; Rother, D.; Bardischewsky, F.; Friedrich, C. G.; Hellwig, P., *Biochemistry* **2010**, *50*, 17-24.
 19. Mengoli, G.; Musiani, M. M.; Schreck, B.; Zecchin, S., *J. Electroanal. Chem. Interfacial Electrochem.* **1988**, *246*, 73-86.
 20. Verghese, M. M.; Ram, M.; Vardhan, H.; Ashraf, S.; Malhotra, B., *Adv. Mater. Opt. Electron.* **1996**, *6*, 399-402.
 21. Verghese, M. M.; Ram, M. K.; Vardhan, H.; Malhotra, B. D.; Ashraf, S. M., *Polymer* **1997**, *38*, 1625-1629.
 22. Faid, K.; Siove, A.; Ades, D.; Chevrot, C., *Synth. Met.* **1993**, *55*, 1656-1661.
 23. Beaujuge, P. M.; Ellinger, S.; Reynolds, J. R., *Adv. Mater.* **2008**, *20*, 2772-2776.
 24. Amb, C. M.; Beaujuge, P. M.; Reynolds, J. R., *Adv. Mater.* **2010**, *22*, 724-728.
 25. Shi, P.; Amb, C. M.; Knott, E. P.; Thompson, E. J.; Liu, D. Y.; Mei, J.; Dyer, A. L.; Reynolds, J. R., *Adv. Mater.* **2010**, *22*, 4949-4953.
 26. Kim, Y.-H.; Hong, J.-I., *Chem. Commun.* **2002**, 512-513.
 27. Anzenbacher, P.; Tyson, D. S.; Juršková, K.; Castellano, F. N., *J. Am. Chem. Soc.* **2002**, *124*, 6232-6233.
 28. Jin, W. J.; Fernández-Argüelles, M. T.; Costa-Fernández, J. M.; Pereiro, R.; Sanz-Medel, A., *Chem. Commun.* **2005**, 883-885.
 29. Liu, Y.; Ai, K.; Cheng, X.; Huo, L.; Lu, L., *Adv. Funct. Mater.* **2010**, *20*, 951-956.
 30. Dong, S.; Ou, D.; Qin, J.; Li, Z., *J. Polym. Sci. A Polym. Chem.* **2011**, *49*, 3314-3327.
 31. García, F.; García, J. M.; García-Acosta, B.; Martínez-Máñez, R.; Sancenón, F.; Soto, J., *Chem. Commun.* **2005**, 2790-2792.
 32. Tomasulo, M.; Raymo, F. M., *Org. Lett.* **2005**, *7*, 4633-4636.
 33. Chung, Y.; Ahn, K. H., *J. Org. Chem.* **2006**, *71*, 9470-9474.
 34. Chung, Y. M.; Raman, B.; Kim, D.-S.; Ahn, K. H., *Chem. Commun.* **2006**, 186-188.

-
35. Chen, C.-L.; Chen, Y.-H.; Chen, C.-Y.; Sun, S.-S., *Org. Lett.* **2006**, *8*, 5053-5056.
 36. Yang, Y.-K.; Tae, J., *Org. Lett.* **2006**, *8*, 5721-5723.
 37. Lee, K.-S.; Kim, H.-J.; Kim, G.-H.; Shin, I.; Hong, J.-I., *Org. Lett.* **2008**, *10*, 49-51.
 38. Ros-Lis, J. V.; Martínez-Mañez, R.; Soto, J., *Chem. Commun.* **2002**, 2248-2249.
 39. Argun, A. A.; Aubert, P.-H.; Thompson, B. C.; Schwendeman, I.; Gaupp, C. L.; Hwang, J.; Pinto, N. J.; Tanner, D. B.; MacDiarmid, A. G.; Reynolds, J. R., *Chem. Mater.* **2004**, *16*, 4401-4412.
 40. Mortimer, R. J.; Dyer, A. L.; Reynolds, J. R., *Displays* **2006**, *27*, 2-18.
 41. Platt, J. R., *J. Chem. Phys* **1961**, *34*, 862-863.
 42. Montilla, F.; Frutos, L. M.; Mateo, C. R.; Mallavia, R., *J. Phys. Chem. C* **2007**, *111*, 18405-18410.
 43. Seo, S.; Kim, Y.; You, J.; Sarwade, B. D.; Wadgaonkar, P. P.; Menon, S. K.; More, A. S.; Kim, E., *Macromol. Rapid Commun.* **2011**, *32*, 637-643.
 44. Kawabata, K.; Goto, H., *Chem. Eur. J* **2012**, *18*, 15065-15072.
 45. Seo, S.; Kim, Y.; Zhou, Q.; Clavier, G.; Audebert, P.; Kim, E., *Adv. Funct. Mater.* **2012**, *22*, 3556-3561.
 46. Galangau, O.; Fabre-Francke, I.; Munteanu, S.; Dumas-Verdes, C.; Clavier, G.; Mallet-Renault, R.; Pansu, R. B.; Hartl, F.; Miomandre, F., *Electrochim. Acta* **2013**, *87*, 809-815.
 47. Kuo, C.-P.; Chuang, C.-N.; Chang, C.-L.; Leung, M.-k.; Lian, H.-Y.; Wu, K. C.-W., *J. Mater. Chem. C* **2013**, *1*, 2121-2130.
 48. Seo, S.; Shin, H.; Park, C.; Lim, H.; Kim, E., *Macromol. Res.* **2013**, *21*, 284-289.
 49. Nakamura, K.; Kanazawa, K.; Kobayashi, N., *Chem. Commun.* **2011**, *47*, 10064-10066.
 50. Liou, G.-S.; Yen, H.-J., *Chem. Commun.* **2013**.
 51. Miomandre, F.; Stancheva, S.; Audibert, J.-F.; Brosseau, A.; Pansu, R. B.; Lepeltier, M.; Mayer, C. R., *J. Phys. Chem. C* **2013**.

-
52. Seo, S.; Allain, C.; Na, J.; Kim, S.; Yang, X.; Park, C.; Malinge, J.; Audebert, P.; Kim, E., *Nanoscale* **2013**, 7321-7327.
 53. Lu, W.; Fadeev, A. G.; Qi, B.; Smela, E.; Mattes, B. R.; Ding, J.; Spinks, G. M.; Mazurkiewicz, J.; Zhou, D.; Wallace, G. G., *Science* **2002**, 297, 983-987.
 54. Lin, T.-H.; Ho, K.-C., *Sol. Energy Mater. Sol. Cells* **2006**, 90, 506-520.
 55. Kang, J.-H.; Oh, Y.-J.; Paek, S.-M.; Hwang, S.-J.; Choy, J.-H., *Sol. Energy Mater. Sol. Cells* **2009**, 93, 2040-2044.
 56. DeLongchamp, D.; Hammond, P. T., *Adv. Mater.* **2001**, 13, 1455-1459.
 57. Unur, E.; Beaujuge, P. M.; Ellinger, S.; Jung, J.-H.; Reynolds, J. R., *Chem. Mater.* **2009**, 21, 5145-5153.
 58. Cristina, P.-G.; Pomposo, J. A.; Alduncin, J. A.; Salsamendi, M.; Mikhaleva, A. b. I.; Krivdin, L. B.; Trofimov, B. A., *Electrochim. Acta* **2007**, 52, 4784-4791.
 59. Krebs, F. C., *Nature Mater.* **2008**, 7, 766-767.
 60. Shin, H.; Kim, Y.; Bhuvana, T.; Lee, J.; Yang, X.; Park, C.; Kim, E., *ACS Appl. Mater. Interfaces* **2011**, 4, 185-191.
 61. Vasilyeva, S. V.; Beaujuge, P. M.; Wang, S.; Babiarz, J. E.; Ballarotto, V. W.; Reynolds, J. R., *ACS Appl. Mater. Interfaces* **2011**, 3, 1022-1032.
 62. Lee, K.-R.; Sotzing, G. A., *Chem. Commun.* **2013**.
 63. Agrawal, A.; Cronin, J. P.; Zhang, R., *Sol. Energy Mater. Sol. Cells* **1993**, 31, 9-21.
 64. Córdoba De Torresi, S. I.; Gorenstrein, A., *Electrochim. Acta* **1992**, 37, 2015-2019.
 65. Dhanasankar, M.; Purushothaman, K. K.; Muralidharan, G., *Solid State Sciences* **2010**, 12, 246-251.
 66. Livage, J.; Ganguli, D., *Sol. Energy Mater. Sol. Cells* **2001**, 68, 365-381.
 67. Macrelli, G.; Poli, E., *Electrochim. Acta* **1999**, 44, 3137-3147.
 68. Nishio, K.; Watanabe, Y.; Tsuchiya, T., *Thin Solid Films* **1999**, 350, 96-100.
 69. Ottaviani, M.; Panero, S.; Morzilli, S.; Scrosati, B.; Lazzari, M., *Solid State Ionics* **1986**, 20, 197-202.

-
70. Ozkan Zayim, E.; Turhan, I.; Tepehan, F. Z.; Ozer, N., *Sol. Energy Mater. Sol. Cells* **2008**, *92*, 164-169.
 71. Rauh, R. D., *Electrochim. Acta* **1999**, *44*, 3165-3176.
 72. Shim, H.-S.; Shinde, V. R.; Kim, H. J.; Sung, Y.-E.; Kim, W. B., *Thin Solid Films* **2008**, *516*, 8573-8578.
 73. Vickers, S. J.; Ward, M. D., *Electrochem. Commun.* **2005**, *7*, 389-393.
 74. Wang, H.; Yan, M.; Jiang, Z., *Thin Solid Films* **2001**, *401*, 211-215.
 75. Neff, V. D., *J. Electrochem. Soc.* **1978**, *125*, 886-887.
 76. DeLongchamp, D. M.; Hammond, P. T., *Adv. Funct. Mater.* **2004**, *14*, 224-232.
 77. DeLongchamp, D. M.; Hammond, P. T., *Chem. Mater.* **2004**, *16*, 4799-4805.
 78. Cieslinski, R. C.; Armstrong, N. R., *J. Electrochem. Soc.* **1980**, *127*, 2605-2610.
 79. Jain, V.; Khiterer, M.; Montazami, R.; Yochum, H. M.; Shea, K. J.; Heflin, J. R., *ACS Appl. Mater. Interfaces* **2009**, *1*, 83-89.
 80. Jia, P.; Argun, A. A.; Xu, J.; Xiong, S.; Ma, J.; Hammond, P. T.; Lu, X., *Chem. Mater.* **2009**, *21*, 4434-4441.
 81. Jia, P.; Argun, A. A.; Xu, J.; Xiong, S.; Ma, J.; Hammond, P. T.; Lu, X., *Chem. Mater.* **2010**, *22*, 6085-6091.
 82. Xiong, S.; Phua, S. L.; Dunn, B. S.; Ma, J.; Lu, X., *Chem. Mater.* **2009**, *22*, 255-260.
 83. Xiong, S.; Wei, J.; Jia, P.; Yang, L.; Ma, J.; Lu, X., *ACS Appl. Mater. Interfaces* **2011**, *3*, 782-788.
 84. Xiong, S.; Xiao, Y.; Ma, J.; Zhang, L.; Lu, X., *Macromol. Rapid Commun.* **2007**, *28*, 281-285.
 85. Argun, A. A.; Cirpan, A.; Reynolds, J. R., *Adv. Mater.* **2003**, *15*, 1338-1341.
 86. Heuer, H. W.; Wehrmann, R.; Kirchmeyer, S., *Adv. Funct. Mater.* **2002**, *12*, 89-94.
 87. Walczak, R. M.; Reynolds, J. R., *Adv. Mater.* **2006**, *18*, 1121-1131.
 88. Poverenov, E.; Li, M.; Bitler, A.; Bendikov, M., *Chem. Mater.* **2010**, *22*, 4019-4025.

-
89. Green, M., *Chem. Ind.* **1996**, 17, 641-644.
 90. Granqvist, C. G., *Handbook of inorganic electrochromic materials*. Access Online via Elsevier: 1995.
 91. Granqvist, C. G., *Sol. Energy Mater. Sol. Cells* **2000**, 60, 201-262.
 92. Granqvist, C. G.; Avendaño, E.; Azens, A., *Thin Solid Films* **2003**, 442, 201-211.
 93. Wang, J.; Khoo, E.; Lee, P. S.; Ma, J., *J. Phys. Chem. C* **2008**, 112, 14306-14312.
 94. Wang, J.; Khoo, E.; Lee, P. S.; Ma, J., *J. Phys. Chem. C* **2009**, 113, 9655-9658.
 95. Seguin, L.; Figlarz, M.; Pannetier, J., *Solid State Ionics* **1993**, 63, 437-441.
 96. Roncali, J., *Chem. Rev.* **1992**, 92, 711-738.
 97. Gunbas, G. E.; Durmus, A.; Toppare, L., *Adv. Funct. Mater.* **2008**, 18, 2026-2030.
 98. Wu, C.-G.; Lu, M.-I.; Chang, S.-J.; Wei, C.-S., *Adv. Funct. Mater.* **2007**, 17, 1063-1070.
 99. Schwendeman, I.; Gaupp, C. L.; Hancock, J. M.; Groenendaal, L.; Reynolds, J. R., *Adv. Funct. Mater.* **2003**, 13, 541-547.
 100. Sonmez, G.; Meng, H.; Zhang, Q.; Wudl, F., *Adv. Funct. Mater.* **2003**, 13, 726-731.
 101. Bulut, U.; Toppare, L.; Yilmaz, F.; Yağcı, Y., *Eur. Polym. J.* **2004**, 40, 2421-2426.
 102. Erden, A.; Sahin, E.; Güllü, M.; Toppare, L., *Eur. Polym. J.* **2006**, 42, 1866-1874.
 103. Camurlu, P.; Şahmetlioğlu, E.; Şahin, E.; Akhmedov, İ. M.; Tanyeli, C.; Toppare, L., *Thin Solid Films* **2008**, 516, 4139-4144.
 104. Pang, Y.; Xu, H.; Li, X.; Ding, H.; Cheng, Y.; Shi, G.; Jin, L., *Electrochem. Commun.* **2006**, 8, 1757-1763.
 105. Chang, C.-W.; Liou, G.-S.; Hsiao, S.-H., *J. Mater. Chem.* **2007**, 17, 1007-1015.

-
106. Cheng, S.-H.; Hsiao, S.-H.; Su, T.-H.; Liou, G.-S., *Macromolecules* **2005**, *38*, 307-316.
 107. Huang, L.-T.; Yen, H.-J.; Chang, C.-W.; Liou, G.-S., *J. Polym. Sci. A Polym. Chem.* **2010**, *48*, 4747-4757.
 108. Liaw, D.-J.; Wang, K.-L.; Chang, F.-C., *Macromolecules* **2007**, *40*, 3568-3574.
 109. Liou, G.-S.; Chang, C.-W., *Macromolecules* **2008**, *41*, 1667-1674.
 110. Liou, G.-S.; Hsiao, S.-H.; Chen, H.-W., *J. Mater. Chem.* **2006**, *16*, 1831-1842.
 111. Liou, G.-S.; Hsiao, S.-H.; Huang, N.-K.; Yang, Y.-L., *Macromolecules* **2006**, *39*, 5337-5346.
 112. Liou, G.-S.; Hsiao, S.-H.; Su, T.-H., *J. Mater. Chem.* **2005**, *15*, 1812-1820.
 113. Liou, G.-S.; Lin, H.-Y., *Macromolecules* **2008**, *42*, 125-134.
 114. Yen, H.-J.; Lin, H.-Y.; Liou, G.-S., *Chem. Mater.* **2011**, *23*, 1874-1882.
 115. Yen, H.-J.; Lin, K.-Y.; Liou, G.-S., *J. Mater. Chem.* **2011**, *21*, 6230-6237.
 116. Hu, Y.-C.; Chen, C.-J.; Yen, H.-J.; Lin, K.-Y.; Yeh, J.-M.; Chen, W.-C.; Liou, G.-S., *J. Mater. Chem.* **2012**, *22*, 20394-20402.
 117. Huang, L.-T.; Yen, H.-J.; Liou, G.-S., *Macromolecules* **2011**, *44*, 9595-9610.
 118. Sotzing, G. A.; Reddinger, J. L.; Katritzky, A. R.; Soloducho, J.; Musgrave, R.; Reynolds, J. R.; Steel, P. J., *Chem. Mater.* **1997**, *9*, 1578-1587.
 119. Witker, D.; Reynolds, J. R., *Macromolecules* **2005**, *38*, 7636-7644.
 120. Beaupré, S.; Breton, A.-C.; Dumas, J.; Leclerc, M., *Chem. Mater.* **2009**, *21*, 1504-1513.
 121. Meng, H.; Chen, Z.-K.; Huang, W., *J. Phys. Chem. B* **1999**, *103*, 6429-6433.
 122. Justin Thomas, K. R.; Lin, J. T.; Tao, Y.-T.; Ko, C.-W., *J. Am. Chem. Soc.* **2001**, *123*, 9404-9411.
 123. Li, Y.; Ding, J.; Day, M.; Tao, Y.; Lu, J.; D'iorio, M., *Chem. Mater.* **2004**, *16*, 2165-2173.
 124. Morin, J.-F.; Leclerc, M., *Macromolecules* **2002**, *35*, 8413-8417.
 125. Huang, J.; Niu, Y.; Yang, W.; Mo, Y.; Yuan, M.; Cao, Y., *Macromolecules* **2002**, *35*, 6080-6082.

-
126. Lmimouni, K.; Legrand, C.; Chapoton, A., *Synth. Met.* **1998**, *97*, 151-155.
 127. Romero, D. B.; Schaer, M.; Leclerc, M.; Adès, D.; Siove, A.; Zuppiroli, L., *Synth. Met.* **1996**, *80*, 271-277.
 128. Blouin, N.; Leclerc, M., *Acc. Chem. Res.* **2008**, *41*, 1110-1119.
 129. Morin, J. F.; Leclerc, M.; Adès, D.; Siove, A., *Macromol. Rapid Commun.* **2005**, *26*, 761-778.
 130. Kihara, N.; Nakayama, H.; Fukutomi, T., *Macromolecules* **1997**, *30*, 6385-6387.
 131. Wang, F.; Lai, Y.-H.; Kocherginsky, N.; Kostas, Y. Y., *Org. Lett.* **2003**, *5*, 995-998.
 132. Wang, F.; Lai, Y.-H.; Han, M. Y., *Org. Lett.* **2003**, *5*, 4791-4794.
 133. Wang, F.; Lai, Y.-H.; Han, M.-Y., *Macromolecules* **2004**, *37*, 3222-3230.
 134. Wang, F.; Lai, Y.-H., *Macromolecules* **2003**, *36*, 536-538.
 135. Wang, X.; Ng, J. K.-P.; Jia, P.; Lin, T.; Cho, C. M.; Xu, J.; Lu, X.; He, C., *Macromolecules* **2009**, *42*, 5534-5544.
 136. Tang, T.; Ding, G.; Lin, T.; Chi, H.; Liu, C.; Lu, X.; Wang, F.; He, C., *Macromol. Rapid Commun.* **2012**, *34*, 431-436.
 137. Sprutta, N.; Siczek, M.; Latos-Grażyński, L.; Pawlicki, M.; Szterenber, L.; Lis, T., *J. Org. Chem.* **2007**, *72*, 9501-9509.
 138. Ito, S.; Ando, M.; Nomura, A.; Morita, N.; Kabuto, C.; Mukai, H.; Ohta, K.; Kawakami, J.; Yoshizawa, A.; Tajiri, A., *J. Org. Chem.* **2005**, *70*, 3939-3949.
 139. Ito, S.; Nomura, A.; Morita, N.; Kabuto, C.; Kobayashi, H.; Maejima, S.; Fujimori, K.; Yasunami, M., *J. Org. Chem.* **2002**, *67*, 7295-7302.
 140. Ito, S.; Kikuchi, S.; Okujima, T.; Morita, N.; Asao, T., *J. Org. Chem.* **2001**, *66*, 2470-2479.
 141. Ito, S.; Iida, T.; Kawakami, J.; Okujima, T.; Morita, N., *Eur. J. Org. Chem.* **2009**, *2009*, 5355-5364.
 142. Jonsson, L., *Acta Chem. Scand. Ser.* **1981**, *B 35*, 683-689.
 143. Arbizzani, C.; Bongini, A.; Mastragostino, M.; Zanelli, A.; Barbarella, G.; Zambianchi, M., *Adv. Mater.* **1995**, *7*, 571-574.

-
144. Mastragostino, M.; Arbizzani, C.; Bongini, A.; Barbarella, G.; Zambianchi, M., *Electrochim. Acta* **1993**, *38*, 135-140.
145. Sankaran, B.; Reynolds, J. R., *Macromolecules* **1997**, *30*, 2582-2588.
146. Kumar, A.; Welsh, D. M.; Morvant, M. C.; Piroux, F.; Abboud, K. A.; Reynolds, J. R., *Chem. Mater.* **1998**, *10*, 896-902.
147. Gaupp, C. L.; Welsh, D. M.; Rauh, R. D.; Reynolds, J. R., *Chem. Mater.* **2002**, *14*, 3964-3970.
148. Sonmez, G.; Sonmez, H. B.; Shen, C. K.; Wudl, F., *Adv. Mater.* **2004**, *16*, 1905-1908.
149. Blankespoor, R. L.; Miller, L. L., *J. Chem. Soc., Chem. Commun.* **1985**, 90-92.
150. Chang, A.-C.; Blankespoor, R. L.; Miller, L. L., *J. Electroanal. Chem. Interfacial Electrochem.* **1987**, *236*, 239-252.
151. Chang, A.-C.; Miller, L. L., *Synth. Met.* **1987**, *22*, 71-78.
152. Daoust, G.; Leclerc, M., *Macromolecules* **1991**, *24*, 455-459.
153. Fall, M.; Assogba, L.; Aaron, J. J.; Dieng, M. M., *Synth. Met.* **2001**, *123*, 365-372.
154. Cihaner, A.; Önal, A. M., *J. Electroanal. Chem.* **2007**, *601*, 68-76.
155. Fungo, F.; Jenekhe, S. A.; Bard, A. J., *Chem. Mater.* **2003**, *15*, 1264-1272.
156. Berlin, A.; Zotti, G.; Zecchin, S.; Schiavon, G.; Vercelli, B.; Zanelli, A., *Chem. Mater.* **2004**, *16*, 3667-3676.
157. Sonmez, G.; Sonmez, H. B.; Shen, C. K.; Jost, R. W.; Rubin, Y.; Wudl, F., *Macromolecules* **2005**, *38*, 669-675.
158. Otero, L.; Sereno, L.; Fungo, F.; Liao, Y.-L.; Lin, C.-Y.; Wong, K.-T., *Chem. Mater.* **2006**, *18*, 3495-3502.
159. Durmus, A.; Gunbas, G. E.; Camurlu, P.; Toppare, L., *Chem. Commun.* **2007**, 3246-3248.
160. Durmus, A.; Gunbas, G. E.; Toppare, L., *Chem. Mater.* **2007**, *19*, 6247-6251.
161. Balan, A.; Gunbas, G.; Durmus, A.; Toppare, L., *Chem. Mater.* **2008**, *20*, 7510-7513.
162. Cihaner, A.; Algi, F., *Adv. Funct. Mater.* **2008**, *18*, 3583-3589.

-
163. Gunbas, G. E.; Durmus, A.; Toppare, L., *Adv. Mater.* **2008**, *20*, 691-695.
164. Balan, A.; Baran, D.; Gunbas, G.; Durmus, A.; Ozyurt, F.; Toppare, L., *Chem. Commun.* **2009**, 6768-6770.
165. Beaujuge, P. M.; Vasilyeva, S. V.; Ellinger, S.; McCarley, T. D.; Reynolds, J. R., *Macromolecules* **2009**, *42*, 3694-3706.
166. Beaujuge, P. M.; Amb, C. M.; Reynolds, J. R., *Acc. Chem. Res.* **2010**, *43*, 1396-1407.
167. İçli, M.; Pamuk, M.; Algi, F.; Onal, A. M.; Cihaner, A., *Chem. Mater.* **2010**, *22*, 4034-4044.
168. Stalder, R.; Mei, J.; Reynolds, J. R., *Macromolecules* **2010**, *43*, 8348-8352.
169. Zhang, X.; Steckler, T. T.; Dasari, R. R.; Ohira, S.; Potscavage, W. J.; Tiwari, S. P.; Coppée, S.; Ellinger, S.; Barlow, S.; Brédas, J.-L., *J. Mater. Chem.* **2010**, *20*, 123-134.
170. Ellinger, S.; Graham, K. R.; Shi, P.; Farley, R. T.; Steckler, T. T.; Brookins, R. N.; Taranekekar, P.; Mei, J.; Padilha, L. A.; Ensley, T. R., *Chem. Mater.* **2011**, *23*, 3805-3817.
171. Sonmez, G.; Shen, C. K.; Rubin, Y.; Wudl, F., *Angew. Chem.* **2004**, *116*, 1524-1528.
172. Amb, C. M.; Kerszulis, J. A.; Thompson, E. J.; Dyer, A. L.; Reynolds, J. R., *Polym. Chem.* **2011**, *2*, 812-814.
173. Amb, C. M.; Dyer, A. L.; Reynolds, J. R., *Chem. Mater.* **2010**, *23*, 397-415.
174. Miyaura, N.; Suzuki, A., *J. Chem. Soc., Chem. Commun.* **1979**, 866-867.
175. Miyaura, N.; Yamada, K.; Suzuki, A., *Tetrahedron Lett.* **1979**, *20*, 3437-3440.
176. Miyaura, N.; Suzuki, A., *Chem. Rev.* **1995**, *95*, 2457-2483.
177. Thomas, S. W.; Joly, G. D.; Swager, T. M., *Chem. Rev.* **2007**, *107*, 1339-1386.
178. Xu, Z.; Chen, X.; Kim, H. N.; Yoon, J., *Chem. Soc. Rev.* **2010**, *39*, 127-137.
179. Zeng, Q.; Cai, P.; Li, Z.; Qin, J.; Tang, B. Z., *Chem. Commun.* **2008**, 1094-1096.
180. Son, J. H.; Jang, G.; Lee, T. S., *Polymer* **2013**.

-
181. Jockusch, S.; Hirano, T.; Liu, Z.; Turro, N. J., *J. Phys. Chem. B* **2000**, *104*, 1212-1216.
182. Namai, H.; Ikeda, H.; Hoshi, Y.; Kato, N.; Morishita, Y.; Mizuno, K., *J. Am. Chem. Soc.* **2007**, *129*, 9032-9036.
183. Kim, Y.; Do, J.; Kim, E.; Clavier, G.; Galmiche, L.; Audebert, P., *J. Electroanal. Chem.* **2009**, *632*, 201-205.
184. Lo ěe, F.; Vuillemin, B.; Oltra, R.; Chaumont, D.; Bourillot, E., *Electrochem. Commun.* **2006**, *8*, 1016-1020.
185. Latonen, R.-M.; Esteban, B. M.; Kvarnström, C.; Ivaska, A., *J. Appl. Electrochem.* **2009**, *39*, 653-661.
186. Salman, H.; Abraham, Y.; Tal, S.; Meltzman, S.; Kapon, M.; Tessler, N.; Speiser, S.; Eichen, Y., *Eur. J. Org. Chem.* **2005**, *2005*, 2207-2212.
187. Schwendeman, I.; Hwang, J.; Welsh, D. M.; Tanner, D. B.; Reynolds, J. R., *Adv. Mater.* **2001**, *13*, 634-637.
188. Padilla, J.; Seshadri, V.; Sotzing, G.; Otero, T., *Electrochem. Commun.* **2007**, *9*, 1931-1935.
189. Suzuki, T.; Hioki, A.; Kurahashi, M., *Anal. Chim. Acta* **2003**, *476*, 159-165.
190. Shan, D.; Mousty, C.; Cosnier, S., *Anal. Chem.* **2003**, *76*, 178-183.
191. Lindsay, A. E.; O'Hare, D., *Anal. Chim. Acta* **2006**, *558*, 158-163.
192. Zacharis, C. K.; Tzanavaras, P. D.; Voulgaropoulos, A. N.; Karlberg, B., *Talanta* **2009**, *77*, 1620-1626.
193. Qian, G.; Li, X.; Wang, Z. Y., *J. Mater. Chem.* **2009**, *19*, 522-530.
194. Grisorio, R.; Dell'Aquila, A.; Romanazzi, G.; Suranna, G. P.; Mastroilli, P.; Cosma, P.; Acierno, D.; Amendola, E.; Ciccarella, G.; Nobile, C. F., *Tetrahedron* **2006**, *62*, 627-634.
195. Omer, K. M.; Ku, S.-Y.; Cheng, J.-Z.; Chou, S.-H.; Wong, K.-T.; Bard, A. J., *J. Am. Chem. Soc.* **2011**, *133*, 5492-5499.
196. Pandalai, S. G., *Recent Research Developments in Chemical Physics*. Transworld Research Network: Kerala, India, 2004; Vol. 5, p 227.
197. Chifotides, H. T.; Dunbar, K. R., *Acc. Chem. Res.* **2013**, *46*, 894-906.

-
198. Krische, B.; Hellberg, J.; Lilja, C., *J. Chem. Soc., Chem. Commun.* **1987**, 1476-1478.
199. Arbizzani, C.; Barbarella, G.; Bongini, A.; Mastragostino, M.; Zambianchi, M., *Synth. Met.* **1992**, 52, 329-339.
200. Ding, G.; Cho, C. M.; Chen, C.; Zhou, D.; Wang, X.; Tan, A. Y. X.; Xu, J.; Lu, X., *Org. Electron.* **2013**, 14, 2748-2755.
201. Li, X.; Liu, A.; Xun, S.; Qiao, W.; Wan, X.; Wang, Z. Y., *Org. Lett.* **2008**, 10, 3785-3787.
202. Qian, G.; Dai, B.; Luo, M.; Yu, D.; Zhan, J.; Zhang, Z.; Ma, D.; Wang, Z. Y., *Chem. Mater.* **2008**, 20, 6208-6216.
203. Qian, G.; Zhong, Z.; Luo, M.; Yu, D.; Zhang, Z.; Wang, Z. Y.; Ma, D., *Adv. Mater.* **2009**, 21, 111-116.
204. Steckler, T. T.; Zhang, X.; Hwang, J.; Honeyager, R.; Ohira, S.; Zhang, X.-H.; Grant, A.; Ellinger, S.; Odom, S. A.; Sweat, D.; Tanner, D. B.; Rinzler, A. G.; Barlow, S.; Brédas, J.-L.; Kippelen, B.; Marder, S. R.; Reynolds, J. R., *J. Am. Chem. Soc.* **2009**, 131, 2824-2826.
205. Yuen, J. D.; Fan, J.; Seifert, J.; Lim, B.; Hufschmid, R.; Heeger, A. J.; Wudl, F., *J. Am. Chem. Soc.* **2011**, 133, 20799-20807.
206. Yuen, J. D.; Kumar, R.; Zakhidov, D.; Seifert, J.; Lim, B.; Heeger, A. J.; Wudl, F., *Adv. Mater.* **2011**, 23, 3780-3785.
207. Zhang, X.; Li, C.; Cheng, X.; Wang, X.; Zhang, B., *Sens. Actuators B Chem.* **2008**, 129, 152-157.
208. Patonay, G.; Antoine, M. D., *Anal. Chem.* **1991**, 63, 321A-327A.

List of Publications

Ding, G.; Zhou, H.; Xu, J.; Lu, X. “Electrofluorochromic detection of cyanide anion using a benzothiadiazole-containing conjugated copolymer”, *Chem. Commun.* 2014, 655–657.

Ding, G.; Cho, C. M.; Chen, C.; Zhou, D.; Wang, X.; Tan, A. Y. X.; Xu, J.; Lu, X. “Black-to-transmissive electrochromism of azulene-based donor–acceptor copolymers complemented by poly(4-styrene sulfonic acid)-doped poly(3,4-ethylenedioxythiophene)”, *Org. Electron.* 2013, 14, 2748–2755.

Chen, C.; **Ding, G.**; Zhou, D.; Lu, X. “Synthesis of poly(aniline-co-3-amino-4-hydroxybenzoic acid) and its enhanced redox activity under highly basic conditions”, *Electrochim. Acta* 2013, 97, 112–119.

Thakur, V. K.; **Ding, G.**; Ma, J.; Lee, P. S.; Lu, X. “Hybrid materials and polymer electrolytes for electrochromic device applications”, *Adv. Mater.* 2012, 24, 4071–4096.

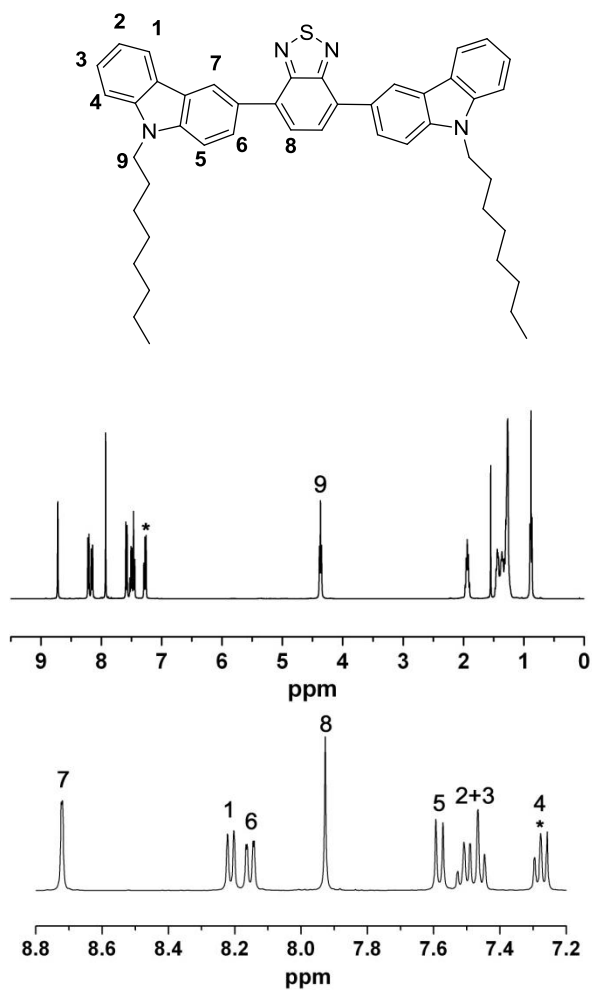
Tang, T.; **Ding, G.**; Lin, T.; Chi, H.; Liu, C.; Lu, X.; Wang, F.; He, C. “Near-infrared responsive conjugated polymers to 1.5 μm and beyond: synthesis and electrochromic switching application”, *Macromol. Rapid Commun.* 2012, 34, 431–436.

Appendix

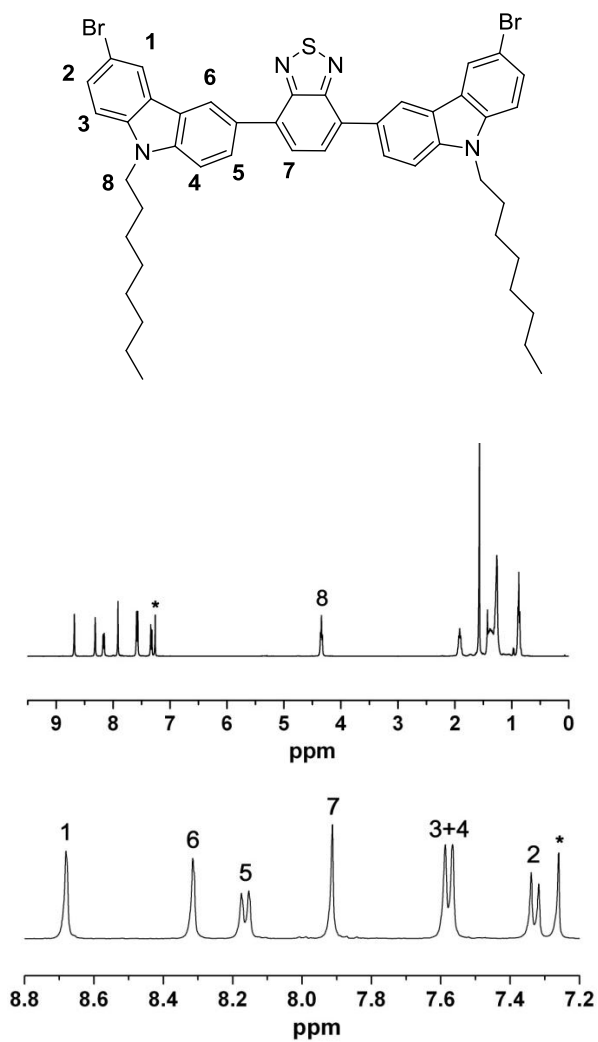
¹H NMR Assignment for Synthesized Compounds

Chapter 4

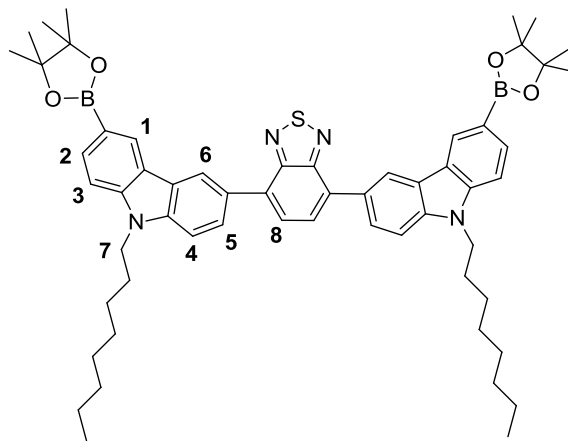
Compound 1

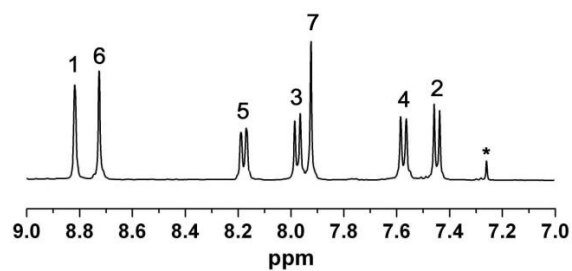
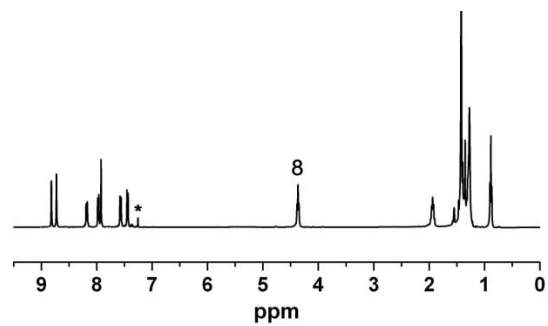


Compound 2

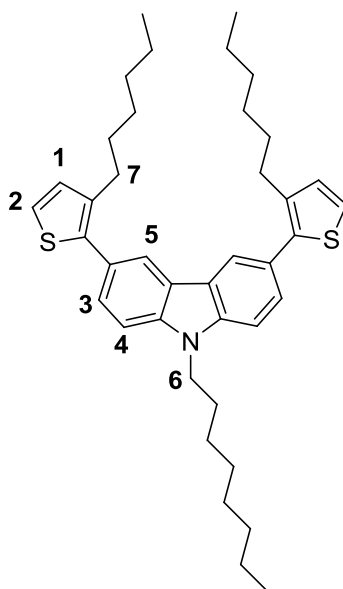


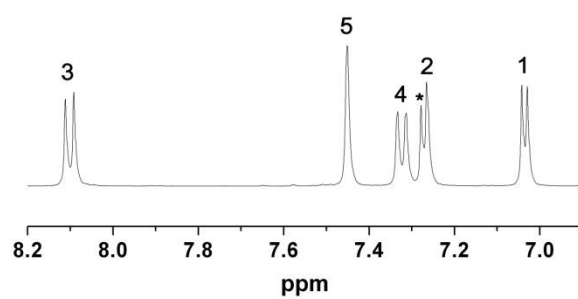
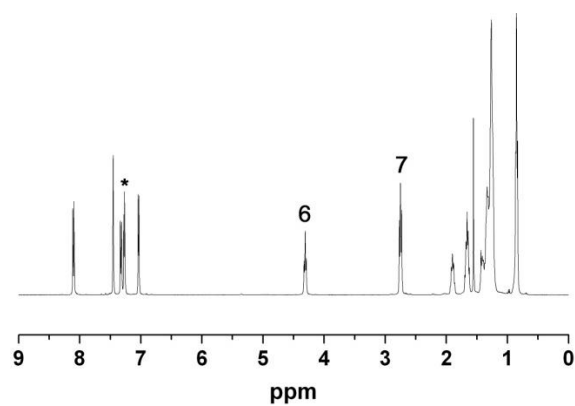
Compound 3



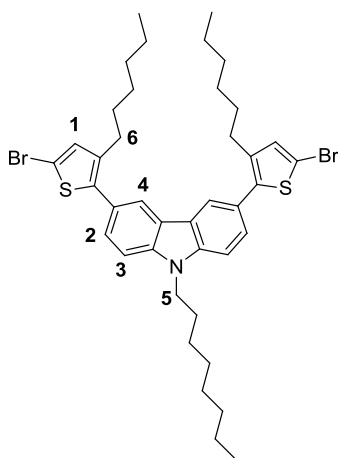


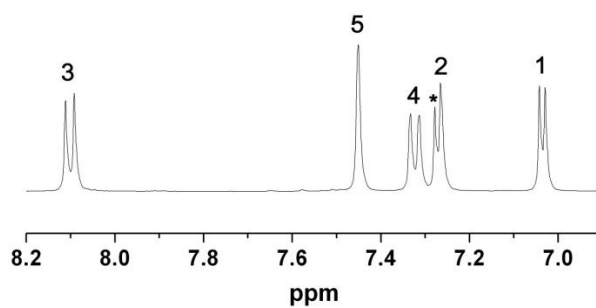
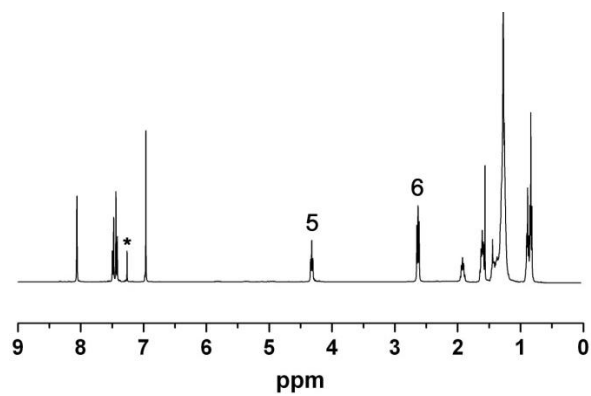
Compound 4





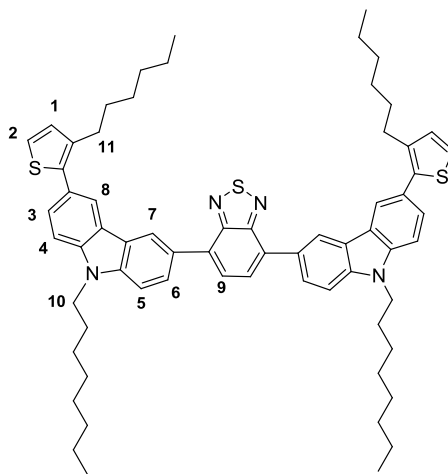
Compound 5

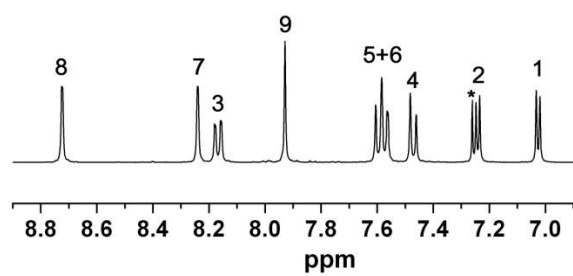
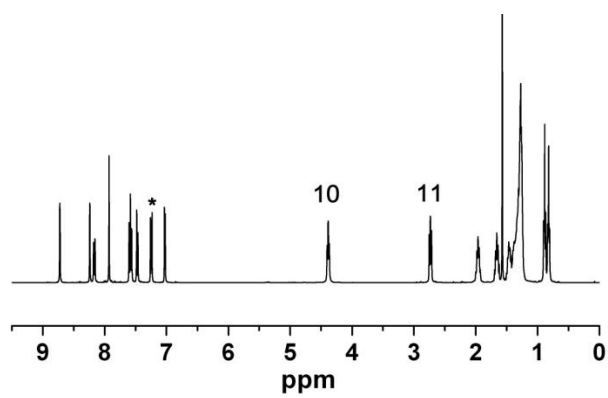




Chapter 5

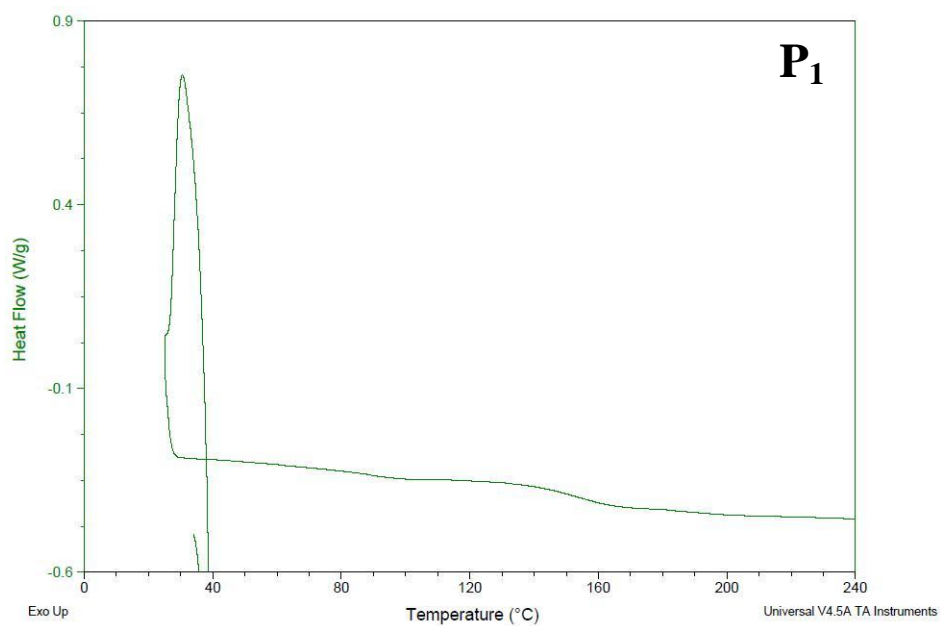
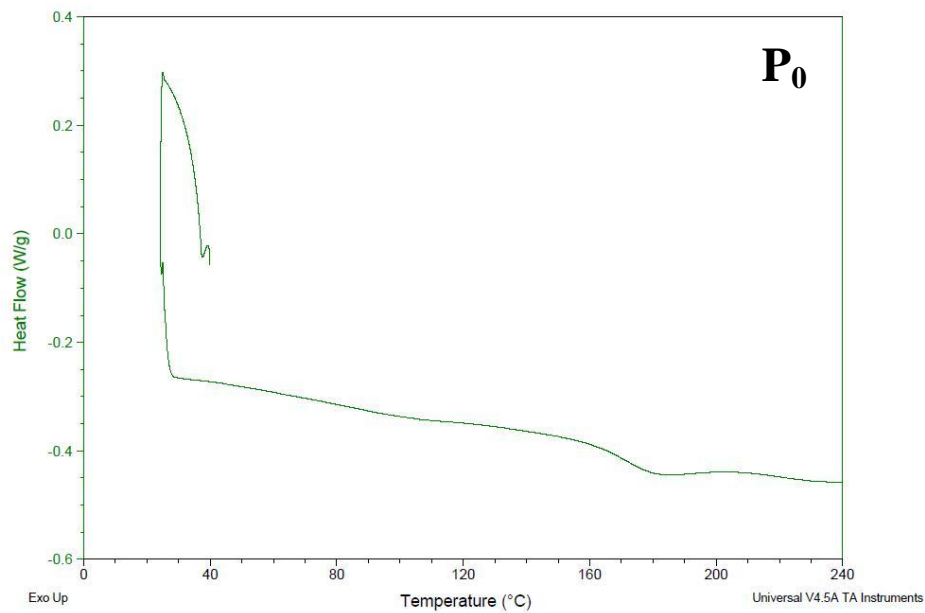
Monomer HT-C-BTD-C-HT

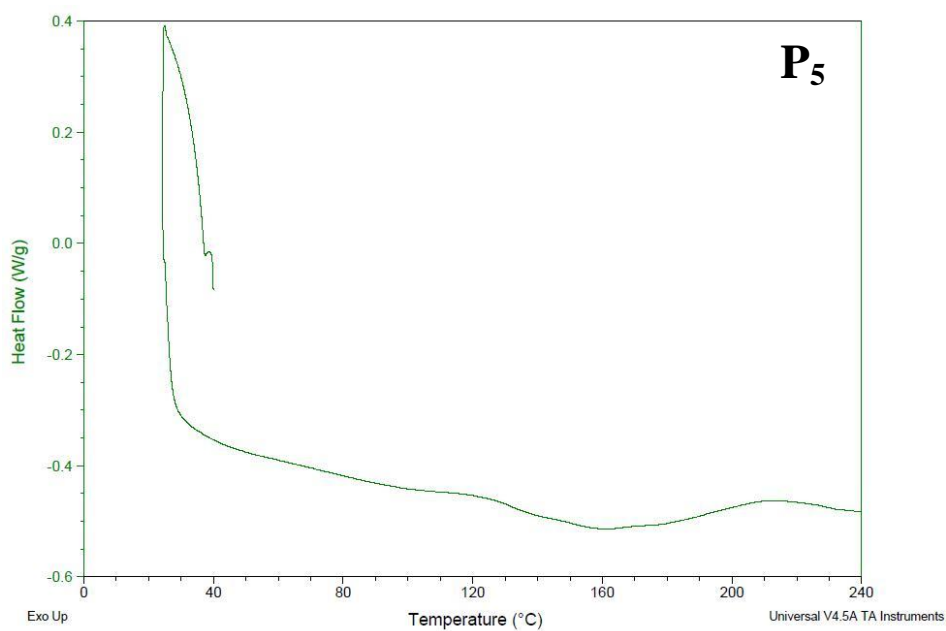
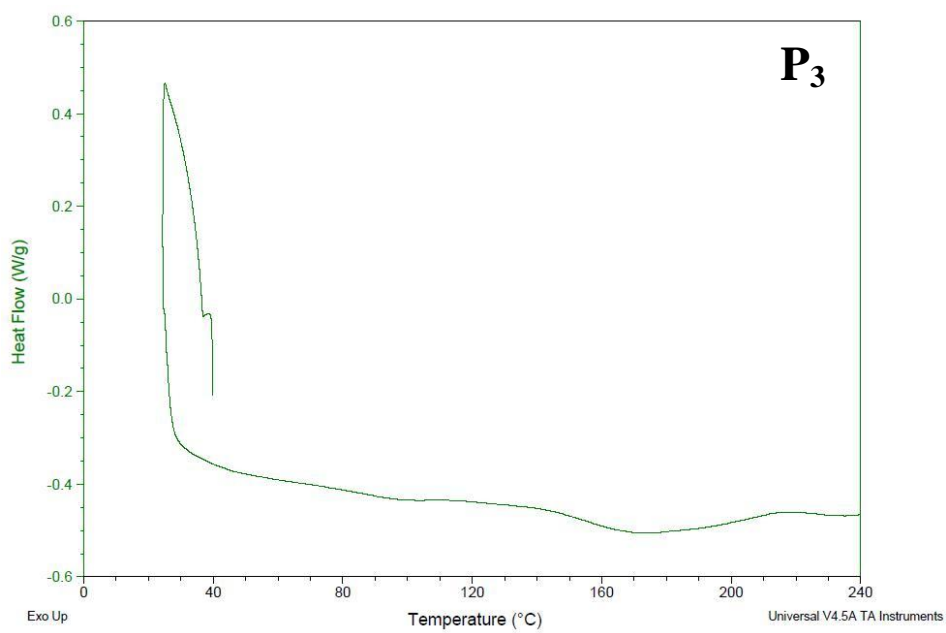


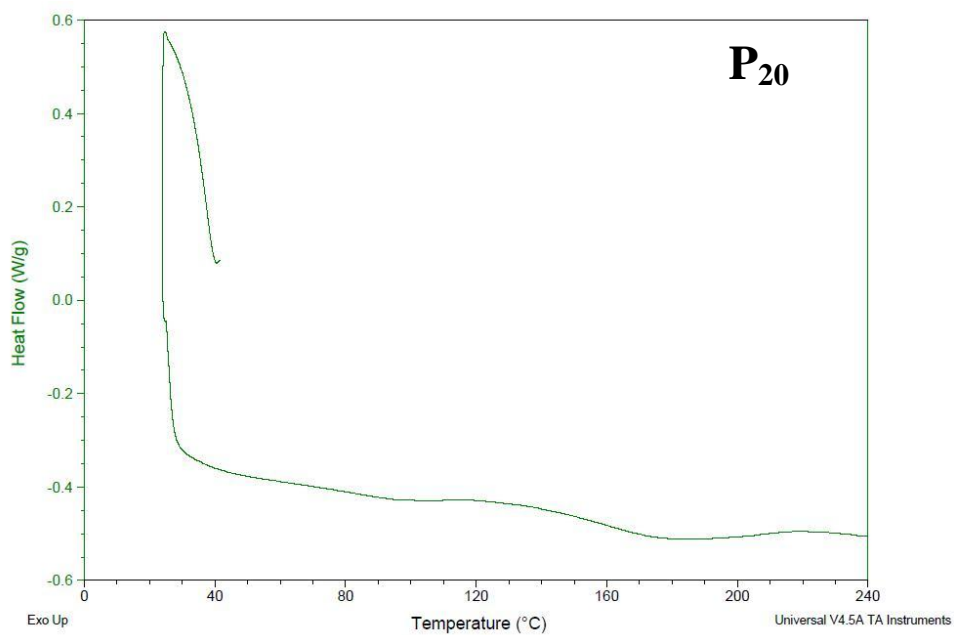


DSC Thermograms of Chemically Synthesized Copolymers

Chapter 3: P₀, P₁, P₃, P₅ and P₂₀







Chapter 4: EFP_C

